Washington University in St. Louis
Washington University Open Scholarship

All Theses and Dissertations (ETDs)

Spring 3-28-2013

Concentration Coding in the Accessory Olfactory System

Hannah Ada Arnson
Washington University in St. Louis

Follow this and additional works at: https://openscholarship.wustl.edu/etd

 Part of the Neuroscience and Neurobiology Commons

Recommended Citation
Arnson, Hannah Ada, "Concentration Coding in the Accessory Olfactory System" (2013). *All Theses and Dissertations (ETDs)*. 1065.
https://openscholarship.wustl.edu/etd/1065

This Dissertation is brought to you for free and open access by Washington University Open Scholarship. It has been accepted for inclusion in All Theses and Dissertations (ETDs) by an authorized administrator of Washington University Open Scholarship. For more information, please contact digital@wumail.wustl.edu.

WASHINGTON UNIVERSITY IN ST. LOUIS

Division of Biology and Biomedical Sciences

Neurosciences

Dissertation Examination Committee:

Timothy E. Holy, Chair

Dennis L. Barbour

Robert W. Gereau

Erik D. Herzog

Daniel Kerschensteiner

Baranidharan Raman

Concentration Coding in the Accessory Olfactory System

by

Hannah Ada Arnson

A dissertation presented to the
Graduate School of Arts and Sciences
of Washington University in
partial fulfillment for the degree
of Doctor of Philosophy

May 2013

St. Louis, Missouri

© Copyright 2013, Hannah Ada Arnson

Contents

List of Figures

List of Abbreviations

AOB: Accessory olfactory bulb

AOS: Accessory olfactory system

AUC: Area under the curve

BAOT: Bed nucleus of the accessory olfactory tract

BNST: Bed nucleus of the stria terminalis

ESP: Exocrine gland secreting peptide

FPR: Formyl peptide receptor

IBI: Interburst interval

ISI: Interspike interval

ITI: Inter-trial interval

MEA: Multielectrode array

MHC: Major histocompatibility complex

MOS: Main olfactory system

MUP: Major urinary protein

OSN: Olfactory sensory neuron

PLC: Phospholipase-C

ROC: Receiver operating characteristic

VNO: Vomeronasal organ

VSN: Vomeronasal sensory neuron

Acknowledgments

I would like to thank the many people who made this thesis possible. From my mentor, Tim Holy, I have learned enormous amounts about science, critical thinking, experimental design, data analysis, programming and mathematics. Most of all, he has imparted the importance of enthusiasm and intellectual curiosity beyond a narrow scientific niche. All of my lab members, past and present, have helped me in some way. Xiaoyan Fu helped me learn MEA recordings, provided me with mouse urine, and performed mass spectroscopy and TLC purification in Chapter 5. Julian Meeks help with much scientific discussion and contributed particularly to the intellectual development of Chapter 3. Zhongsheng Guo and Jian Wang provided technical assistance and fixed many computer disasters. Everyone else, too many to name individually, has given scientific and life advice and made the lab a great place. I deeply appreciate the friendships formed over the past several years.

I would like to acknowledge my thesis committee for scientific advice, discussion and for helping make this work better. The Cognitive, Computational and Systems Neuroscience (CCSN) pathway provided funding and overall enriched my graduate experience. I like to think that my thesis encompasses the multi-discimpinary spirit of CCSN. CCSN outreach played an invaluable role in my scientific development, improving my communication skills and providing an alternate perspective. All of the support staff in Anatomy and Neurobiology and the Division of Biology and Biomedical Sciences made any administrative aspects of graduate school operate so seamlessly.

Thanks to my friends at Wash U and beyond for making graduate school not only bearable, but fun. I would especially like to acknowledge the Lulus.

This thesis would not be if not for the endless support and encouragement of my family, my parents, my brother and my grandmother. My parents made this all possible by giving me the best educational opportunities, allowing me to pursue my passions and making it so easy for me to be here today.

Finally, I would like to thank Michael Morgan, for being there for me and encouraging me to be the best scientist, musician and person possible. All of his kindness, enthusiasm, humor, help and honesty has meant so much to me. I will be forever grateful to the neuroscience program for bringing us together.

Funding for this work was provided by NSF IGERT 0548890 (HAA), NIDCD RO1 DC005964 (TEH), and NIDCD R01 DC010381 (TEH).

ABSTRACT OF THE DISSERTATION

Concentration Coding in the Accessory Olfactory System

by

Hannah Ada Arnson

Doctor of Philosophy in Biology and Biomedical Sciences

in Neurosciences

Washington University in St. Louis, 2013

Associate Professor Timothy E. Holy, Chairperson

Understanding how sensory systems encode stimuli is a fundamental question of neuroscience. The role of every sensory system is to encode information about the identity and quantity of stimuli in the environment. Primary sensory neurons in the periphery are faced with the task of representing all relevant information for further processing by downstream circuits, ultimately leading to detection, classification and potential response. However, environmental variability potentially alters stimulus properties in non-relevant ways. Here, we address these problems using the mouse accessory olfactory system (AOS) as a model. The AOS is an independent olfactory system possessed by most terrestrial vertebrates, although not humans, and is specialized to detect social cues. It mediates behaviors such as reproduction, aggression, and individual identification. Non-volatile compounds found in urine, including sulfated steroids, are the main source of AOS stimuli. Vomeronasal sensory neurons (VSNs), the primary sensory neurons of the AOS, are located in the base of the nasal cavity, and they detect the identity and quantity of stimuli. However, like other sensory cues, urine is subject to environmental modulation through mechanisms such as evaporation and dilution that affect the concentrations of ligands in non-biologically relevant ways. Ideally, the AOS represents stimuli in ways that are stable across condition.

In the scope of this thesis, I explore how the AOS represents concentration at the levels of the individual neuron, the circuit and the whole animal. Using extracellular recordings of explanted tissue, we characterized how VSNs encode stimuli. VSNs fired predominantly in trains of action potentials with similar structure during spontaneous and stimulus-driven activity. Using pharmacological and genetic tools, we demonstrated that the signal transduction cascade influences the

structure of both spontaneous and stimulus-driven activity. Then, we explored the representation of concentration of sulfated steroids by VSNs and the circuit mechanisms by which the AOS can represent concentration information in a manner invariant to environmental uncertainties. We identified ratio-coding as a means for stable concentration representation. The ratio of the concentrations of non-volatile ligands found in urine will not change following urine evaporation or dilution, while the individual concentrations will. This property allows for both insensitivity to changes in absolute concentration and sensitivity to changes in relative concentration. Using extracellular recording and computational modeling, we have demonstrated that VSN activity can be used to robustly encode concentration using ratios. Finally, we attempted to develop a novel behavioral assay to investigate how mice detect AOS stimuli.

1 Introduction

A central goal of neuroscience is to understand sensory perception, an enormous task involving questions posited at all levels of the nervous system. How do sensory neurons represent information? What patterns or features of action potentials are responsible for transmitting essential information? How do circuits extract relevant information about a stimulus? Can strictly controlled elements of animal behavior be used to provide insight into the structure and function of the nervous system? These are all questions I will be addressing in the scope of this thesis as related to concentration coding in the mouse accessory olfactory system (AOS). When most people think of olfaction, they think of the main olfactory system (MOS); receptor neurons in the nose detect small airborne, or volatile, compounds. Mice, along with most terrestrial animals (not humans, see section 1.2.3), also posses an accessory olfactory system, a specialized olfactory system involved in detecting cues related to social communication.

While ultimately neuroscientists are interested in understanding neural coding in humans, studies in other animals are more tractable. The mouse AOS has several benefits. From the point of view of a model circuit it is relatively compact, as reviewed in more detail in Section 1.2.4 (Figure 1.1). Detection begins with receptor neurons in the nose. Then there are a few areas of central processing before output at the hypothalamus. The AOS's appeal is apparent upon comparison with the monkey visual circuit which involves a dozen or so cortical areas [1], or even the MOS, involving multiple cortical areas, the amygdala, and striatum [2]. The AOS is also an experimentally accessible system. The sensory epithelium in the nose can be removed and recorded from for long periods of time (see Section 2). Genetic manipulations in the mouse have produced useful mutants.

Even though humans lack an equivalent system, the mouse AOS is interesting for its own sake. The AOS detects social cues including compounds such as pheromones, individual identifiers, and

metabolic byproducts. This system mediates essential behaviors in the animal kingdom — reproduction, identification, aggression. While animal social behavior is fascinating, it is something in which we truly lack insight. By studying the AOS, we can gain understanding as to what drives certain animal behaviors. This thesis will cover the following areas of AOS function and sensory coding: understanding how receptor neurons represent sensory information, exploring how sensory neurons and neural circuits represent the amount of stimuli, and developing a behavioral assay of AOS detection.

1.1 Intensity coding

Sensory systems detect and encode the amounts of stimuli in the environment. How they do so is a matter of active research. The quantitative study of intensity perception and coding began in the seventeenth century by the German psychophysicist Ernst Weber. Weber's law states that the just noticeable difference between two stimuli is proportional to the magnitude of the stimulus; small changes in high-intensity stimuli are less noticeable than small changes in low-intensity stimuli. This law was furthered in the mid-1800s by Gustav Fechner, who stated that subjective sensation is proportional to the logarithm of the stimulus intensity (the Weber-Fechner law) [3]. Since the 1800's, there have been different views as to how stimulus and perceived intensities are related, however, psychophysicist proposed that subjective intensity and neural representation are linearly related [4, 5]. Here, I will focus on the neural representation of stimulus intensity.

On the surface, understanding how neural circuits represent concentration appears to be straightforward. More stimulus leads to an increase in firing in peripheral sensory neurons that propagates to downstream circuits and is decoded as more stimulus. However, peripheral neurons are encoding more than just the intensity of a single stimulus dimension. Stimuli are typically complex mixtures; a song is a combination of many pure tones and the smell of coffee consists of a myriad of odors. Peripheral neurons must detect all aspects of the entire stimulus scene. An increase in firing can mean more of one stimulus, the presence of a different amount of another stimulus, or some combination. How might a downstream circuit disambiguate this increase in firing and recognize a stimulus as the same given different amounts? How can sensory systems achieve perceptual stability in the face of varying intensities? Perceptual stability occurs as we are able to recognize an object despite

changes in light levels or recognize a sound be it near or far. Eliminating all intensity information is not a feasible solution, as intensity is still a meaningful and perceptible dimension. Therefore, the brain must be capable of representing sensory information in an intensity invariant manner while simultaneously representing information about the stimulus intensity as an aspect of stimulus quality. The neural basis of intensity invariance has been explored in multiple sensory systems including olfaction, vision and audition with proposed mechanisms ranging from adaptation [6, 7] to spike timing [8] to dendritic nonlinearities [9]. A more thorough exploration of concentration coding and invariance in the main olfactory system is discussed below.

1.1.1 Intensity coding in the main olfactory system

Concentration-dependent responses of the main olfactory system have been well characterized. The concentration response of main olfactory sensory neurons (OSNs) is described by the Hill Model in which there is some minimum threshold followed by a monotonic increase and then saturation. The dynamic range spans one log-unit, on average, with considerable variability [10, 11, 12]. OSNs project into the main olfactory bulb where neurons expressing the same receptor type converge and synapse in structures referred to as glomeruli. In the rodent main olfactory bulb, increasing the concentration of odorants leads to the recruitment of additional glomeruli [13, 14, 15, 16]. Individual glomeruli also have larger dynamic ranges than reported in OSNs, potentially due to pooling of many OSNs with different sensitivities, effectively extending the dynamic range [15].

The difference in patterns of activation of glomeruli within the main olfactory system poses a potential difficulty in decoding; can an animal recognize an odor across concentrations? If so, how can an animal recognize an odor as a constant percept given disparate patterns of activation? Animals, including humans, are generally able to recognize many odors across a range of concentrations [17, 18, 19, 20, 16], however, there are notable exceptions of odor quality changing with increasing concentration. Humans perceive lower concentrations of the odorant indole as pleasant and floral and higher concentrations as putrid [21]. Drosophila are attracted to apple cider vinegar at low concentrations, yet this attraction decreases with increasing concentration [22]. Honeybees conditioned to detect an odorant displayed a reduced conditioned response to concentrations other than that used in initial training, suggesting that different concentrations may be perceived differently

[23].

Despite limited evidence that particular odors undergo changes in quality over a range of concentrations, there is a high degree of perceptual stability. There have been several theoretical models as to how concentration-invariant perception occurs. One such model relies on inhibition within the olfactory bulb. As concentration increases, more glomeruli are activated. If total inhibition scales with this activation, then the pattern of glomerular activation can be maintained; increasing inhibition can normalize the signal onto downstream neurons, effectively returning the representation to an odor-specific map [16]. Spike timing has also been proposed as a means of generating concentration invariance. Olfactory receptor neurons show decreased latency to fire with increasing concentration [24, 25, 26, 27]. Latency to spike will then maintain a certain order with the most sensitive receptor neurons activated first, and so on, providing a code that is stable across concentrations [28, 2, 25]. Temporal information across a large population of neurons may provide a concentration invariant readout of stimulus in the locust olfactory system [29]. A model proposed by Hopfield suggests that if one assumes that receptor-ligand interactions lead to a log-linear response, then the ratio of activated receptors will be constant over the dynamic range of the receptor. By reading out the ratio of occupied receptors, a concentration-invariant representation of odor can be achieved [30, 31]. Uchida and Mainen went on to demonstrate behaviorally that rats can use odor ratios. Rats were unable to discriminate mixtures with the same ratio and different absolute concentrations across a ten-fold concentration range [32]. However, a basic assumption of the ratio model is that the dynamic range of receptor neurons is constant across neurons. If some receptors saturate, then the ratio is no longer constant. Olfactory receptor neurons have variable dynamic ranges, as measured by the Hill coefficient in the Hill model [10], complicating implementation of the ratio model. However, by pooling populations of sensory neurons with variable dynamic ranges, the log-linear portion of concentration representation can be increased [15](see Section 4).

1.2 The accessory olfactory system

1.2.1 A note about the term "pheromone"

The term "pheromone" was originally coined in 1959 by Karlson and Luscher [33]. According to their original publication, pheromones are "defined as substances which are secreted to the outside by an individual and received by a second individual of the same species, in which they release a specific reaction" [33]. While originally defined in the context of insect behavior (the first chemically defined pheromone, Bombykol, was published that same year by Butenandt and colleagues [34]), Karlson and Luscher postulate the use of pheromones beyond insects and invertebrates and suggest they are likely detected by chemosensory organs [33]. While the terminology is relatively new, the idea that a chemical emitted by one animal may serve as an attractant or behavioral modifier of another, has long been known, dating back to the ancient Greeks who realized that female dogs in heat attracted male dogs from some distance [35].

While it is clear that chemical communication is pervasive among animals, plants and even single celled organisms [36], the definition of what falls under the umbrella of the term pheromone and what does not is still a matter of debate. Does this term apply to complex odors or only those of a single compound or blend? Are learned odors that still have social valance pheromones or only those with innate responses? What about compounds used to communicate across species such as in a predator-prey relationship? Historically, the AOS detects pheromones and the MOS detects every-day smells [37]. However, recent work suggests that the two systems operate in tandem, with the MOS detecting social as well as non-social odors [38, 39, 40, 41]. Also, many proposed ligands for the AOS fail to meet the strict definition of pheromones as small molecules used for conspecific signaling (see Section 1.2.5). The AOS in reptiles is involved in detecting food odors, decidedly non-pheromonal in nature [42]. There is also a great deal about AOS function and ligands that is of yet unknown. Recent work identified sulfated steroids as a main class of ligands activating the AOS [43, 44]. However, no behavioral function has been definitively attributed to these compounds. Therefore, can we call them pheromones? To avoid making any categorization about ligand function, I will avoid "pheromone" when it is not clearly indicated or historically used, instead opting for the term "social odor" or "social cue".

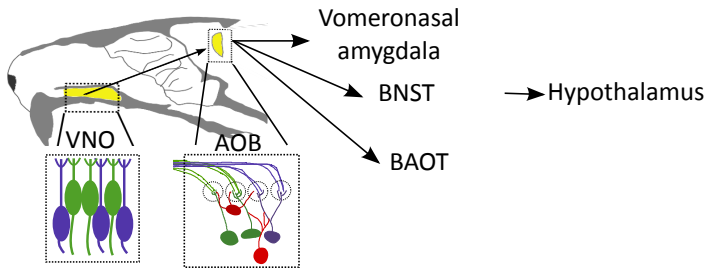

Figure 1.1: Anatomy of the AOS. A sagital view of the nasal cavity of the mouse. The VNO projects to the AOB. The AOB projects primarily to the vomeronasal amygdala, but also to the bed nucleus of the stria termanalis (BNST) and the bed nucleus of the accessory olfactory tract (BAOT). These areas then project to the hypothalamus. Reciprocal projections are not shown. The VNO insert illustrates the striated nature of the tissue and the general structure of VSNs. The AOB cartoon demonstrates the pooling of VSN axons into glomeruli, the dotted circles. There, they synapse with mitral cells (green and purple cells). Inhibitory interneurons are indicated in red. The mouse drawing is modified with permission from T. Holy.

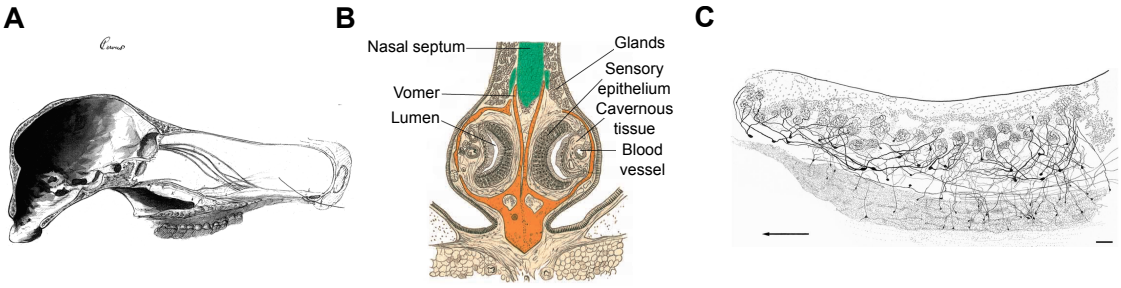

Figure 1.2: Historical portrayal of the AOS. **A**, Jacobson's drawing of a sagital view of the deer (cervus) head (date unknown). The VNO and AOB are shown with connecting nerves. Reproduced from [45]. **B,** A drawing by Von Mihalkovics (1899) of a cross section of the mouse nasal septum illustrating the VNO structure. Reproduced from [45] and modified to enlarge the labels. **C,** A drawing of the rat AOB by Larriva-Sahd (2008). Reproduced from [46]

1.2.2 AOS history and function

Historical knowledge about the AOS began with the discovery of the vomeronasal organ (VNO) by Ludvig Jacobson (1783-1843) in 1811, although the VNO may have been reported as early as 1703 [47]. Figure 1.2A is of a drawing by Jacobson of the deer AOS. Termed the Jacobson's organ for many years, it was renamed as the vomeronasal organ (or "organon vomeronasal") in 1895 [48]. Since its discovery, the vomeronasal organ has been thought to be, in part, a sensory organ, potentially assisting in the sense of smell [48]. Its similarity to other olfactory systems was confirmed in 1884 by Retzius [49, 45], suggesting a chemosensory role. Early electrophysiological investigation of the accessory olfactory bulb (AOB) by E.D. Adrian did not evoke any response from odorants, rather only from mechanical stimulation. However, Adrian postulated that the VNO may respond to slow chemical changes in the nasal fluid [50]. Beginning in the 1950s, pheromonal effects in mice were explored and many were found to be elicited by urine and to depend on intact olfactory systems [42].

AOS involvement has been demonstrated in behaviors directly related to mating. After undergoing vomeronasal removal, male mice demonstrated reduced copulation [51, 52]. Upon exposure to female odors, male mice lacking a VNO also showed a decreased testosterone surge [53]. Male mice bred with a genetic ablation of the VNO (a null mutation of the TrpC2 gene, a required component of the vomeronasal sensory neuron (VSN) signal transduction machinery) appear unable to discriminate between sexes, indiscriminately mounting both males and females while maintaining normal male-female copulation [54, 55].

Female attraction to male odor likely involves AOS cues [56, 57], and female copulatory behavior may be regulated by the AOS as well. A study of female mouse sexual behavior found that when the VNO was genetically rendered non-functional, females displayed male-specific behavior such as mounting, suggesting that the AOS may be involved in repressing neural circuitry that gives rise to sexually dimorphic behaviors [58]. However, another report involving surgical removal of the VNO failed to replicate male-like sexual behavior in females [59].

Both male and female aggression have ties to the accessory olfactory system. When presented with an unfamiliar male, or the urine from an unfamiliar male, a male mouse will display aggressive

behaviors [60] if the AOS is intact [61, 51, 54, 62, 63, 55]. However, deficits in male-male aggression have also been demonstrated in mice with intact accessory but non-functional main olfactory systems [64]. Female mice are also known to be aggressive, particularly while lactating. While fertility and most maternal behavior such as pup retrieval and nursing were not profoundly affected following vomeronasal removal in female mice, a reduction in aggression in lactating females was observed [65].

There are several more specific, canonical AOS-dependent phenomena. One such behavior is the Lee-Boot effect, or estrus suppression among group housed females [66]. Mice undergoing VNO removal prior to group housing failed to show estrus suppression, and those already undergoing estrus suppression returned to estrus following removal of the VNO [67]. This effect was likely due to urinary cues from other female mice [68]. The Whitten effect, induction of estrus by male odors, was initially found to be induced by the presence of males or male-soiled bedding [69]. Stimulation of the AOB, medial amygdala, or bed nucleus of the stria terminalis (BNST), all areas in the accessory olfactory pathway, leads to a surge in lutenizing hormone, inducing ovulation [42]. While estrus induction was believed to be due to a volatile compound found in male urine [70], it was later suggested to be dependent on a functional AOS [71] and the effect was blocked in rats [72] and in goats [73] following VNO removal or ablation. The Vandenbergh effect involves acceleration of puberty in immature female mice following exposure to a male or male odor [74]. This effect requires the presence of an intact VNO or intact connection from the VNO to AOB [75, 76].

One of the most frequently studied AOS behaviors is the Bruce effect. Also termed pregnancy block, this behavior describes the reduced frequency of fertilized egg implantation in the uterus following exposure to a novel male [77, 78] or male odor [79, 80] soon after mating. Exposure to the stud male or another female does not result in pregnancy block. The requirement of the accessory olfactory system was later demonstrated [81, 82] and putative circuitry involves noreadrenergic stimulation of the AOB and subsequent endocrine involvement [83], although the circuitry may be less clear than previously thought [84].

The requirement of the AOS for the Bruce effect implies that AOS cues are sufficient to discriminate between two males (or males of different strains) or between males and females. Individual recognition is also important in more general mate choice [85]. Another example of individual recog-

nition using urinary cues is in the case of scent marking [86]. The activity of neurons within the AOS is indicative of sex and strain based on urinary cues [87, 88]. However, it is unclear as to what individual components of urine drive individual identification (see section 1.2.5 for more discussion).

Identification of conspecifics, sexual and aggressive behaviors all have strong ties to the AOS. Behaviors occur both at the level of endocrine control and overt observable responses. However, some controversy within the field remains as to the AOS-dependance of specific behaviors and to the identity of evoking stimuli.

1.2.3 The AOS in humans

Since the discovery of the the VNO two-hundred years ago, humans were thought to possess, at most, a rudimentary sensory organ [48] (although the organ may have originally been discovered in humans [47]). There is strong evidence for a vomeronasal organ-like structure in human embryos, however it decreases in size and complexity until being unobservable at embryonic ages ranging from 19 to more than 30 weeks [89, 90]. Human adults frequently have a pit or depression in the nasal cavity in a location consistent with the VNO on one or both sides of the nose [91]. However, the pit reportedly contains varying degrees of structure, from none [91] to pseudo-stratified cell layers [92]. While there are some reports that "neuron-like" cells may exist [93, 91], the cells lack clear hallmarks of VSNs such as clearly defined axons and expression of Olfactory Marker Protein, a marker of chemosensory receptor neurons [91, 94], indicating a lack of chemosensory function [92, 91, 94].

The genetic machinery required for VSN function is also lacking in the human genome. The TrpC2 channel, required for VSN function in mice, is a non-functional pseudogene in the human genome [95, 96]. Vomeronasal receptor genes are present in the human genome, but the majority of evidence suggests that they are also pseudogenes [97, 98], although one vomeronasal receptor-like gene may be expressed in human main olfactory epithelium [99]. Interestingly, using genetic tracing of a range of species, it is likely that the first mutation to render TrpC2 non-functional occurred in the ancestors of old world monkeys and apes 25–40 million years ago, with other VNO related genes likely mutating around the same time. This timeframe coincides with the likely rise in trichromatic vision in old world primates, suggesting chemosensory social signaling may have been co-opted by

visual signals [100, 96].

It remains relatively uncontroversial that humans lack a functional AOS (despite papers such as Foltan and Sedy [101], which claims that behavioral changes following facial surgery are the result of damage to the VNO, without any evidence of a functional human AOS). However, humans may or may not make use of "pheromonal" communication through main olfactory channels. Human mother-infant recognition has an olfactory component, evidence of the use of social-odors in humans. An infant prefers its mother's odor over that of another new mother, and mothers are able to recognize their baby by smell alone after limited contact [102]. A classical study by Martha McClintock proposed that human menstrual synchrony, a well observed pheromone-dependent behavior in mice (Section 1.2.2), is evidence of human pheromones [103]. However, these results remain controversial, with numerous reports presenting experimental and statistical flaws in the original study (for example, [104]). Other examples of putative human pheromones are androstenone, a known MOS-dependent pig pheromone [105] and androstadienone, a related compound, both found in men's sweat. While there is some evidence that female behavior may be modified by these compound (i.e. [106]), the ability to even detect the compound is variable and genetically determined [107, 108] questioning the utility and universality of these cues. Despite the advertisements in the back of magazines suggesting otherwise, the extent to which humans use pheromones, mediated necessarily by the main olfactory system, remains controversial [109, 110, 94].

1.2.4 AOS anatomy

The vomeronasal organ Detection in the mouse AOS begins with the receptor neurons located in the VNO. A drawing of a cross section of the VNO from 1899 is shown in Figure 1.2B. The VNO, a mucus-filled, blind ended tube in the base of the nasal cavity, is made up of a neuroepithelium in which the receptor neurons are located and a blood vessel that serves as a pump. As AOS stimuli are non-volatile (see Section 1.2.5), the mouse must make direct contact with the stimuli. The pump then draws stimuli into the nasal cavity and into contact with the receptor neurons. Little is known about the function of the VNO pump in the mouse, but in hamsters it is active in response to novel stimuli [111]. In addition, sympathetic nerve activity elicits pump activity [112, 113].

The neuroepithelium is primarily made up of sensory neurons, VSNs, as well as supporting

cells and secretory ducts [45]. The VNO also contains solitary chemosensory cells innervated by the trigeminal nerve, which are thought to detect noxious substances, preventing their entrance to the VNO [114]. VSNs consist of a cell body, a dendrite sent to the surface of the tissue, and an axon. The dendrite of the VSN contains multiple microvilli, upon which the receptors involved in chemosensation are located [115] (Figure 1.1). VSN axons fasciulate into bundles at the base of the VNO to form the vomeronasal nerve. From there they travel along the nasal septum, through holes in the cribiform plate, along the medial face of the main olfactory bulb, ultimately terminating in the AOB [116].

VSNs consist of a diverse group of neurons, expressing around 300 different G-protein coupled receptors [110] of three main types, V1Rs, V2Rs, and formyl peptide receptors (FPRs). Each neuron is thought to express one or two [117] receptors. The VNO is organized into apical and basal regions; cell bodies of VSNs are segregated based on receptor expression. V1R-expressing neurons, coupled to the G-protein $G_{\alpha i}$, reside in the apical portion while V2R-expressing neurons, utilizing the $G_{\alpha o}$ G-protein, reside in the basal layer [118, 119, 120, 121, 122]. The V2R population has further been subdivided into those expressing H2-Mv, nonclassical major histocompatibility (MHC) genes [123, 124] and those not expressing this family of genes. The H2-Mv family has been postulated to aid in receptor trafficking or to form a complex with the receptor [125]. The most recently discovered class of receptors, FPRs, have members coupling with both $G_{\alpha i}$ receptors in the apical layer and $G_{\alpha o}$ in the basal layer [126, 127].

The accessory olfactory bulb From the vomeronasal organ, VSNs project into the AOB where they terminate in discrete structures referred to as glomeruli (Figures 1.1, 1.2C). There, VSNs synapse with the dendrites of mitral cells (also termed large principle cells [46]), the principal neurons projecting out of the AOB. A single VSN terminates in multiple glomeruli [128, 46], and a glomerulus receives input from many VSNs expressing the same receptor type [128, 116]. Projecting VSNs maintain the segregation observed in the AOB — neurons from the apical and basal layers of the VNO project to the anterior and posterior AOB, respectively [46, 120]. Mitral cells also maintain spatial segregation, with their cell body and dendrites residing in the anterior or posterior zone of the AOB [129, 46]. Mitral cells within the AOB send dendrites to multiple glomeruli [46,

130, 131, 132]. Some evidence suggests that the multiple glomeruli are receiving input from VSNs expressing the same receptor, making mitral cell input redundant [131], while other studies suggest that a population of mitral cells are receiving disparate input, establishing a point of information integration [132]. A functional study of AOB mitral cells suggests that integration across multiple processing streams is at most, a limited occurrence. However, multiple receptors may have similar response profiles, potentially explaining the difference between the different studies [44].

There also exists local circuitry within the AOB. Numerous types of interneurons reside in several layers of the AOB [46] and include inhibitory neurons (GABA-positive), potentially excitatory neurons, and those expressing markers for neuromodulators such as tyrosine hydroxylase [133]. The AOB also receives input from other brain areas. There are reciprocal connections with the amygdala and bed nucleus of the stria terminalis (BNST), the bed nucleus of the accessory olfactory tract (BAOT), and non-reciprocal input from the hippocampus and brain stem areas of the locus ceruleus and dorsal raphe nucleus [134, 135, 46, 59, 136, 84, 137].

The medial amygdala and beyond Mitral cells in the AOB project primarily to a region in the amygdala referred to as the "vomeronasal amygdala", consisting of the medial and posterior medial amygdala. Mitral cells also project to the BNST and BAOT [138, 139] (Figure 1.1). Anatomical segregation originating in the VNO persists in some areas of the amygdala [140, 141] and not in others [142, 141]. Evidence suggests that a V1R/V2R division persists even at the level of the hypothalamus [143], and a retrograde tracer study suggests that only the anterior AOB projects to the BNST [141]. Within the amygdala there are areas receiving input from both the MOS and AOS [59, 144]. From the amygdala, the AOS continues on to output in hypothalamic regions including the preoptic area and other regions of the hypothalamus involved in sexual behavior and hormonal regulation [145].

1.2.5 Stimuli of the AOS

The AOS detects non-volatile social cues found in naturalistic stimuli such as urine and other bodily secretions. Urine, or soiled bedding, is important in AOS mediated behaviors [80, 146, 147] and is a potent source of activity in the AOS [148, 149, 150, 151, 87, 88, 113]. In a study involving

awake-behaving recording from the mouse AOB, responses were observed only when the animal made direct contact with the ano-genital and head regions of another animal [151], suggesting a role in non-volatile compound detection. In this section, I will discuss AOS stimuli along with controversies surrounding particular ligands.

Proteins Proteins and peptides have long been thought to play a role in accessory olfactory system behaviors (i.e. [152]). To date, several specific peptidergic ligands have been suggested including MHC peptides [153, 154], major urinary proteins (MUPs), either as a means to bind other compounds [155, 146, 156] or as isolated ligands [157, 62], ESP peptides [158], and formyl peptides [126, 127]. With the exception of ESP peptides, which are found in the exocrine glands, all other peptides are postulated to be present in urine.

Peptidergic ligands have been proposed to mediate several different behaviors. ESP1, a male specific peptide, enhanced female sexually receptive behavior upon detection [159]. MUPs have been implicated in male-male aggression [62], predator avoidance behavior [160] or individual recognition of wild mice [146]. A specific MUP found selectively in males, nicknamed "darcin", may attract [56] and induce spacial preference in females [57]. MHC peptides have also been suggested as a signal for individual and mate recognition [153], however, Roberts et al suggests MUPs as a more robust and diverse signal for individual recognition [56].

Some controversy remains as to whether or not MHC peptides and MUPs are actual AOS ligands; these compounds have failed to elicit activity in the VNO in independent electro- and opto-physiological assays [43, 161].

Volatile compounds While the AOS is generally thought of as detecting non-volatile stimuli, there are reports of urinary volatile compounds stimulating the AOS and eliciting behaviors thought to be mediated by the AOS. Compounds such as 2-heptanone, pentyl acetate and isobutylamine reportedly evoke AOS-mediated behaviors such as puberty delay [162] and maternal aggression [163] and activate VSNs [164, 163, 165, 166, 38]. However, other studies have failed to find AOS activity in response to these putative ligands [151, 43, 161], and a study demonstrated that VNO removal had no effect on amygdalar responses to 2-heptanone [167]. Behavioral effects of these compounds

can be explained by the role of the main olfactory system. The MOS is known to respond to "pheromones" [147] and likely plays a role in many reproduction and aggression related behaviors. The discrepancy in physiological findings are more difficult to explain. Many of the studies finding responses to volatiles are plagued by methodological problems such as a lack of negative controls (for example [163]), single stimulus presentation (for example [165]), and responses to non-consecutive concentrations [166]. Chapter 3 examines VSN spontaneous activity and its impact on stimulus detection, particularly outlining the importance of using multiple repeats to reduce false positive responses [168]. This suggests that AOS stimuli truly are non-volatile in nature.

Sulfated steroids Sulfated steroids make up a class of compounds found in mouse urine [43]. Sulfated steroids may be responsible for up to 80% of the activity that female mouse urine elicits in the VNO [43] and may activate up to a quarter or a half of apical VSNs [161]. A few specific sulfated steroids have been isolated from (Balb/c) female mouse urine, including corticosterone-21-sulfate, a derivative of the hormone corticosterone. Other commercially available sulfated steroids evoke activity in the VNO and AOB, although have not been identified as endogenous ligands [43, 44]. Sulfated steroids are derivatives of steroid hormones, which are involved in regulating much of an animal's internal function such as metabolism, stress and reproduction. The amount and identity of these compounds present in urine may be indicative of the internal state of a conspecific, an important piece of information about a potential mate or competitor. For example, the levels of circulating corticosterone increase following a stressful experience. Nodari et al demonstrated that levels of sulfated corticosterone found in urine followed the same pattern and increased following stress [43]. Sulfated steroids have also been identified as pheromones in the goldfish [169] and sea lamprey [170]. The potential biological relevance and robust elicited activity suggest that sulfated steroids may serve as a meaningful stimuli for the AOS and therefore are the main class of stimuli that I will be using for the scope of this thesis.

1.2.6 Sensory/concentration coding in the AOS

Anatomy and function of the AOS have been studied for many years, yet it is only in more recent years that studies have investigated how stimuli, neurons, and anatomy interact for coding purposes.

Here I will review what is known about how VSNs and the AOB encode sensory information.

Sensory coding in the VNO Many behaviors attributed to the AOS require discrimination of sex and identity from urine or other bodily excretions. As the exact ligands responsible are unknown, there has been much investigation into how the AOS may be capable of making these discriminations using urine. Individual neurons in the VNO respond preferentially to male or female urine [150, 87, 171]. Knowing the relative affinities of populations of VSNs is sufficient to discriminate sex [150], and the activity of a small population of cells responding only to male or female urine may be required for this discrimination [87]. Urine from different strains also activate the VNO differentially [87, 171], allowing for reliable discrimination between both sex and strain using population activity of VSNs (Tolokh et al, under revision). Information encoded by VSNs in response to urine is sufficient for proper sex and individual (or strain) identification.

Concentration tuning in the AOS has been explored both using urine and individual ligands as stimuli. A monotonic relationship between concentration and response was found in urine [150, 87] and in sulfated steroids [43, 171]. Different concentrations of urine also activate different populations of VSNs, with some subset possibly responding only to low concentrations of urine [171] (however, see Section 3.3.3 for an alternate explanation). Further investigation into how VSNs represent concentration will be discussed in Chapter 4.

Knowledge of ligand-receptor pairs is very limited in the AOS. ESP1, a peptide present in male facial secretions, has been linked to a specific vomeronasal receptor [159]. A small number of sulfated steroids have also been paired with receptors [172]. Using populations of neurons stimulated with a battery of different sulfated steroids, repeated patterns in receptor neuron activity were identified, allowing for a non-genetic approach to identify receptor "processing streams" [44, 161]. This functional classification of VSN coding allows for investigations in downstream circuitry and information processing [44].

While the above studies address the issue of stimulus representation and processing, little work has been done in understanding how stimulus information is represented at the level of action potentials. Numerous studies have explored the channel physiology of VSNs and have helped establish the ion channel expressions and currents involved in VSN activity (i.e. [173, 174, 175, 176]). In

Chapter 3 of this thesis, I will address the issue of sensory coding on the level of individual action potentials in VSNs [168].

Sensory coding in the AOB Early electrophysiolgical investigation into AOB coding first focused on the relationship between the pump and activity in the AOB, establishing a temporal link between the two [112]. This early study demonstrated that the response kinetics of the AOB occur on a slow timescale due to to VNO pumping. More recent recordings from the AOB in awake behaving mice confirmed this slow dynamic, with an average time from stimulus contact to an observable AOB response of 3.6 seconds [151] or more than 4 seconds [113]. In anesthetized or ex-vivo preparations in which stimulus is delivered directly into the VNO through a cannula, the time to observe a response is decreased [88, 44], suggesting that pump dynamics may play a role in shaping the temporal profile of a stimulus response. This is not unexpected as the dynamics of the sniff cycle are known to play an essential role in stimulus coding in the MOS [177].

Circuitry within the AOB influences stimulus representation. VSN input converges in glomeruli, effectively averaging the signal across many neurons. As a consequence, the variability of VSN responses is greater than that in mitral cells [44]. Inhibitory responses in mitral cells have been observed due to inhibitory interneurons within the AOB [151, 88, 44, 113]. Lateral inhibition shapes the response of mitral cells and is essential in sex discrimination of urine [88].

1.3 Motivation and intent

This thesis will cover multiple aspects of concentration coding of sulfated steroids in the AOS. As demonstrated by Nodari et. al., the amount of sulfated steroid present in urine can be directly related to the behavioral state of the mouse, suggesting that ligand quantity provides meaningful information. However, encoding ligand concentration is a more difficult task than may be initially apparent. Naturalistic stimuli like urine sit in the environment in unknown conditions potentially leading to evaporation or dilution. The absolute concentration of ligands will then change for reasons that are not necessarily biologically relevant. Ideally, the AOS is able to extract concentration information in a way that is robust to these environmental variabilities.

Before one can understand how the sensory system may encode concentration, an understanding

of how sensory neurons encode information is required. As reviewed in section 1.2.6, there is limited knowledge as to how VSNs respond to stimuli and what indicates a response. In Chapter 3 of this thesis, I explore how VSNs represent information, from extracellular firing patterns to sensory transduction involvement.

Once an understanding of general stimulus information is achieved, investigation can progress to an exploration of circuit mechanisms involved in concentration representation. I propose that the AOS represents concentration as a ratio of multiple compounds; when urine is evaporated or diluted, the relative concentration of non-volatile stimuli remains unchanged. This provides insensitivity to environmentally-mediated changes in absolute concentration while still providing information about relative changes in concentration of individual compounds. A way in which a neural circuit can represent ratios is through the use of logarithms — the log of the ratio is equal to the difference of logs. Using extracellular recordings from populations of VSNs in response to a range of concentrations of sulfated steroids and computational modeling based on known circuitry, we demonstrate that the AOS is capable of log-ratio coding of concentration, thus providing evidence that ratios may be used.

The ultimate goal of this investigation is to follow sensory coding of concentration all the way from signal transduction and single cell behavior to the behavior of the animal. In the final section, I discuss an attempt at developing a novel behavioral assay that would be the first to allow a mouse to self-report the detection of an AOS stimulus. This assay can be used to test the hypothesis proposed in Chapter 4 suggesting that ratios are used to encode concentration. AOS-mediated behaviors are generally thought to involve innate functions such as endocrine regulation, aggression, or mating. Therefore, it is possible that processing of social cues through the AOS is unconscious, making it impossible for an animal to indicate detection. While successful at training mice to detect sensory cues, we have not yet been successful in demonstrating detection of sulfated steroids. Therefore, we were unable to shed light on ratio coding or the perceptibility of sulfated steroids.

Over the course of this thesis, I hope to advance understanding of concentration representation in the accessory olfactory system as well as provide a more general understanding of how sensory systems may cope with environmental uncertainty.

2 Common methods

Parts of this chapter have previously appeared in Arnson and Holy 2011 [168] and Arnson and Holy (submitted)

2.1 Solutions and stimuli

All sulfated steroids were purchased from Steraloids Inc (Newport, RI), and all other chemicals were obtained from Sigma (St. Louis, MO), unless otherwise indicated. Stock solutions of steroids were dissolved in either methanol or deionized water. The following steroids, referred to by their Steraloid catalog number, were used: A0225, A6940, A7010, A7864, P3817, P2135, P3865, P8168, P8200, Q1570, Q2525, Q3910, Q5545; the exact molecular identities of these compounds are as documented previously [43, 44] (Figure 2.1). Ringer's solution contained 115 mM sodium chloride, 5 mM potassium chloride, 2 mM calcium chloride, 2 mM magnesium chloride, 25 mM sodium bicarbonate, 10 mM HEPES, and 10 mM D-(+)-glucose and was equilibrated by bubbling with 95% O2/5% CO2. High potassium Ringer's solution substituted 50 mM potassium for equimolar sodium. Urine was collected from 3 month old BALB/c female mice or CBA male mice and flash frozen in liquid nitrogen as previously described [43].

2.2 Electrophysiological recording

Adult male mice 6 weeks of age or older of the B6D2F1/J strain (Jackson Laboratory, Bar Harbor, ME) were used in all recordings unless otherwise indicated. All experimental protocols followed the United States Animal Welfare Acts and National Institutes of Health guidelines and were approved by the Washington University Animal Studies Committee.

Dissection and recording procedures were performed as previously described [150, 43, 178] unless otherwise indicated; briefly, intact vomeronasal epithelia were isolated and mounted on a multielec-

trode array. The vomeronasal epithelium was removed from the bony capsule, and the neuroepithelium was mechanically dissected as an intact sheet from the basal lamina. It was then held in place on the electrode array using a nylon mesh. Sulfated steroids were diluted with Ringer's immediately before the recording session. Sulfated steroids were used at a maximum of 11 concentrations, ranging from 1 nM to 100 μM, in approximately 3-fold increasing intervals. Final methanol concentration in the stimulus solution was never higher than 0.1%. All experiments included a minimum of 2 negative control (Ringer's) stimuli as well as a vehicle control containing 0.1% methanol in Ringer's. A positive control of Ringer's solution containing 50 mM potassium was also used. Stimuli were dispensed using an HPLC pump (Gilson 307) (Gilson, Middleton, WI), and a robotic liquid handler (Gilson 215) capable of taking samples from prepared tubes and injecting them in a HPLC valve (Gilson 819 injection module). This robot was controlled by the Gilson 735 software. Continuously bubbled Ringer's solution alternated with stimuli to produce continuous flow over the epithelium; the flow was heated to a temperature of 35 °C and aimed directly at the epithelium. The timing of stimulus delivery (HPLC valve switch) was monitored electrically and fed back to the acquisition software. Stimuli were presented for 10 sec in a randomized order. Delivery was repeated in a newly randomized order 4–6 times.

Extracellular recording was performed using multielectrode planar arrays (ALA Scientific Instruments, Westbury, NY) (10 µm flat titanium nitride electrodes isolated with silicon nitride) where electrodes were 30 µm apart, in two fields of 6×5 electrodes each. Electrical signals were amplified with a MEA 1060 amplifier (ALA Scientific Instruments), acquired at 10 kHz with a data acquisition card (National Instruments, Austin, TX) and saved to disk. We used custom data acquisition and data analysis software based on COMEDI (http://www.comedi.org) and Matlab (The MathWorks, Natick, MA).

2.3 Data analysis

2.3.1 Spike sorting

This and all subsequent analyses were performed in Matlab (Mathworks Inc, Natick, MA). Following acquisition, single units were isolated using custom software. Spikes were sorted based on waveform

shape across all electrodes using methods similar to those described previously [179, 180]. All single units had clear refractory periods of approximately 25 ms or more.

In response to the highest concentrations of sulfated steroids, the spike amplitude in a few of the responsive cells progressively decreased during the response such that we were unable to record their activity using extracellular electrodes for up to a few seconds [44]. Our choice of firing rate metric (section 2.3.2) compensates for this phenomenon. See Section 3.3.3 for a further discussion of this phenomenon.

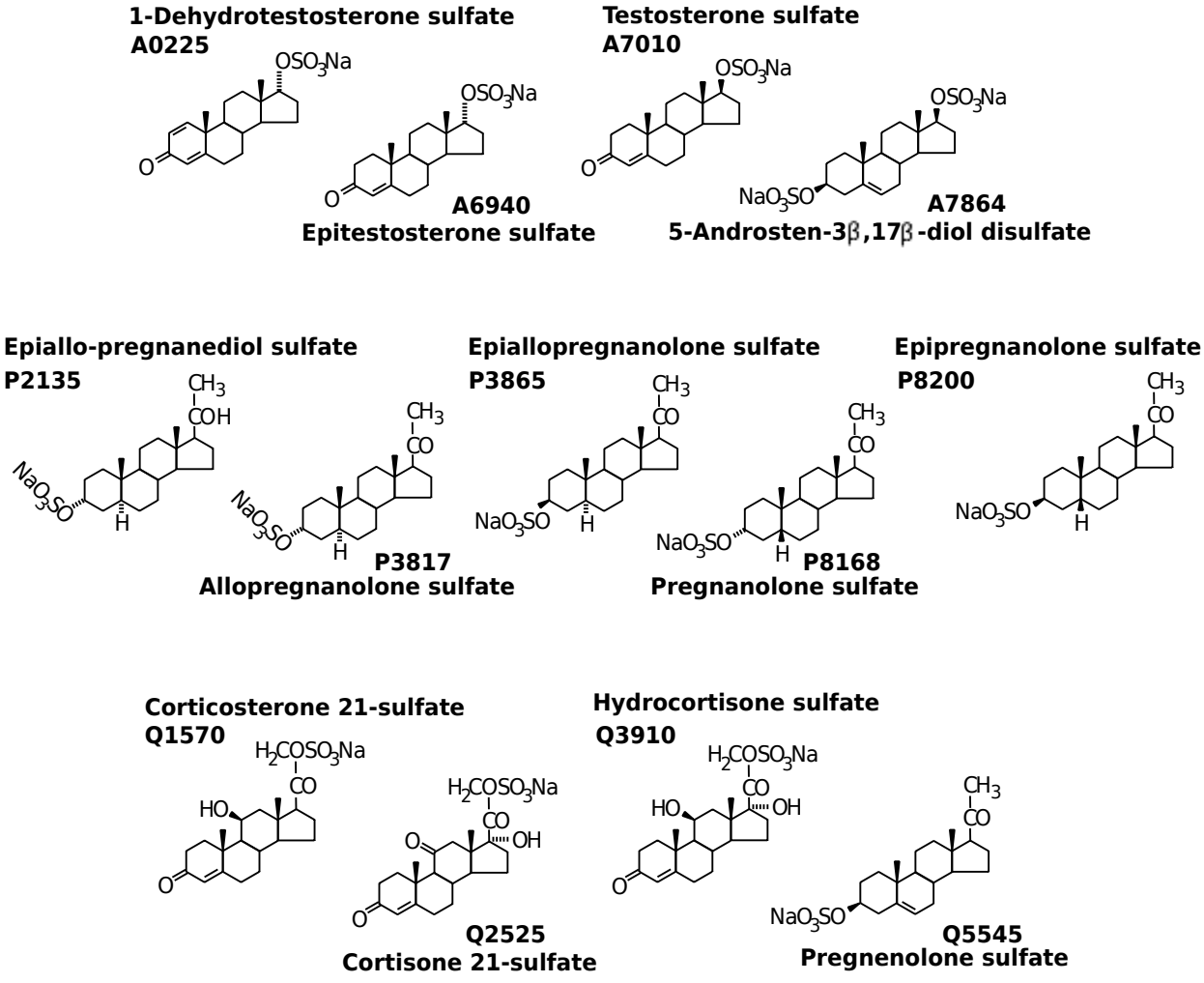

Figure 2.1: Sulfated steroids. The structures of all sulfated steroids used are displayed.

2.3.2 Firing rate metrics

Six firing rate metrics were used — Δr_{fixed}, Δr_{burst}, Δr_{max}, Δr_{avgmax}, $\Delta r_{monotonic}$ and $\Delta r_{synaptic}$. Using Δr_{fixed}, the firing rate was calculated for each trial over a 10 sec time window both prior to and during stimulation. The pre-stimulus firing rate was subtracted from the peri-stimulus firing rate to compute a Δr for each trial, which was then averaged across trials.

Δr_{burst} computed the number of bursts per sec. A burst was defined as three or more spikes with at most 100 ms between spikes (Section 3.3.2). A 10 sec time window both prior to and during stimulation was used to calculate the average burst rate across all trials. To compute the Δr value, the pre-stimulus bursting rate was subtracted from the average peri-stimulus bursting rate and then averaged across trials.

Δr_{max} used a time window of variable length to calculate the cumulative firing rate at the time of each spike following stimulation. On each trial, the time window that produced the maximum firing rate was used. A baseline firing rate was computed as with Δr_{fixed}. The peri-stimulus firing rate was averaged across all trials and the averaged baseline firing rate was subtracted to calculate Δr.

Δr_{avgmax} was computed similarly to Δr_{max}. A time window of variable length, set independently for each distinct stimulus was used. The window started with stimulus onset and ended at the point yielding the maximum firing rate, averaged over the window and across all trials of this stimulus. The time window was constrained to be at least 1 sec in duration and at most 20 sec following stimulus onset. A baseline firing rate was computed by averaging the firing rate across trials for 10 sec prior to stimulus delivery. The Δr value was calculated by subtracting the baseline firing from the peri-stimulus firing rate.

$\Delta r_{monotonic}$ takes into account the observation that the peak response following stimulus delivery occurs with equal or shorter latency with increasing concentration. The peri-stimulus response was measured using an automated algorithm that finds the global maximum cumulative firing rate across all trials for each stimulus concentration such that the time window is of equal or shorter length with increasing concentration (see Optimal monotonic time windows for details). A baseline firing rate was computed using a time window equal to that used following stimulation.

The final metric, $\Delta r_{synaptic}$, is based on a biologically plausible metric in which the spike train was convolved with an exponential function with a time constant of 500 ms [181]. The resulting filtered spike trains from each trial were averaged. The peak value prior to stimulus delivery was subtracted from the peak value post stimulus delivery to calculate the Δr value.

In all metrics, the response period was delayed from the start of stimulus delivery on a preparation-by-preparation basis (average approximately 2 sec). The offset was determined by measuring the activity across all electrodes in a particular recording using 250 msec time bins. The offset was set as the time bin prior to an increase in net activity following stimulus delivery onset. Much of this time was likely due to delay associated with the liquid traveling through the stimulus device as well as variability in the placement of the perfusion tip.

Optimal monotonic time windows for computing $\Delta r_{monotonic}$ This metric optimizes the time window over which to integrate firing rate, subject to the constraint that the length of the time window varies monotonically, if at all, with stimulus concentration. This does *not* imply that the firing rate itself is monotonic with concentration. Let the index i refer to all trials using a particular stimulus identity at a given concentration, and suppose that we have N different concentrations of the same ligand. $i = 1$ corresponds to the highest concentration at which this ligand is applied, and $i = N$ corresponds to the lowest, with all others arranged in order of decreasing concentration. Let $R_i(t)$ be the firing rate, averaged over both trials and time, starting from the beginning of the trial (offset some time after valve opening) until time t. To compute $\Delta r_{monotonic}$, we seek a set of window ending times t_i such that the sum

$$S(T) = \sum_{i=1}^{N} R_i(t_i) \tag{2.1}$$

is maximized ($S^\star$ will denote the maximum), subject to the constraint that the time windows are monotonic in i, that is, $t_{i+1} \leq t_i$ with all t_i satisfying $0 \leq t_i \leq T$ for some maximum trial duration T. This is a global optimization problem, and so it would seem to require a comprehensive search in an N-dimensional space, which even for $N \approx 11$ (as here) is a prohibitively-expensive computational problem. However, the problem can be solved much more efficiently using a dynamic programming

approach. Consider the (partial) sum over a restricted time window $T' \leq T$ and just the n highest concentrations,

$$S_n^\star(T') = \max_{t_{i+1} \leq t_i,\, 0 \leq t_i \leq T'} \sum_{i=1}^{n} R_i(t_i). \tag{2.2}$$

Suppose we know the global optimum for these n concentrations at any arbitrarily-chosen time $T' \leq T$; then we can construct the solution for the first $n+1$ concentrations for any time T'' satisfying $T' \leq T'' \leq T$ by realizing that

$$S_{n+1}(T'') = S_n^\star(T') + R_{n+1}(t_{n+1}) \qquad \text{with} \quad T' \leq t_{n+1} \leq T''. \tag{2.3}$$

Hence the optimal solution $S_{n+1}^\star(T'')$ can be found by considering all possible pairs (T', t_{n+1}) satisfying $T' \leq t_{n+1} \leq T''$. To make this practical, we divide time into K discrete bins (we used 20 bins in all analyses). Once the solution for $n+1$ is found, the process can be repeated until the solution for N is obtained.

Thus, with this dynamic programming (i.e., inductively over n) approach, a problem that seemed to be $O(K^N)$ in time and $O(N)$ in storage can be solved in $O(NK^2)$ time and $O(NK)$ storage. MATLAB code implementing this global optimization can be downloaded from `http://holylab.wustl.edu`.

2.3.3 Mutual information

The utility of each response metric was evaluated by computing the reliability of the relationship between the measured response r and the stimulus concentration c. This was evaluated using the mutual information I, [182]

$$I(r, c) = H(r) + H(c) - H(r, c) \tag{2.4}$$

where H is the total entropy. Entropy was calculated based on the following equation:

$$H = -\int \mathrm{d}\mathbf{z}\, p(\mathbf{z}) \log_2 p(\mathbf{z}) \tag{2.5}$$

To compute H, it was necessary to first estimate the probability distribution of firing rates and

concentrations from the data. To obtain a reasonable estimate, entropy was calculated only on cells from experiments in which each stimulus was presented a minimum of 20 times each. 7–9 concentrations of sulfated steroids were used.

The probability distribution of each variable was estimated by a kernel density analysis [183] using a Gaussian kernel. The joint probability distribution was calculated as:

$$p(x,y) = \frac{1}{2\pi\sigma_1\sigma_2 n}\sum_j e^{-\frac{(x-x_j)^2}{2\sigma_1^2}-\frac{(y-y_j)^2}{2\sigma_2^2}} \tag{2.6}$$

where n is the number of repeats, x_i is firing rate on the ith stimulus presentation, y_i is a value corresponding to log-concentration (see below) used for that stimulus presentation, and $\sigma_1$and $\sigma_2$are the smoothing widths for firing rate and concentration, respectively. Single-variable probability distributions were calculated using one-dimensional analog of Eq. 2.6,

$$p(x) = \frac{1}{n\sqrt{2\pi\sigma}}\sum_j e^{\frac{-(x-x_j)^2}{2\sigma^2}} \tag{2.7}$$

Entropy was calculated as

$$H_\sigma = -\frac{1}{n}\sum_i \log_2 p(\mathbf{z}_i), \tag{2.8}$$

where the $\mathbf{z}_i$ are observed values for the parameter $\mathbf{z}$. This formula is derived from the continuous expression of Eq. 2.5 using the "bootstrap" approximation $p(z) \approx \frac{1}{n}\sum_i \delta(z - z_i)$, where δ is the delta function. The notation H_σ is used to emphasize that the value of the entropy depends upon the smoothing width σ.

The optimal smoothing widths σ_1 and σ_2 were determined by cross-validation, splitting the full data set into two halves and choosing the σ's to maximize the summed log-likelihood (i.e., minimizing the entropy) calculated from one half (z_j) when evaluated at the points z_i' of the second half. A total of 100 random splits of the data set were used, and the cross-validated entropy was calculated by averaging over these splits. Optimization was done on the joint distribution by direct search, testing 2250 combinations of two log-spaced sets of smoothing widths that ranged over four orders of magnitude. This resulted in separate σ's for concentration and firing rate; once chosen, these same smoothing widths were also used for the one-dimensional distributions.

Stimulus concentration was indexed by an integer c from the range 1–7 or 9 (1 nM becomes 1, 3 nM becomes 2, etc.) and thus spaced evenly on the log-concentration axis. The concentration variable was therefore discrete. Because cross-validation fails for discrete data, the y_j of Eq. 2.6 were obtained by "dithering" the integer values, adding a random number evenly distributed between 0 and 1. This allowed us to treat concentration as a continuous variable for the purpose of cross-validation.

To compare the utility of each metric, we calculated $I(r, c)$ for each firing rate metric on single-units. Normally, 5 repeats were used for each stimulus, however at least 20 repeats were used for these analyses (see Supplemental Figure 2B). For metrics that used a variable time window, to mimic "ordinary" usage these time windows were set based on a grouping of only 5 out of the 20-plus repeats. Multiple such groups were used so that a a Δr value was calculated for each trial.

2.4 Quantifying sensory responses in VSNs across concentrations

Frequently in sensory neurobiology, the response of a cell to a stimulus is determined by counting the number of action potentials during a fixed period. However, the tendency of VSNs towards spike amplitude decrement at high stimulus concentrations (Section 2.3.1 and Figure 3.6) introduces a potential experimental artifact in this measurement. Therefore, the traditional way of measuring firing rates may not provide an accurate representation of the sensory response of VSNs. We set out to explore possible metrics to best capture the neural response. To do so, we measured the response of VSNs to many repeats of a concentration series of sulfated steroids and quantified the response using six metrics, which differ only in terms of the mechanisms used to choose the time interval over which the response is averaged and whether spikes or bursts are used. We compared these metrics based on the amount of information [184] they conveyed about stimulus concentration.

The six metrics Δr_{fixed}, Δr_{burst}, Δr_{max}, Δr_{avgmax}, $\Delta r_{monotonic}$ and $\Delta r_{synaptic}$ are illustrated in Figure 2.2 using a cell that was stimulated with 11 concentrations of Q1570. The response as measured by each metric is plotted in Figure 2.2 (bottom). Δr_{fixed} used a fixed 10 sec time window (gray box) across all concentrations and trials. In this example cell (Figure 2.2A), the apparent response decreased at the two highest concentrations due to an apparent silencing of the response late in the time window; we verified this silencing to be an artifact of spike amplitude decrement (see

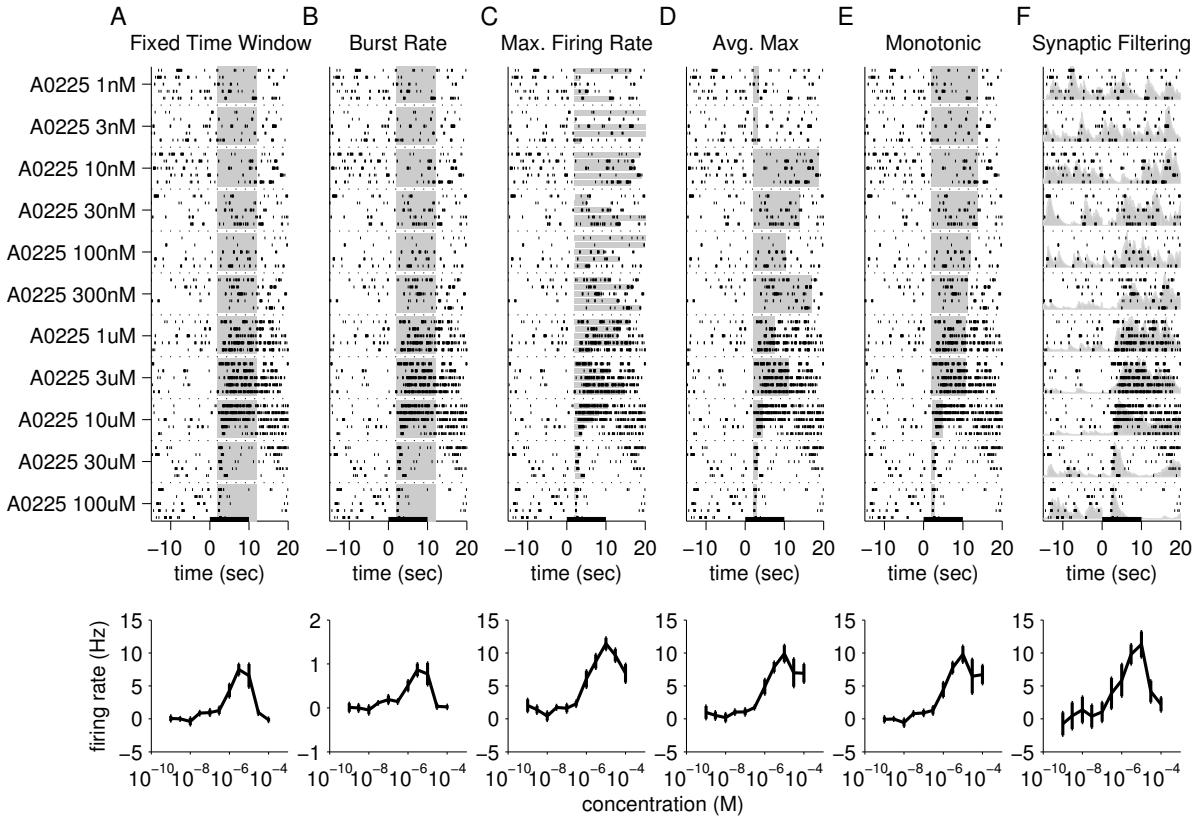

Figure 2.2: An illustration of six different firing rate metrics. Raster plots for the same cell are displayed in the top half of each panel. The black bar indicates the period of stimulus delivery. For the first five metrics (A–E), the analysis window is indicated by the gray box (top). **A**, Response of an example cell using Δr_{fixed}, a fixed time window metric. In A–E, a baseline firing rate was computed by averaging a time window of equal length and was then subtracted from the post-stimulus firing rate to calculate Δr. The resulting values are plotted below. **B**, Response of the cell over the same time window was measured in bursts per second using the metric Δr_{burst}. **C**, A variable time window metric, Δr_{max}, maximizing the firing rate since the beginning of each trial. **D**, A variable time window metric, Δr_{avgmax}, maximizing the average firing rate across all trials. **E**, A metric using time windows that vary monotonically with concentration, $\Delta r_{monotonic}$. **F**, A "synaptic filtering" metric, $\Delta r_{synaptic}$. The gray curves represent the average of five low-pass filtered spike trains. The post-stimulus firing rate was calculated by taking the maximum peak value. The pre-stimulus baseline firing rate was calculated by taking the maximum peak value prior to stimulus delivery.

Figure 3.6). Since the main difference that we identified between spontaneous and stimulus-evoked activity was the time between subsequent bursts (Chapter 3), we measured the rate of bursting using the second metric, Δr_{burst} (Figure 2.2 B). This metric calculated the number of bursts in a fixed 10 sec time window across trials and subtracted a baseline burst rate. As burst properties remained similar between baseline and stimulus-evoked activity (Chapter 3), one would expect the firing rate calculated by this metric to be a scaled version of the number of spikes/sec within the same time window (Δr_{fixed}), and indeed this is what we observed. A variable time window that found the maximum firing rate on a trial-by-trial basis was used to calculate Δr_{max}. This metric performed well in capturing the response at high concentrations (Figure 2.2C). However, because the algorithm accumulated spikes across time until a maximum rate was reached, this metric was especially sensitive to spontaneous bursting, as is reflected in the integration time window for the first few concentrations. Figure 2.2D used Δr_{avgmax}, finding the maximum firing rate averaged across all trials of the stimulus. This metric performed similarly to Δr_{max}. $\Delta r_{monotonic}$ utilized a globally optimal time window with the constraint that the window be decreasing or stationary with increasing concentration. This metric also captured the increasing nature of the response relative to concentration, as shown in Figure 2.2D. The concentration-response curve was similar to that observed using Δr_{max} and Δr_{avgmax}, however, $\Delta r_{monotonic}$ and Δr_{avgmax} were less sensitive to spontaneous bursting on a trial-by-trial basis. The fifth metric, $\Delta r_{synaptic}$, was based on the idea that synaptic transmission is subject to low-pass filtering. Therefore, each spike train was convolved with an exponential decay function with a time constant of 500 ms, and the maximum value of the average filtered spike train was used to compute Δr. This metric also appeared to be sensitive to spike amplitude decrement (Figure 2.2E), although the degree will vary based on the time constant.

Ultimately, the ideal metric captures a maximal amount of information about what the neuron is representing. Therefore, we compared the aforementioned six metrics in terms of how much information they captured about the stimulus concentration. Mutual information reflects the amount of information (in bits) across concentrations that is captured by the Δr's. To measure information, we performed at least 20 repeats of each of 7–9 concentrations of a single sulfated steroid. For each of the six metrics, we measured the trial-by-trial Δr values for each cell across concentration, and used the distribution of values to compute the mutual information (see Section2.3.3, Figure 2.3B).

The mutual information is shown in Figure 2.3C. Each metric conveys a variable amount of information depending on the cell. This is largely due to the variance in the nature of the responses we observe, predominantly due to concentration threshold differences. The mutual information of non-responsive cells hovered around 0, as expected (Figure 2.3C, gray lines). Responsive cells that displayed lower mutual information values tended to show responses only at the one or two concentrations, while the other cells were responsive at lower concentrations.

Consistently, Δr_{max}, Δr_{burst}, and $\Delta r_{synaptic}$ captured the least amount of information. Δr_{fixed}, $\Delta r_{monotonic}$ and Δr_{avgmax} captured similar amounts of information. In cases where spike amplitude decrement was observed (2/8 cells), $\Delta r_{monotonic}$ and Δr_{avgmax} were more slightly informative than was Δr_{fixed} (Figure 2.3, blue lines). In other cases, Δr_{fixed} was consistently less informative. When cells did not display spike amplitude decrement, the response windows chosen by the algorithms computing $\Delta r_{monotonic}$ and Δr_{avgmax} were approximately fixed across concentrations, as in calculating Δr_{fixed}. Therefore, we found that $\Delta r_{monotonic}$ and Δr_{avgmax} provided more information than the other metrics did for the "difficult" cells, while these two metrics were as good or better than the other metrics for cells with stable responses. $\Delta r_{monotonic}$ and Δr_{avgmax} are the most robust and flexible of these metrics when measuring VSN responses across concentration, and therefore these two metrics will be used in subsequent investigations.

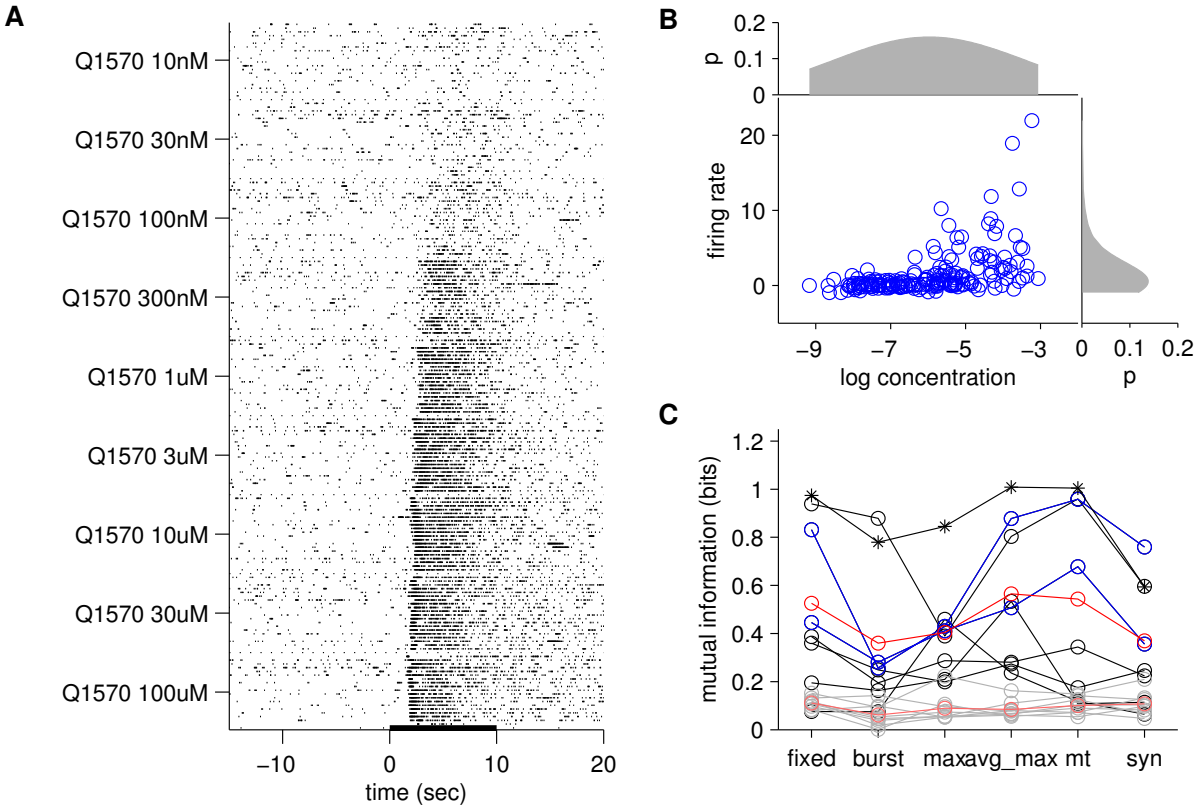

Figure 2.3: Comparison of firing rate metrics using mutual information. **A**, To calculate mutual information, a large number of repeats were needed (see Section 2.3.3). An example cell was stimulated with 20 repeats of 9 concentrations of Q1570. The black line indicates the period of stimulus delivery. **B**, Joint distributions of concentration and firing rate, each trial is indicated by a single circle. Concentrations were dithered to facilitate display and for the purposes of cross-validation to set the smoothing length scale. The resulting marginal distributions are shown by the gray curves along each axis. **C**, Mutual information for 8 cells using the 6 firing rate metrics. The black lines indicate cells that appeared responsive. The line with the asterisks corresponds to the cell shown in **A**. The gray lines correspond to cells that did not appear to be responsive at any concentration. The blue lines indicate cells that experienced spike amplitude decrement. The bright red line shows the average mutual information for responsive cells. The light red line indicates the average mutual information for non-responsive cells.

3 Chemosensory burst coding by mouse vomeronasal sensory neurons

This work is modified from Arnson and Holy, 2011 [168]

3.1 Introduction

A central goal of sensory neurobiology is to reveal how neurons encode information about the environment. This goal has many facets, including efforts to understand the nature of the stimulus (e.g., reviewed in [185, 186]), the mechanisms of sensory transduction [187, 188, 189, 190, 110, 191], and the representation of stimulus information in patterns of action potentials [182, 192, 193]. The ability to decode information about the natural environment is heavily influenced by neuronal "noise"; depending on the particular neurons and circuits, responses can be reliable at the level of single action potentials [192] or show sufficient variability that many spikes and/or large populations of neurons are required for accurate decoding [193].

The accessory olfactory system (AOS) is a distinct chemical sense found in most tetrapods. This system is specialized to detect non-volatile compounds used in social communication. Chemical stimuli are pumped into the vomeronasal organ (VNO), where vomeronasal sensory neurons (VSNs) that express individual receptor proteins from large families [110] encode the identity and concentration of ligands via their spiking activity. In the mouse, the AOS is an attractive system for exploring sensory coding and its functional relevance, in part because of the modest number of processing stages between sensory input and behavioral output [42]. While physiological investigation of this sensory system is quite recent, there has been progress in identifying VSNs ligands and key components of the sensory transduction cascade, in characterizing the electrical properties of the sensory neurons, and in understanding how large-scale properties of the stimulus (such as the sex or strain of a conspecific) determine VSN responses [110, 147].

While these studies give insight into the sensory responses of VSNs, there has been little work bridging the gap from ligand to the fundamental unit of neuronal signaling, the single action potential. To obtain a clearer understanding of how sensory transduction is coupled to firing, we performed multielectrode array (MEA) recordings of the intact vomeronasal epithelium in response to a battery of sulfated steroids over a range of concentrations. Observing a significant level of spontaneous activity, we explored the implications this noise has on decoding sensory responses. We then investigated the structure of this activity as well as stimulus-driven activity to better understand what features of a response may communicate sensory information. We observed that VSNs predominantly fired bursts of spikes; while stimulus delivery increased the frequency of bursting, the characteristics of individual bursts were remarkably unchanged by the presence of stimulus. Given these similarities, we investigated the root of burst structural stability. By blocking or eliminating part of the signal transduction machinery, we altered the structure of spontaneous activity, suggesting that the signal transduction cascade is involved in both spontaneous and stimulus-driven activity. These results provide a first look at how sensory transduction and the firing properties of VSNs impact the encoding scheme of primary sensory neurons in the accessory olfactory system.

3.2 Materials and methods

3.2.1 Solutions and stimuli

Ringer's solution and sulfated steroid stimuli were as described in Section 2. Low potassium Ringer's was made with 0.5 mM potassium, substituting equimolar sodium. Low sodium Ringer's solution was made with 57.5 mM sodium and 57.5 mM choline chloride. Urine from BALB/C mice was collected as described in Section 2. The PLC inhibitor U-73122 and the inactive analogue U-73343 were presented at 10 μM and dissolved in DMSO, for a final DMSO concentration of 0.67%. In all recordings involving these drugs, a vehicle containing 0.67% DMSO in Ringer's solution was used.

3.2.2 Electrophysiological recording

Unless otherwise indicated, animals and electrophysiology was performed as described in Section 2. Recordings using TrpC2$^{-/-}$ animals used a line of mice in which the TrpC2 channel is genetically

ablated [54]. Adult males of the same age range were used.

3.2.3 Data analysis

Spike sorting This and all subsequent analyses were performed in Matlab (Mathworks Inc, Natick, MA). Following acquisition, single units were isolated using custom software. Spikes were sorted based on waveform shape across all electrodes using methods similar to those described previously [179]. All single units had clear refractory periods of approximately 25 ms or more.

Characterizing a stimulus response

Unless otherwise indicated, Δr was calculated using the $\Delta r_{monotonic}$ metric for stimuli presented over a range of concentrations (See Section 2 for details). For stimuli presented for a single concentration such as diluted female mouse urine and Ringer's solution, Δr_{fixed} was used. A response was determined to be statistically significant if it differed from the Ringer's control using a rank-sum test with a p-value threshold of 0.05 with a minimum Δr of 2 Hz. To control for methanol and Ringer's artifacts, Δr was computed for the vehicle and Ringer's solution stimuli. No cells in this data set were found to have a significant Ringer's response.

Characterization of VSN firing properties All firing property analyses were performed on sorted single-units. When indicated, firing was divided into a non-stimulus period and a stimulus-response period. All non-stimulus periods included activity during the 30 sec prior to stimulus presentation, which corresponds to 30 – 60 sec following the previous stimulus, for all stimuli. Stimulus-evoked activity corresponds to the 30 sec following stimulus onset (using sulfated steroid or 1:100 diluted female mouse urine) if the change in firing rate, or Δr, was judged statistically significant.

Interspike interval Interspike interval (ISI) was calculated by taking the difference in spike times between adjacent action potentials. All interspike interval frequency histograms represent the probability of observing that particular ISI for the given cell. This was calculated according to the method outlined by Reich et al [194]. To accommodate the wide range of relevant time scales in the ISI distribution, we used bin sizes that span logarithmically increasing intervals, for a total of 200

time bins ranging from 1 ms to 14.5 sec in width. Histogram frequency was calculated by dividing the bin count by the total number of ISIs. Figure 3.5D shows the mean histogram across 126 cells — the error bars represent standard error. All subsequent population firing property figures represent the mean and standard error of the histograms across the population, unless otherwise indicated.

Determination of a burst We define a burst as 3 or more spikes fired with an ISI < 100 ms. This ISI criteria is based on the ISI distribution (Figure 3.5). A dominant peak was observed at approximately 40 ms, corresponding to bursting activity, and a second smaller peak was present at approximately 1 sec. 100 ms corresponds to the end of the first peak. As this pattern was consistently observed across cells, this burst definition was used for all cells.

Burst measurements Interburst interval (IBI) is defined as the time between the last spike of a burst and the first spike of the following burst. The burst duration corresponds to the time between the first and last action potential within a burst. The within-burst ISI was calculated by computing the ISI of each spike within the burst, while keeping track of the spike position within the burst. Spike position relative to the end of the burst was also computed where the last spike was counted as 1, the second last as 2, and so on. The within-burst ISI was normalized to the maximum within-burst ISI on a cell-by-cell basis.

The role of repeats in stimulus reliability

Fano factor To determine the variability of cells, we calculated the Fano factor, or the variance divided by the mean, as a function of time according to the method described by Rieke et al [182]. The continuous spike train from each cell was divided into a series of time bins ranging in width from 1 ms to 100 sec. The spike count in each time bin was computed. The variance and mean of the spike counts across time bins were computed to give the Fano factor.

Receiver operating characteristics We explored the reliability of single and small numbers of trials using analyses based on receiver operating characteristics (ROC) [195, 196] as described by Dayan and Abbott [197]. This allows for the computation of performance — if an ideal observer

is presented with the Δr value calculated based on measurements from n-repeats of the stimulus presentation, the performance indicates the percentage of times the observer would correctly guess a true positive response or a true negative response using a given threshold. A sulfated steroid at 100 μM was used for a "true positive" stimulus, using only cells that clearly responded to this stimulus at that concentration with a $\Delta r >$ 2 Hz and $>$ 2 standard deviations above zero. The "true negative" stimulus corresponded to Ringer's solution stimuli and steroids that did not elicit a response at any concentration. Each were presented 5 times to the cell.

Each ROC was calculated using Δr values computed from a set number of repeats (from 1 to all 5) for the "true positive" sulfated steroid stimulus and the "true negative" negative stimulus. To simulate the relative sparseness of ligand responses across VSNs, all negative stimuli were pooled. The same number of repeats were drawn from this pool as were drawn from the responsive pool.

A range of thresholds (z), from the minimum Δr to the maximum Δr value, changing by 1 spike/sec were used. At each threshold point, we computed the false alarm rate $\alpha: p(\Delta r \geq z|-)$ and the true positive rate $\beta: p(\Delta r \geq z|+)$ using the following equations:

$$\alpha = \frac{1}{n}\Sigma\Delta r_{Ringer's} \geq z \qquad \text{and} \qquad \beta = \frac{1}{n}\Sigma\Delta r_{Steroid} \geq z \tag{3.1}$$

where n is the number of re-sampled Δr values. This resulted in an α and β value for each threshold z. α and β are plotted as shown in Figure 3.3. A separate curve is generated for each number of repeats used. This was done 100 times using 100 blocks of n repeats randomly drawn from the observed Δr values, and the α and β values for each Δr were averaged across realizations. The resulting normalized area under the curve (AUC) is equal to the performance of an ideal observer in a 2 alternative forced choice task [195, 197] similar to the presented task (either the stimulus evokes a response or it does not). We computed the AUC using the TRAPZ function in MATLAB.

Correlations in VSN activity To determine whether or not correlations existed across VSNs, we looked at the spike times of all cells recorded on a single preparation (n = 14 preparations). Using 10 ms time bins, we measured the distribution of time differences between all spikes fired by all pairs of cells within a 10 sec window both before and after the spike.

3.3 Results

We set out to explore the impact of sensory transduction and firing properties of VSNs on coding in the AOS using MEA recordings of the intact vomeronasal epithelium. We probed VSN function by stimulating with dilute female mouse urine and a concentration series of 13 synthetic sulfated steroids ranging from 1 nM to 100 μM (see Solutions and Stimuli). We sorted spikes from individual VSNs (Figure 3.1A,B gray rasters) and could follow the spontaneous and stimulated activity of these neurons across multiple trials (Figure 3.1A–C). As has previously been reported [43, 44, 171], VSNs increased their firing rate in response to sulfated steroids with a monotonic dependence on concentration (Figure 3.1D). We noted high levels of activity, both stimulated and spontaneous, consistent with previous reports [150, 43].

High levels of spontaneous firing lead to noise in the signal, potentially making it more difficult to decode. Therefore, we set out to examine the role that this spontaneous activity has on coding in the AOS.

3.3.1 Spontaneous activity of VSNs leads to high variability in firing

In some cases, tonic spontaneous neural activity is thought to add to the reliability of signal detection by downstream decoders [182]. However, sporadic spontaneous activity may also present hurdles to reliable signal detection. For example, if a spontaneous increase in activity coincided with the stimulus period, a trial could be classified as falsely responding to a stimulus (e.g., Figure 3.1A, trial 3). If activity coincided with the baseline period preceding stimulus delivery, then one may record a false negative. Therefore, we set out to explore how this noise affects the fidelity of response identification. To do so, we measured the effect of pooling activity across multiple trials, thus reducing the effect of noise, on the variability of stimulus-response detection using receiver operating characteristic (ROC) analysis [195]. Across 6 preparations, a total of 61 cleanly-isolated cells were tested with 100 μM Q3910, of which 4 were classified as responsive to this ligand (Figure 3.2). Each cell was also stimulated with 4 individual Ringer's solution controls and 2 additional sulfated steroids each at 11 different concentrations. If a cell did not respond to the additional sulfated steroids at any concentration, those trials were also counted as negative trials (e.g. Figure

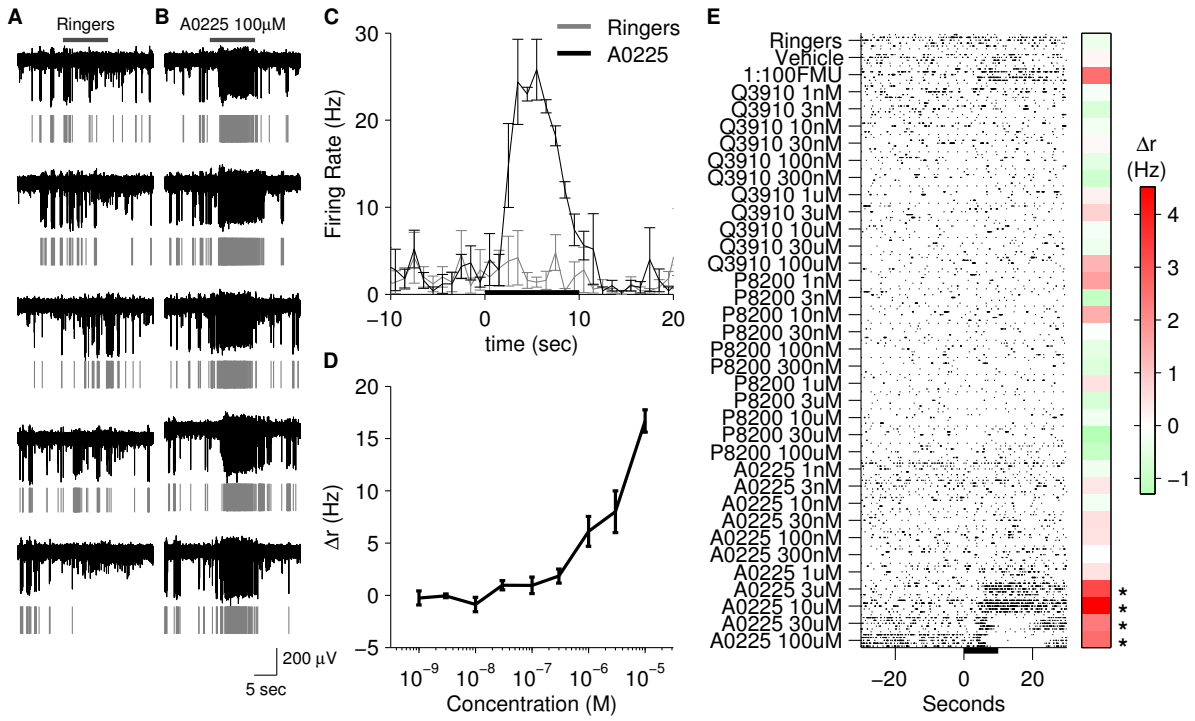

Figure 3.1: MEA recordings of VSNs. **A,** 30 sec of activity recorded on a single electrode across five repeats during stimulation with Ringer's solution. These repeats were interleaved with presentations of other stimuli, not shown, for a total recording time of approximately 200 min. The dark gray bar indicates the 10 sec stimulus window. The activity of one single unit is indicated by the gray rasters below each electrode trace. Note the high level of spontaneous activity prior to and during stimulation with a negative control. **B,** The same cell as shown in **A** during stimulation with $100\,\mu M$ A0225. Note the increase in firing that is consistent across trials. **C,** The peri-stimulus time histogram (PSTH) of the average activity for this cell in response to Ringer's solution (gray) and $100\,\mu M$ A0225 (black). Error bars reflect the sem across trials at each time point (bin size 1 sec). **D,** The response of a different cell to increasing concentrations of A0225. The change in firing rate, Δr, is plotted as a function of delivered concentration. Error bars reflect the sem across trials. **E,** Activity of an example cell. Each stimulus was presented 5 times for 10 sec, as indicated by the black bar on the x-axis. The red-green colored bar to the right of the raster plot indicates the Δr values for that particular stimulus averaged across the 5 trials. The asterisk indicates that the stimulus elicited a statistically significant response ($p < 0.05$, t-test). Firing rate values are indicated by the scale bar to the right.

3.3A). This gave us a distribution of 5 responsive trials and anywhere from 20 (4 Ringer's solution controls, 5 repeats) to 130 (2 negative steroids at 11 concentrations plus 4 Ringer's) non-responsive trials. Having a large number of negative trials mimics, in an interpretable fashion, the more common task of identifying sparse actual responses from frequent negative responses. Using the observed distributions of firing rates (Figure 3.3B), we calculated the frequency at which an ideal observer would correctly classify responses using a range of different thresholds. By comparing this classification with the known classification, we measured the frequency of true positive and false positive classification rate (Figure 3.3C).

The activity of an example cell is shown in Figure 3.3A. Depending on the number of trials used and choice of firing rate (Δr) threshold, responses to the active stimulus ("true positives") may be confounded with apparent responses to the negative stimuli ("false positives") (Figure 3.3C). The ROC analyses for all 4 responsive cells are shown in Figure 3.3D,F–H (top). The area under the curve (AUC) represents the probability that an ideal observer would correctly identify a response as positive or negative, and therefore corresponds to the reliability of the data [197]. The AUC using 1–5 repeats for each example cell is shown in Figure 3.3E,F–H (bottom). In the first example cell, comparing one active trial to one inactive trial resulted in correctly classifying the response 79% of the time. Functionally, this translates to incorrectly identifying a ligand as active or missing a truly active ligand approximately 20% of the time; if 30 ligands were tested on this cell using only one trial, we would be wrong about our assessment of activity for 6 of the ligands. Using as few as 4 repeats, the likelihood of correct classification climbed to 100%. Reliability varied across cells; two other cells (Figure 3.3F, G respectively) showed similar rates of misclassification using few trials and high reliability using 5 trials, while the final cell (Figure 3.3H) was reliable using only 1 trial. For non-responsive cells, the same analysis yielded detection at chance levels (data not shown), indicating (as expected) that the steroid and Ringer's solutions were indistinguishable. The majority of responsive cells were not reliable when using single trials, suggesting that VSNs are noisy neurons to the point where pooling of information is required.

This analysis emphasizes the utility of pooling information, either across trials or across neurons. However, it does not address any questions about underlying causes of VSN noise. This led us to look in more detail at the variability of VSN spiking statistics across time scales, in terms of the

ratio of the variance to the mean, or Fano factor [182]. A Fano factor of 1 indicates that the spiking follows Poisson statistics — each spike is independent, not influenced by the prior history of the spike train [182]. A Fano factor less than 1 indicates that there is less variance than predicted by a Poisson model, while a larger value indicates greater variance. To calculate this, we divided the spike train of all cells into time bins of various widths (Figure 3.4A) and computed the mean and variance of the number of spikes within each bin (Figure 3.4B). Figure 3.4 C–E plots the Fano factor as a function of bin width with corresponding interspike interval (ISI) histograms of individual cells (C, D) or of the population (E). We found that across all cells, the Fano factor hovered near 1 for smaller time bins until increasing drastically for larger time bins. Therefore, if one were to investigate a response, for example over 10 sec of activity (Materials and Methods), the average Fano factor is approximately 100 (Figure 3.4C), or 2 orders of magnitude larger than that of a Poisson process, indicating considerable variability associated with assessing a sensory response across the given timescale. This implies that spikes fired by VSNs were not independent of each other, and that some structure in activity may exist.

To gain some insight into the mechanism underlying this noise, we explored the relationship between the Fano factor time scale and the ISI distribution of the cell. We found that this point of inflection corresponded to the peak in the ISI histogram, most frequently at around 40 ms. The increase in Fano factor at times longer than a single ISI indicates that successive spikes are not independent, as for example, might be observed with burst firing.

3.3.2 VSNs tend to fire in bursts

The Fano factor analysis suggested that some structure exists in the spike trains of VSNs, beginning at time scales coinciding with a peak in the ISI histogram. Therefore, we investigated the detailed firing properties of VSNs, both during spontaneous activity (the 10 sec prior to stimulus delivery) and during stimulus-evoked activity ($p < 0.05$ rank sum test and $\Delta r > 2$ Hz). Taking a closer look at the firing patterns of VSNs, we observed that spontaneous activity occurred in two distinct patterns. Most cells (108/126) fired repeated trains of action potentials in rapid succession (Figure 3.5A, middle) while the remaining cells fired action potentials with longer ISIs (Figure 3.5A, top). Across the population, the spontaneous firing rate was 0.7 Hz with a standard deviation of 0.6 Hz

and a range of 0.2–3.8 Hz ($n = 126$ cells) (Figure 3.5B). Excluding the slow firing minority group, the average spontaneous firing rate was also 0.7 Hz with a slightly smaller standard deviation of 0.5 Hz and a range of 0.2–3.45 Hz. We also counted the number of spikes during a significant response to chemical stimuli ($n = 36$ cells). The mean firing rate was 3 Hz with a standard deviation of 2 Hz and a range of 0.5–9.0 Hz. While spontaneous activity was lower than stimulus-evoked activity, the firing rate distributions overlapped (Figure 3.5B).

We looked across all clearly sorted single units, and found that rapidly-firing neurons had several consistent features. Their ISI histograms, shown in Figures 3.5C and D, showed a dominant peak at approximately 40 ms during both spontaneous and stimulated activity. This consistency, across both the population and under different stimulus conditions, allowed us to use a uniform definition of "bursting," as three or more spikes fired with ISIs of less than 100 ms (Figure 3.5C–D, methods). The responsive neurons had a slightly higher probability of being in the bursting mode, as demonstrated by a higher "burst peak" in the population ISI histogram, while the spontaneous ISIs showed a large peak in the bursting mode with a second smaller peak at approximately 1 sec. The ISI histogram suggested that while responsive VSNs showed a tendency to spend more time bursting, the peak burst ISI of 40 ms was maintained in both conditions. Therefore, the observed increase in firing rate during a stimulus response was not due to a sizable shift in the overall ISI distribution.

Since we recorded many cells simultaneously (ranging from 3–31 cells in each preparation), we explored whether activity, and more specifically, bursting across cells were correlated. We found no evidence of correlations across cells (data not shown), suggesting that the origin of activity is independent across cells.

3.3.3 Membrane properties of VSNs affect spike measurement

Over the time course of a response, we observed a phenomenon such that the amplitude of the VSN action potentials occasionally decreased to the noise level for several seconds, making it impossible to follow the activity of such a cell using extracellular recording. This effect, which we term "spike amplitude decrement" (shown in Figure 3.6), displayed a strong concentration dependence, appearing predominately at the highest tested stimulus concentrations. For example, in response to 30 μM of a sulfated steroid Q3910, we observed a protracted increase in firing (Figure 3.6A top). When

stimulated with 100 μM of Q3190, the same cell exhibited a transient increase in firing, followed by an extended silence (Figure 3.6A bottom). The insert in Figure 3.6A illustrates the rapid decrease in the action potential amplitude over 2 sec until it was no longer larger than the noise. Note that despite the decrease in amplitude, spiking apparently continues for as long as the spikes can be distinguished from noise. The concentration dependence of this phenomenon is illustrated in Figure 3.6B. Spike amplitude decrement occurred in 5/15 cells that were responsive to the top two or more concentrations of a sulfated steroid. It is possible that this phenomenon occurred more frequently: spike amplitude decrement makes spike sorting more challenging and may bias against identifying cells that display this phenomenon.

Because we observed a change in spike amplitude rather than a slowdown in firing rate, we hypothesized that the amplitude changes were not due to sensory adaptation, but rather to membrane properties — that strong depolarization of the membrane prevents voltage gated sodium channels from recovering from inactivation, thus leading to a decrease in action potential size. A similar phenomenon has been demonstrated using whole cell recordings from V1R neurons following current injection [174], which bypasses the sensory transduction apparatus. In an attempt to test the hypothesis that this is a membrane property, we performed multielectrode array recordings using low Na^+ Ringer's solution and low K^+ Ringer's solution (see Solutions and Stimuli). By lowering Na^+ concentration, both the sodium Nernst potential and the amount of current through Na channels should decrease, potentially reducing the likelihood of spike amplitude decrement. Low K^+ Ringer's solution should lower resting potential and increase the outward, hyperpolarizing current through K channels, thus increasing the likelihood of voltage gated Na channel recovery from inactivation, thereby decreasing spike amplitude decrement. The results of these experiments are shown in Figure 3.6C. With modified Ringer's solutions, within the limits of trial-to-trial variability, we continued to observe spike amplitude decrement at the same stimulus concentrations and with similar latencies. A possible explanation is that other conductances were continuing to depolarize the neurons [173, 198, 174, 199], or that the changes in driving force were not sufficient to alter the kinetics of Na channel inactivation.

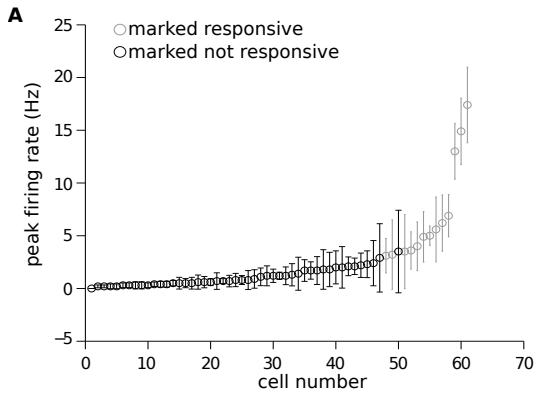

Figure 3.2: Firing rates used to determine a "true" response in ROC analysis. The change in firing rate in each cell is plotted with the standard error across trials. The cells are plotted in order of increasing firing rate. The gray bars represent cells that did not pass our significance criteria of a maximum firing rate above 2 Hz and firing that is at least 2 standard errors above baseline activity. The black bars did meet our criteria.

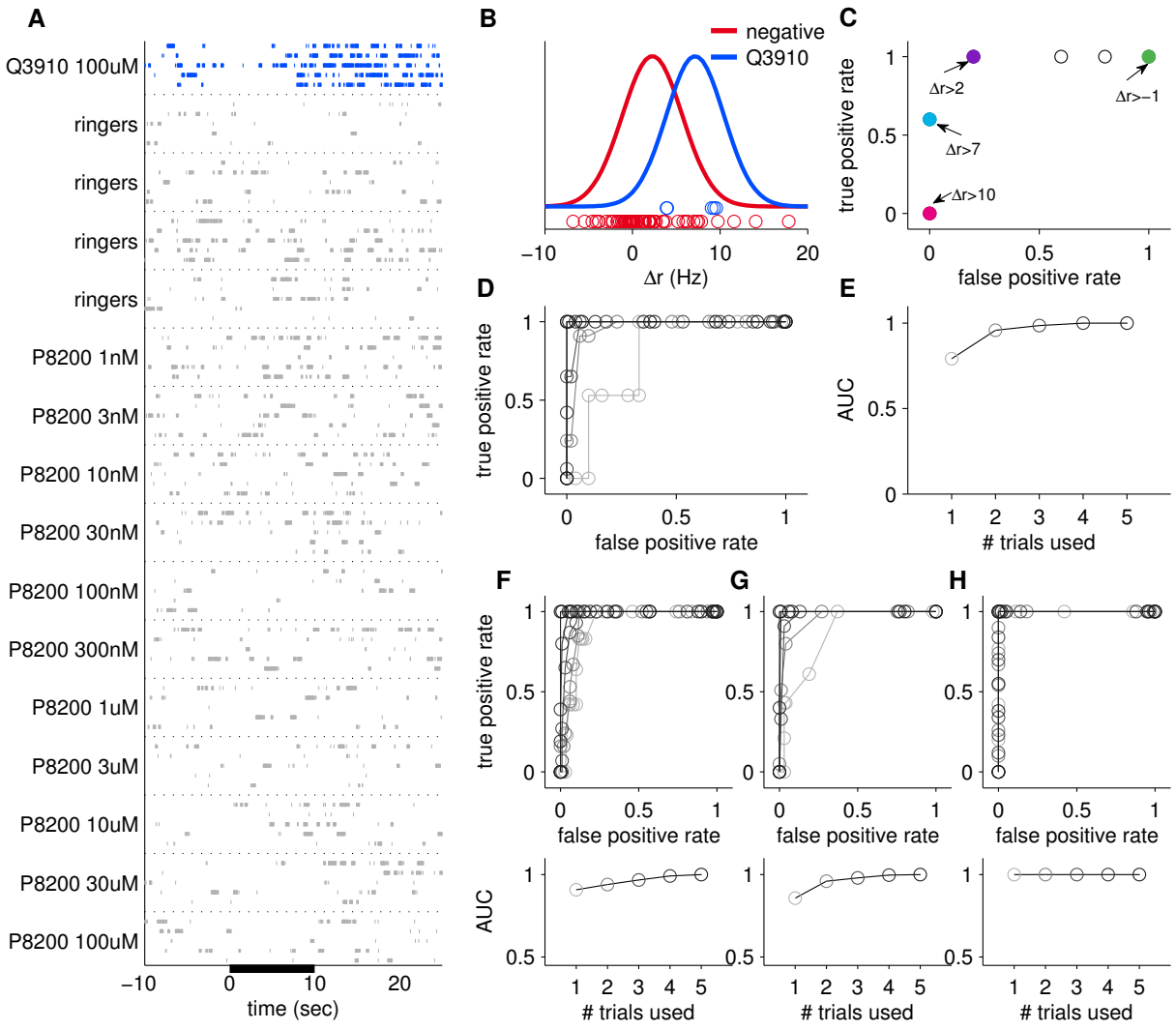

Figure 3.3: Variability of VSNs limits the reliability of detection. **A,** Raster plot of the activity of a representative cell in response to an active sulfated steroid (blue), Ringer's controls (gray) and a sulfated steroid that does not activate this cell (gray). Each stimulus was presented during the time indicated by the black bar for five separate interleaved trials. This cell was used in panels **A**–**E**. **B,** Mean firing rate change upon stimulation. The circles represent the firing rate change, Δr, calculated on each trial of active stimulation (blue) or inactive stimulation (red). The distribution of firing rates is represented by a Gaussian distribution based on the mean and standard deviation of Δr across trials. While the mean response to negative controls is near zero, spontaneous activity leads to multiple negative trials with high firing rates. **C,** Results of classification of responses based on Δr as a function of threshold (ROC analysis). Each dot corresponds to the rate of true and false positives that would be observed using the indicated criterion value for this cell using 5 responsive trials and 5 non-responsive trials, drawn randomly from the distribution. For example, when a threshold of 2 Hz was used (purple), 100% of true positives were correctly classified, however, there was a 20% false positive rate. Even using 5 trials, for no value of threshold could one distinguish the two categories with perfect reliability. **D,** ROC analysis using 1–5 repeats. False positive and true positive classification rates were computed using 1 (light gray) to 5 (black) trials of both responsive and non-responsive stimuli randomly drawn from the distribution shown in **B** and averaged over different combinations. **E,** The AUC (area under the curve) summarizes the reliability of detection. The AUC values using 1–5 repeats computed from the figure in **D** are shown. Reliability increases with the use of more trials. **F**–**H,** ROC analyses for the three additional responsive cells.

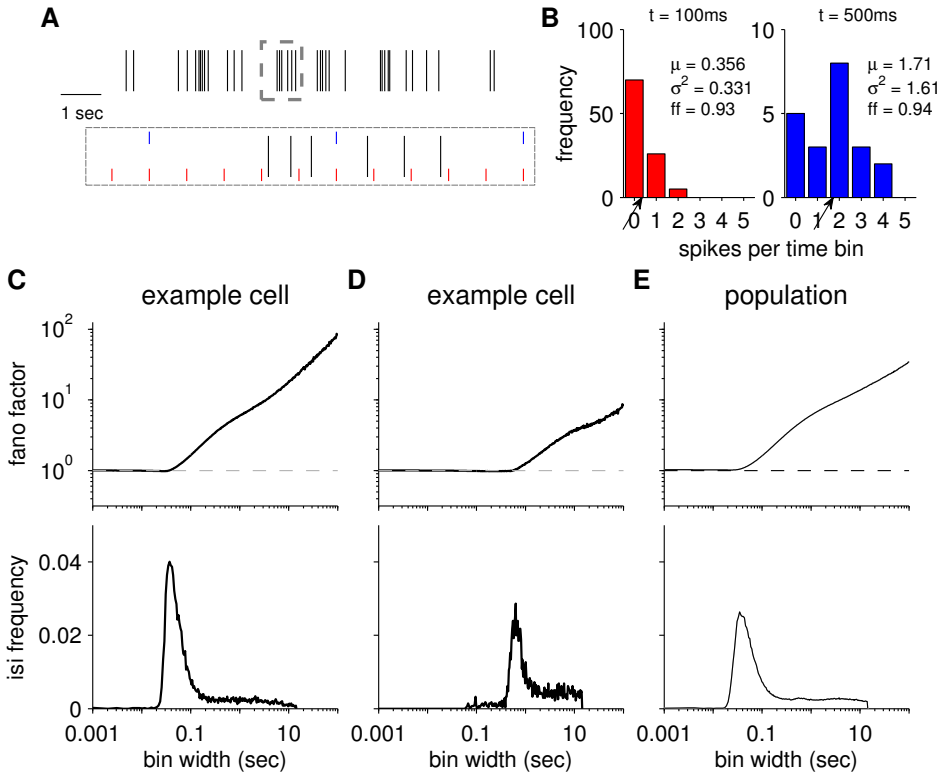

Figure 3.4: Variability of VSNs. **A,** A 10 sec interval of activity of an example cell (same as in **C**). Each line represents an action potential. The boxed area is shown on a different time scale on the bottom. The red and blue lines indicate example time bin divisions used when calculating the fano factor — 100 ms (red) and 500 ms (blue). **B,** A spike count for each time bin using 10 sec of activity was calculated and the mean and variance across all time bins was computed, for both 100 ms (red) and 500 ms (blue) time bins. The ratio of variance over mean gives the Fano factor, shown in the text in **B**. The arrow points to the mean spike count value. **C,** The variance divided by the mean (Fano factor) is plotted for a representative cell as a function of time bin (top). The corresponding ISI frequency histogram for that cell is plotted below. The Fano factor increased when measured at time bins larger than the peak of the ISI histogram, approximately 40 ms. **D,** A cell with lower levels of activity is shown here. The Fano factor still increased at time bins larger than the peak ISI. **E,** The average Fano factor and ISI histogram are shown. The black lines correspond to the mean±sem.

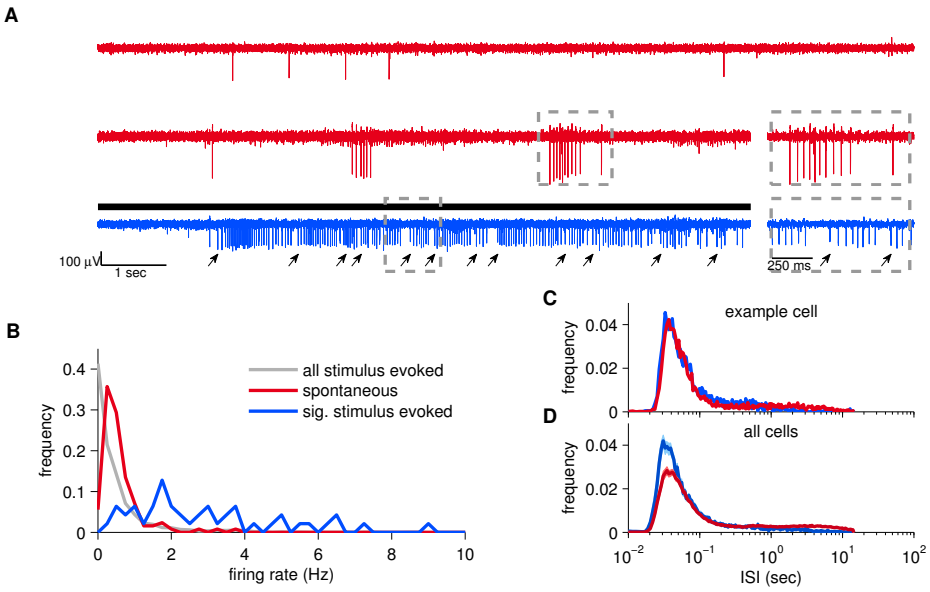

Figure 3.5: Firing properties of VSNs. **A,** Three modes of activity (from top to bottom): tonic firing, spontaneous bursting, and responsive bursting. We did not observe a response to stimulus delivery from any tonically firing cells. The insert at the middle right shows a 1 sec close up of the spontaneous burst. (Bottom) The arrows indicate the start time of each individual burst that make up the protracted period of activity. The insert at the bottom right shows a 1 sec close up of the stimulus driven activity. Two bursts can be observed at this magnification, with arrows indicating the starting spike of each. Note the similarity between each stimulus-driven burst and the spontaneous burst. Voltage off of three different electrodes from three different preparations is shown. The bar indicates when the stimulus (Q3910 30 μM)was delivered. **B,** The distribution of spontaneous (126 cells) (red) and stimulus-evoked (36 cells) (blue) firing rates. The number of spikes in the 10 sec prior to stimulus delivery (red) or number of spikes in the 10 sec following stimulation (blue) was counted and averaged across trials to obtain the rate. Only responsive stimuli were used to compute stimulus-evoked values while the period prior to all stimuli were used to compute spontaneous activity. The gray line represents the activity of all 126 cells following all stimulus presentations (40–42 stimuli per cell, 126 cells). Stimulus driven increases in firing rates were rare. **C,** Normalized interspike interval histogram of a single cell during spontaneous activity (red) and stimulus-evoked activity (blue). A detailed look at the activity of this example cell is shown in Figure 3.1**E**. **D,** The ISI histogram across the all single units. The dark lines indicate the mean and the lighter lines indicate the sem. Note the similarity of the red and blue distributions in **C** and **D**.

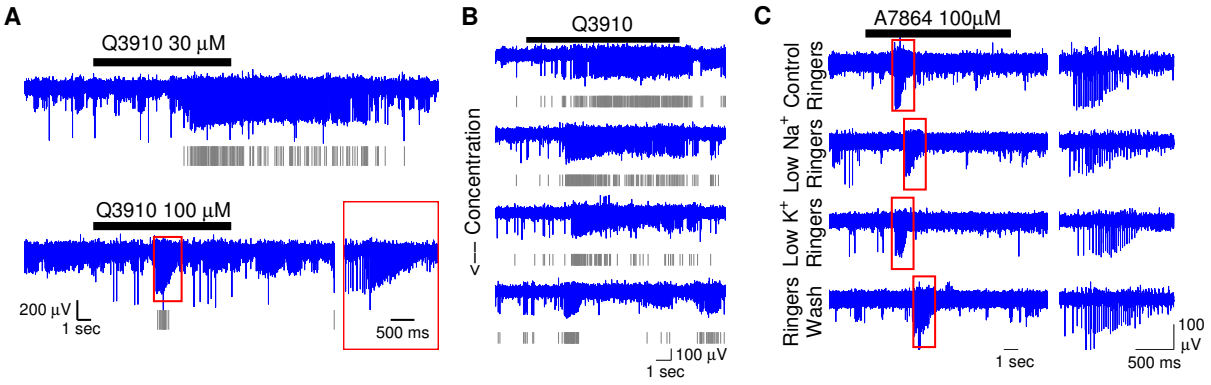

Figure 3.6: Spike amplitude decrement. The bar indicates when stimulus was delivered. The gray ticks below the trace indicate spikes fired by the sorted unit. **A**, A cell stimulated with 30 μM of Q3910 (top) displayed a protracted response. The same cell was stimulated with 100 μM of Q3910 (bottom). There was a transient response followed by a period of silence. A detailed view of the response (insert) reveals a rapid decrease in the amplitude of the action potentials. **B**, Another cell was stimulated with increasing concentrations of Q3910 (increasing from top to bottom). Clear spike amplitude decrement was observed with increasing concentration. At the highest concentrations, firing of the cell stopped (or became unmeasurable) but later resumed. **C**, Modified Ringer's solutions were used to address the issue of spike amplitude decrement. The period inside the red box is shown in greater detail on the right. We observed spike amplitude decrement when the tissue was in regular Ringer's solution, low Na^+ Ringer's and low K^+ Ringer's. Each modified Ringer's solution was followed by a regular Ringer's solution wash. The dynamics of spike amplitude decrement did not appear to be substantially modified by changes in the Ringer's ion concentration.

3.3.4 Similarities in bursting properties during stimulation and spontaneous activity

Our previous analyses suggested that bursting, both spontaneously and during stimulation, underlies activity of VSNs. We wondered whether fine details of the burst structure might provide valuable clues in distinguishing sensory responses from noise, so we investigated the timing of spikes between and within bursts.

The distribution of burst durations for a single example cell is shown in Figure 3.7A. The mean burst duration of this cell was 246.6 ± 6.2 ms (mean±sem; $n = 29581$ bursts) and 247.7 ± 9.7 ms ($n = 3155$ bursts) during spontaneous and stimulus-evoked activity, respectively. The length of bursts was found not to be statistically different between the two conditions ($p = 0.94$, t-test). Of the 36 cells that were significantly responsive, burst duration during spontaneous and stimulus evoked firing differed significantly in only 11 cells (t-test, $p < 0.05$). Even in these cells, the average

difference in burst length between spontaneous and stimulus evoked conditions was 80 ms, on the order of only one or two interspike intervals. Overall, the cells with stronger responses (Δr>4 Hz), showed slightly longer bursts during stimulation on the order of a single spike while cells with weaker responses did not (data not shown). Burst length across the population is presented in Figure 3.7B. Averaging across the population, the difference in burst duration between stimulus-evoked (327.8 ± 5.5 ms) and spontaneous (279.7 ± 1.4 ms) activity was statistically significant ($p < 0.01$); however, the difference between the two conditions was approximately 50 ms, on the order of only a single interspike interval.

As the burst duration differed minimally between stimulus evoked and spontaneous activity, we next investigated the spike timing within bursts to see if there was evidence of sensory adaptation [176] or other similar phenomenon during a response. A slowdown in firing was frequently observed towards the end of a burst. In Figure 3.7C we plotted the normalized ISI versus spike position within the burst for the first 5 spikes and last 5 spikes for the representative cell. We found that across all bursts, the first 5 spikes slightly accelerated their timing to reach a plateau and the final 5 spikes demonstrated an increased ISI, indicating a slowdown in firing. In both stimulus-evoked and spontaneous conditions, the same trend of acceleration and slight deceleration was observed for this cell ($p > 0.05$, t-test at each point). Across all single-units, the first 5 spikes showed an initial decrease in the ISI followed by an eventual increase in the ISI during both spontaneous and stimulus-evoked bursting, as shown in Figure 3.7D. Only the first spike of each of the two metrics (first 5 and last 5 spikes) were significantly distinguishable between stimulus-evoked and spontaneous conditions ($p < 0.05$, t-test), despite the fact that the timing of over 3000 ISIs were compared ($n = 3285$ ISIs). This suggests that there is minimal difference in spike timing within bursts during stimulation and spontaneous activity.

3.3.5 The time between bursts decreases during a response

Thus far, we observed limited differences in firing statistics between spontaneous and stimulus-evoked activity, differences too small to explain the increase in firing during a response. We next investigated the time between bursts, or the IBI. This metric is related to the burst frequency, and was investigated by measuring the interval between the last spike in one burst and the first

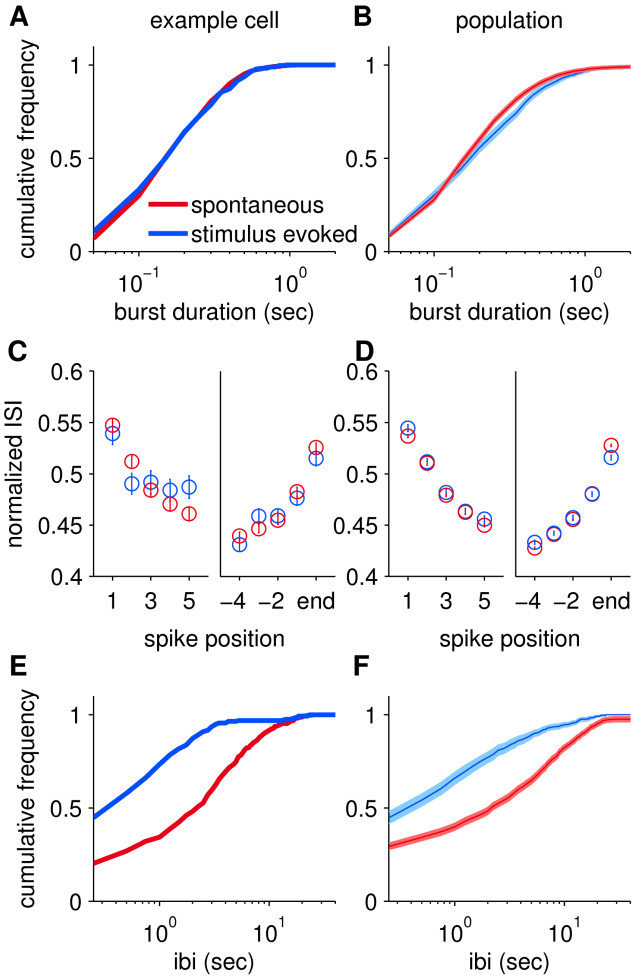

Figure 3.7: Bursting properties of VSNs. **A**,**C** and **E** were calculated using the same cell (see Figure 3.1**E**) and **B**, **D** and **F** were calculated using all cells. Spontaneous activity of all cells is indicated by the red line, and stimulus-evoked activity from responsive cells is shown in blue. The burst duration was calculated for an example cell (**A**) and across the entire population (**B**), as measured by the time between the first spike in a burst and the last spike in that same burst. The center line of the cumulative probability histogram represents the mean and the lighter lines represent the standard error. Note the similarity between burst duration during spontaneous and stimulus-evoked activity. **C** and **D,** Relative timing of the first and last 5 spikes within a burst. The circles represent the mean with error bars indicating the standard error. In both the single cell example (**C**) and across all cells (**D**), there was an initial acceleration in firing followed by a slowdown in firing at the end of the burst. **E,** The time between consecutive bursts for a single cell and for the population (**F**). The inter-burst interval was significantly shorter during a stimulus response than it was during spontaneous activity.

spike in the following burst. Figure 3.7E shows the cumulative frequency histogram of the IBI for a representative cell, both during spontaneous and stimulus-evoked activity. During spontaneous activity, the average between-burst interval was 3.8 ± 0.2 sec while it was 1.45 ± 0.2 sec in response to a stimulus ($p < 0.01$, t-test). This increase in burst frequency is illustrated in Figure 3.7E by the leftward shift of the responsive curve. In 21/36 responsive cells, stimulus caused a decrease in the IBI as compared to spontaneous activity (t-test, $p < 0.05$). Of the 15 cells that did not display a significant difference in IBI, 10 similarly had decreased IBI (and 4 had increased IBI) during stimulus-driven activity, but these changes did not meet our significance criteria largely due to the sparseness of these cells' responses. Across the population, the mean burst-spacing was significantly different between conditions ($p < 0.01$, t-test), at 4.15 ± 0.04 sec and 1.58 ± 0.05 sec for spontaneous and stimulus-evoked activity, respectively.

Overall, the firing properties of VSNs demonstrated a tendency towards low rates of spontaneous activity (almost 1 Hz), consisting of both bursts and single spikes. While the probability of bursting increased during a stimulus response, the properties of burst duration and timing within bursts remained similar to that observed during spontaneous activity. The most prominent difference observed was that the time between bursts decreased during sensory responses. These results suggest that the primary feature in stimulus encoding involves the burst frequency or timing between bursts rather than a change in spike timing or longer burst duration.

3.3.6 Signal transduction pathway is involved in shaping spontaneous activity

The similarity of bursts during both spontaneous activity and stimulus responses suggests that they are generated by a common mechanism. One possibility is that initiation of bursting is controlled by the membrane properties of the soma [200, 201]; another possibility is that bursts are triggered by the signal transduction cascade, and that this cascade is sometimes activated spontaneously.

To distinguish between these possibilities, we first exploited the fact that vomeronasal sensory transduction is Phospolipase C (PLC) dependent [150, 110]. We treated vomeronasal tissue with the PLC inhibitor U-73122 ($10\,\mu M$) or its inactive structural analogue U-73343 ($10\,\mu M$) while stimulating with sulfated steroids and 50 mM K^+ Ringer's solution. Consistent with previous work [150], the PLC inhibitor successfully eliminated receptor-dependent responses in 14/16 responsive

cells ($n = 49$ cells) (Figure 3.8A) and responses were greatly reduced in the other two cells. Activity due to K^+ induced depolarization is thought to bypass any signal transduction machinery, which is consistent with the maintenance of K^+ Ringer's solution response during treatment with U-73122 in all but 2 cells that were active throughout the recordings (Figure 3.8B). Cells still maintained some degree of spontaneous activity in the absence of PLC activity (Figure 3.8C), but the average firing rate dropped from 0.8 Hz to 0.3 Hz. The reduced firing rate is reflected by a smaller-amplitude peak in the population ISI histogram (Figure 3.8D). While bursting was maintained during PLC block, the overall structure appeared qualitatively different (Figure 3.8C). We found that U-73122 slowed the rate of firing within bursts (Figure 3.8E) and increased the time between bursts (Figure 3.8F). However, the most striking feature was that bursts were significantly reduced in length from 240.7 ms to 122.4 ms (Figure 3.8E). One interpretation of these results is that signal transduction machinery plays a role in shaping spontaneous, as well as stimulus driven, activity in VSNs, potentially both in terms of the total amount of firing as well as sculpting the dynamics of individual bursts.

However, pharmacological intervention may have effects on machinery other than the intended target. Therefore, we also used a line of mice in which TrpC2, the ion channel previously demonstrated to be required for ligand-driven responses in VSNs [54], is knocked out. This affects the signal transduction cascade at a point downstream of PLC. Consistent with previous reports [54, 43], these TrpC2$^{-/-}$ mice no longer displayed stimulus-driven responses yet did respond to high K^+Ringer's solution (Figure 3.9A) ($n = 28$ cells). As observed during PLC inhibition, spontaneous activity was reduced in the mutant mice compared with wild type (WT) mice yet bursting persisted (Figure 3.9B). The ISI histogram indicated a reduced peak at the shortest firing latencies (Figure 3.9C). In contrast with the results from U-73122, the burst duration in TrpC2$^{-/-}$ VSNs was remarkably similar to that found in the WT VSNs (Figure 3.9D). The phenomena of acceleration at the beginning and deceleration at the end were also similar, with slightly slower firing in the mutant mice (Figure 3.9E). The time between bursts was greatly reduced in the absence of functional TrpC2 channels (Figure 3.9F), consistent with the overall decrease in activity.

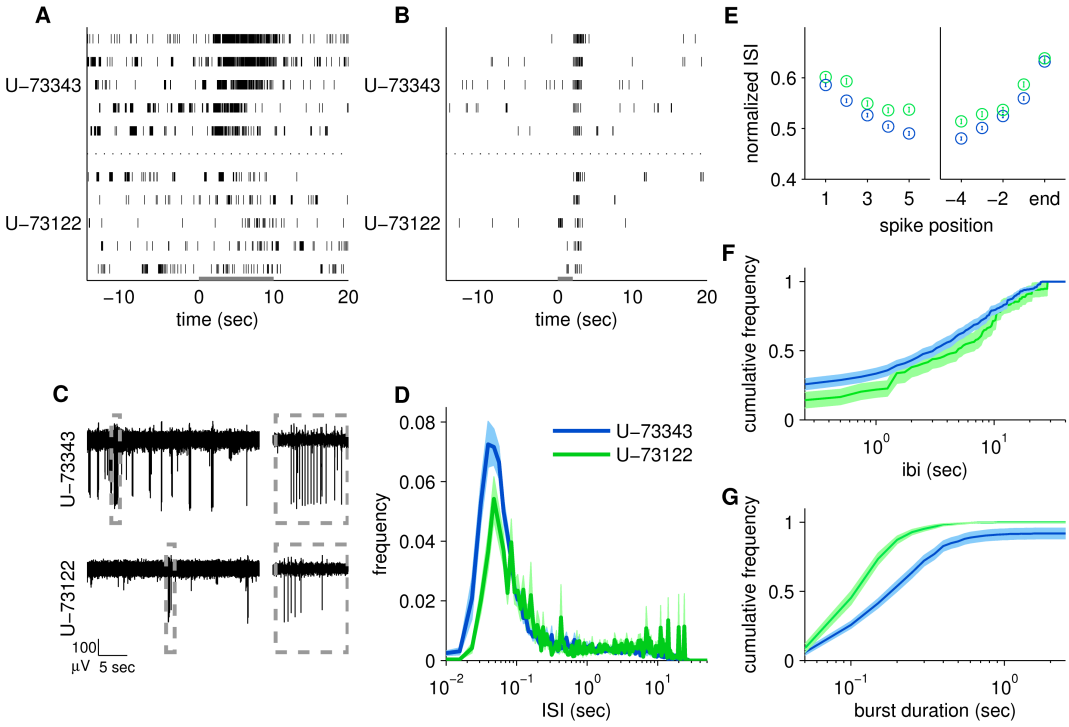

Figure 3.8: Blocking the signal transduction cascade affects spontaneous VSN activity. **A,** a raster plot showing the response of a cell to 10 μM A0225 while being treated with the inactive U-73343 (top) and the active U-73122 (bottom). The gray bar indicates the time over which stimulus was delivered. Stimulus driven, not spontaneous, activity was eliminated in the bottom condition. **B,** a raster plot showing the activity of a different cell in response to 50 mM K^+ Ringer's solution. The response was maintained in both conditions. **C,** Activity on a single electrode during Ringer's solution stimulation in the presence of U-73343 (top) and U-73122 (bottom). Activity was greatly reduced in the bottom panel, and the bursts were shorter, as illustrated by the boxed off region showing 1 sec of activity from each trace. **D,** the ISI histogram for the population of 49 cells that were treated with U-73343 (blue) and U-73122 (green). There is a slight rightward shift following PLC inhibition, suggesting a slowdown in activity. This figure, and those in subsequent panels, use activity measured in the absence of stimulus. **E,** the relative timing of the first and last five spikes within a burst. The time between spikes was slightly increased following drug treatment. **F,** the cumulative frequency histogram of the interburst interval across the population. There was more time between bursts during PLC inhibition. **G,** the cumulative frequency histogram of burst duration across the population during treatment with U-73343 (blue) and U-73122 (green). The PLC inhibitor treatment lead to a reduction in burst duration.

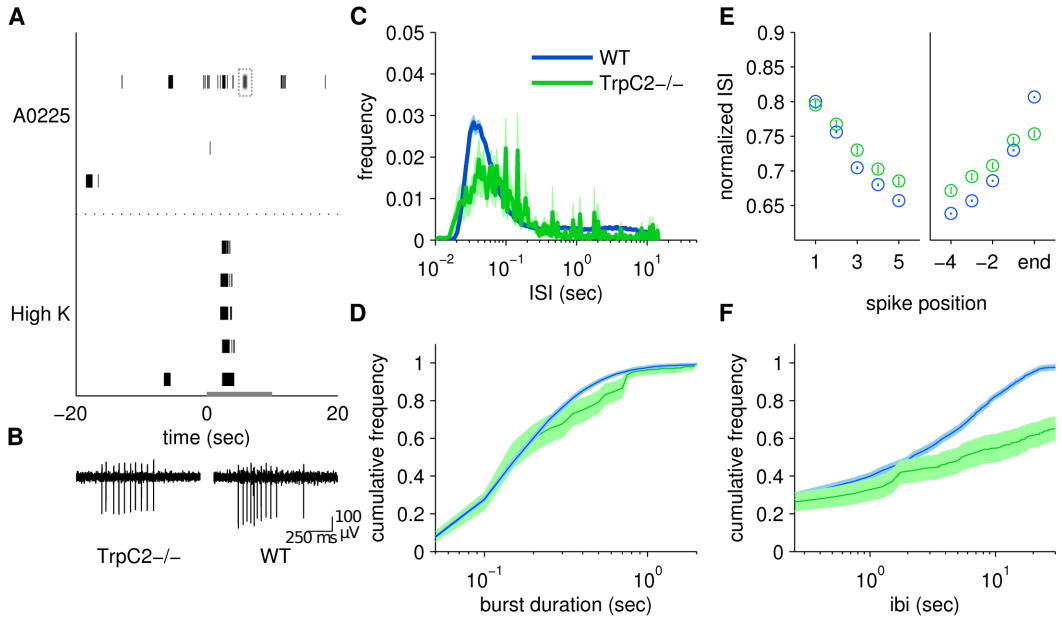

Figure 3.9: The TrpC2 channel is involved in shaping spontaneous activity. **A,** Stimulus driven activity was abolished in the mutant VNOs (top). Activity in response to 50 mM K^+ Ringer's solution persisted (bottom). Spontaneous activity was also reduced. The gray bar indicates the duration of stimulus delivery. The gray box around a burst of activity (top) is blown up in **B** (left). **B,** A close up of bursting activity in TrpC2$^{-/-}$ (left) and wild type (right) animals. The WT activity is taken from Figure 3.5**A** middle insert. **C,** The ISI histogram of spontaneous activity from 28 cells from mutant animals (green) and 126 cells from wild type animals (blue). The WT histogram is the same as in Figure 3.5**C**. **D,** The cumulative frequency histogram of burst duration in mutant (green) and wild type (blue) VSNs. In this and all subsequent panels, the WT spontaneous activity is taken from Figure 3.7. The overall burst duration in the mutant VNO was similar to that in WT VNO. **E,** The ISI of spikes within a burst. The spikes within TrpC2$^{-/-}$ VSN bursts (green) were slightly slower overall than spikes from WT animals (blue). **F,** The timing between bursts was greatly increased in the mutant animals (green) compared to the WT animals (blue).

3.4 Discussion

The murine accessory olfactory system has been subject to a number of recent studies spanning both sensory neurons and downstream circuits [43, 88, 87, 44, 113, 171]; however, the question of how information is being represented at the level of individual spikes has not been explored. In this study, we aimed to elucidate the physiological properties of VSNs that relate to how stimulus information is encoded, and to explore the implications of these properties for decoding sensory responses.

3.4.1 VSNs use a "burst rate" code for representing sensory information

A large body of literature in neuroscience has been devoted to exploring mechanisms by which neurons encode sensory information, such as through spike rates or spike timing [182]. Bursts have been reported to encode sensory information in numerous systems including in olfactory receptor neurons [202, 203]. In various brain regions, the utility of bursts has been attributed to encoding information by burst duration [204, 205, 206], number of spikes within the burst [202], or within-burst interspike interval [207].

We first explored the within-burst ISIs and the burst duration and observed only minimal differences in these characteristics between stimulus-response and spontaneous conditions, suggesting that VSNs were not encoding stimulus characteristics using intra-burst differences. In our preparation, we also found little evidence to suggest that the precise timing of individual spikes was important. VSNs fired both in bursting and non-bursting modes, with very high variability (Figure 3.4), which implies that codes depending upon fine details of spike timing may be insufficiently robust. Moreover, the timing of spikes within bursts is nearly independent of sensory stimulation (Figure 3.5). However, a caveat of this (and all other published investigations of VSN activity) is the *ex vivo* preparation. *In vivo*, detection of stimuli is elicited by active pumping of the VNO [111], and it remains possible that pumping imposes a more detailed temporal structure on sensory encoding in the VNO. It is also possible that the natural kinetics of VSNs are upset by the *ex vivo* preparation. While great care was taken to maintain the integrity of the vomeronasal epithelium, it is possible that the ion concentration of our Ringer's solution differs from that of the VNO lumen

(currently unknown).

Overall, we observed that an increase in burst frequency signaled a sensory response. Therefore, we propose that VSNs encode sensory information via a burst rate code, in which bursts are the unit, rather than individual spikes. In this scheme, a burst code is approximately equal to a rate code, as the spike count and duration of bursts was approximately fixed (Figure 3.5).

If bursts are not contributing additional coding information, that begs the question as to the purpose of bursts. It has been proposed that bursts increase the fidelity of synaptic transmission [208, 200]. It is possible that there is low coupling between VSN spikes and mitral cells within a glomerulus, and the presence of bursts may increase the probability that a stimulus will elicit a response in the AOB. Mechanistically, a possibility explored below is that bursts are a by-product of sensory transduction or the membrane properties of VSNs.

3.4.2 VSNs and sensory adaptation

Using MEA recordings, we found no clear evidence of sensory adaptation in VSNs in the form of a diminished stimulus response over time. This is consistent with much of what has been previously reported [150, 171], although other studies have reported some degree of adaptation [176]. In our experiments, repeated stimulus deliveries did not lead to a decrease in the response magnitude or duration in individual cells (i.e. Figures 3.1,3.3A)).

Across the duration of a single trial, we observed two phenomena that we believe to be membrane properties rather than sensory adaptation, which would involve second messenger activation. Over the course of an individual burst, there was slowdown in firing (Figure 3.7C). However, this occurred both in the presence and absence of stimulation, suggesting that this phenomenon is linked to the membrane properties that give rise to bursting.

The second relevant phenomenon was spike amplitude decrement. In response to the highest tested concentrations of sulfated steroids, action potential amplitude tended to decrease into the noise level for seconds before returning after cessation of stimulation (Figure 3.6). This is similar to what has been observed in the main olfactory system [209, 210] in response to high concentrations of odorant, and is thought to be due to sodium channel inactivation.

Our attempts to address the issue of whether spike amplitude decrement was a membrane rather

than sensory phenomenon were inconclusive (Figure 3.6), likely due to the presence of non-sodium conductances [173, 198, 174, 199], and the relative balance of inward and outward currents. However, this phenomenon is very similar to what was observed by Ukhanov et al using whole cell recording during current injection into a V1R neuron. During current injection, the neurons rapidly began to oscillate and fire broad, complex spikes [174]. Extracellular recording measures the capacitive current, which is approximately proportional to the first derivative of the trans-membrane potential that is recorded intracellularly, or $^{dV_m}/_{dt}$ [211]. Offline analysis of published intracellular V1R waveforms [174] revealed a first derivative signal that falls well below the initial amplitude (data not shown), and likely well below threshold on an MEA electrode, similar to what we observed (Figure 3.6). Such phenomena have been directly observed in hippocampal neurons [212].

Interestingly, Ukhanov et al observed this activity pattern only in V1R and not V2R neurons [174]. A study by Hagendorf et al reported that the presence of a particular potassium channel, Ether-a-go-go related gene (ERG) channel, extended the dynamic range of VSNs, likely by aiding in fast recovery from voltage gated sodium channel inactivation. Cells with reduced expression of the ERG channel displayed pronounced spike amplitude decrement [175]. The authors found ERG channels only in basal, V2R-expressing neurons. There is evidence that urine, and therefore presumably sulfated steroids, fairly selectively activates apical, V1R-expressing neurons in the VNO [213, 161], potentially providing an explanation for cellular mechanisms of spike amplitude decrement.

3.4.3 Implications of VSN properties on the coding and measuring of olfactory information

We observed that variability in VSN spike trains increased dramatically at time bins greater than the peak in the ISI histogram (typically around 40 ms, Figure 3.5). Therefore, when measuring a sensory response, which is typically done over seconds with VSNs [43, 44], variability in the signal was large. This potentially can lead to misclassification (Figure 3.3) of ligand responses.

While this variability affects us as experimenters, it presumably also plays a role in how the AOS processes information. A common role by which systems can increase the reliability of highly variable systems is by pooling activity across a population [182]. The approximately 150,000 neurons of the VNO [214] express approximately 300 different receptor types; consequently many cells will

be expressing the same receptor type in any given VNO. In the AOS, multiple VSNs expressing the same receptor type project to a limited number of glomeruli in the AOB [128, 116, 131, 132], meaning that there exists significant pooling of similar inputs. This pooling may allow the system to obtain a more reliable signal by averaging across redundant information, as indeed has been observed when comparing VSN responses to those of AOB neurons [44]. Given the capacity for pooling across many cells, it is indeed possible that the unreliability of individual neurons may be an acceptable price to pay for mechanisms of sensory transduction or firing that might increase sensitivity to weak stimuli.

Physiological recordings are typically blind to the molecular identity of the cells. As a proxy for pooling of common signals, we therefore use multiple repeats of the same stimulus on a given cell to explore the implications of variability on signal detection (Figure 3.3). By pooling across multiple repeats, the reliability of the signal increased. These results support the idea that stimuli are represented by population activity *in vivo*, and emphasize the importance of performing multiple repeats of stimuli.

3.4.4 Implications for chemosensory transduction

For many neurons, an increase in firing rate corresponds to a decrease in the ISI. Surprisingly, VSNs fired in bursts that maintained similar spike timing properties regardless of stimulation status. This poses an interesting question as to the nature of the signal transduction cascade: how can ligands trigger bursting without substantively modifying the membrane properties during a burst?

One possible mechanism is that intrinsic membrane properties alone drive bursting. However, this interpretation appears to be in conflict with the observation that burst frequency was significantly reduced by altering the sensory transduction cascade (Figure 3.8,3.9). An alternative hypothesis is that activation of the G-protein is effectively quantal, where a single temporally-isolated quantum corresponds to a single burst. If the signal transduction cascade is occasionally activated spontaneously, this mechanism would be predicted to produce stereotyped bursting even in the absence of stimulation. This interpretation appears to be consistent with an overall decrease in spontaneous activity (Figure 3.8,3.9) and decrease in burst length when PLC is inhibited (Figure 3.8). However, while the rate of initiating bursts was greatly reduced in TrpC2$^{-/-}$ VSNs, the

burst length was not significantly altered, although there was a slight slowdown of spikes within the bursts (Figure 3.9). Overall, the uniformity of burst structure and the change in spontaneous activity following intervention in various components of the signal transduction cascade argue that signal transduction machinery is involved in triggering spontaneous activity, while membrane properties may play the major role in the burst structure.

4 Robust encoding of concentration in the accessory olfactory system

This chapter is modified from Arnson and Holy (submitted)

4.1 Introduction

Sensory systems have a remarkable ability to extract relevant information from a noisy and inconsistent environment. For example, the visual system is able to identify an object despite variability in observation angle or size [215]. A sound can be identified independent of volume or intensity [6], and a smell can be recognized as a particular odor over a range of concentrations [17, 216, 18]. Sensory stability, particularly in the face of changing conditions, has been subject to numerous investigations in multiple sensory systems, including olfaction [217, 32, 2, 29].

A central mystery is how olfactory percepts can be relatively constant despite dramatic changes in the raw peripheral representation of odors as stimulus concentration is varied [15]. In principle, one possible computational strategy is through the use of ratios: if an odor has two components, A and B, the ratio of their concentrations is constant even if the absolute concentration is subject to environmental influences. This notion is supported by behavioral observations such as the attraction of moths to particular pheromone blends [218] and the ability of rats to make choices based on ratios of components [32].

How might a neural circuit represent ratios? One possibility is through the use of logarithms — the log of a ratio is equal to the difference of logarithms ($\log \frac{A}{B} = \log A - \log B$). This requires neural circuitry to represent the logarithm of concentration and compute the difference, which could be accomplished through inhibitory circuitry found throughout the brain. Logarithmic representation of sensory stimuli has a long history, dating back to early psychophysicists Weber and Fechner [3] and has been previously proposed as a neural mechanism for computing ratios [32, 30]. However, to

our knowledge no direct neural evidence of logarithmic or ratio coding exists in an olfactory system.

Here we explored the potential computation of logarithms and ratios by the accessory olfactory system (AOS), an independent olfactory system present in most terrestrial vertebrates. The AOS detects social cues from complex mixtures of stimuli, used by organisms to make behavioral decisions about reproduction and aggression conditional upon the status of other members of the social group. Behavioral and physiological state is known to be reflected in changes in the relative concentrations of components of stimuli such as urine [43], but absolute concentrations are expected to be highly variable [219] (Figure 4.1A). Using multielectrode array recordings of accessory olfactory sensory neurons located in the vomeronasal organ (vomeronasal sensory neurons, VSNs) we demonstrate that a logarithmic representation of concentration, and in turn log-ratio of concentration of two components, may be robustly calculated from the firing rates of VSNs. These results demonstrate the feasibility of quantitative "olfactory scene segmentation" using the responses of neurons with mixed selectivities for individual odorants.

4.2 Materials and Methods

All stimuli, solutions, and electrophysiological recordings were as described in Section 2. The following sulfated steroids were used in this study: A0225, Q1570 and Q3910. Sulfated steroids were used at a maximum of 9 concentrations, ranging from 10 nM to 100 μM, in approximately 3-fold increasing intervals. Binary mixtures were prepared by making 1:1 mixtures of chosen dilutions of pure compounds, so that each individual mixture component was half the concentration of the original solution of pure compound.

4.2.1 Data analysis

Spike sorting and electrophysiological recordings were performed as described in Section 2.

Determining firing rate Change in firing rate of a cell, Δr, was calculated using the Δr_{avgmax} metric, described in Section 2. Due to time lags within the delivery system and variability in the placement of the stimulus pipette, an offset was allowed between the time at which stimulus delivery began and stimulus reached the tissue. The offset was determined by measuring the activity across

all electrodes in a particular recording using 250 msec time bins. The offset was set as the time bin prior to an increase in net activity following stimulus delivery onset, with values ranging from 1.25 to 4.75 sec.

A response was determined to be statistically significant if it differed from the Ringer's control using a rank-sum test with a p-value threshold of 0.05 with a minimum Δr of 2 Hz. To control for methanol and Ringer's artifacts, Δr was computed for the vehicle and Ringer's solution stimuli. No cells in this data set were found to have a significant Ringer's or vehicle response. Because of the large number of stimuli and cells examined (see below), to further exclude false positives we used the Hill equation (described in more detail below) to model the response of each cell to the stimulated compounds based on the fits described below. Cells with predicted firing rates not exceeding 1 Hz at any concentration were excluded from further analysis. A total of 22 cells were excluded in this round (4.4% of the total population, consistent with a statistical cutoff of $p = 0.05$). By eye, none of the excluded cells appeared to be responsive.

Concentration characterization To compute the response properties of individual cells, the change in firing rate in response to a range of concentrations was fit with three models — a log-concentration model, a rectified log-concentration model, and a Hill model. The log-concentration model, a model in which the firing rate rises linearly with the logarithm of concentration, was computed by fitting the cell's firing rates (r) across concentrations to the equation $r = \alpha \log \frac{c}{c_{ref}} + \beta$, where α is the slope (Hz), c is the stimulus concentration (M), c_{ref} is a normalizing factor to make concentration unit-less and is equal to 1 M, and β is the offset (Hz). Firing rates computed on each trial were used (4–6 per stimulus).

The rectified log model differed from the above model in that below a minimum concentration threshold, c_0, firing was equal to a baseline firing rate r_0, or if $c < c_0, r = r_0$ and if $c \geq c_0, r = \alpha \log \frac{c}{c_0} + r_0$.

The Hill equation fit was calculated by fitting the firing rate of the cell to the Hill equation,

$$r = r_0 + r_\infty \frac{(c/K)^n}{1 + (c/K)^n}$$

where r_0 is the baseline firing rate, r_∞ is the maximum firing rate for the cell, c is the stimulus concentration, K is the binding affinity of the cell to each ligand, and n is the Hill coefficient. Using the 4–6 repeats of each concentration of each single steroid stimulation, r_0, r_∞, K, and n were all fit to minimize χ^2. We started from a simplified "flat" model, progressing to a linear model, a Hill model with $n = 1$, and finally the full Hill model. This progressive increase in the number of parameters reliably led to fits that, by eye, appeared consistent with the global optimum and avoided getting trapped in local minima. The value of n, indicating cooperativity, was initially allowed to be between 0 and 5. We found that cells with n-values at or near 5 consistently were responsive only to the highest concentration, providing too little data to constrain model parameters. These cells were excluded from all analyses involving the Hill parameters. For subsequent analyses, these cells were refit with the Hill model with a fixed n of 1. Importantly, when fitting the responses of a cell to two different pure compounds, the only parameter that was permitted to differ for the two compounds was K; the remaining parameters were jointly optimized for both compounds.

Mixtures were also fit with a Hill model incorporating competitive binding of different compounds within the mixture,

$$r = r_0 + r_\infty \frac{(c_1/K_1 + c_2/K_2)^n}{1 + (c_1/K_1 + c_2/K_2)^n},$$

using r_0, r_∞, K, and n values from the pure compound Hill equation fits. Because the validity of the Hill equation fit requires approximate saturation to at least one tested compound, only the 24 most-sensitive cells were used to investigate competitive binding. Saturation was determined by a K value of $10\,\mu M$ or less.

Log-Concentration modeling In order to determine whether populations of VSNs could be used to reconstruct log-concentration, we used a linear model, $\log(\hat{c}) = \mathbf{w} \cdot \mathbf{r}$ where ĉ is an estimate of the concentration presented, $\mathbf{r}$ is a vector containing the responses of each cell to the presented concentration of that compound, and $\mathbf{w}$ is the vector of weights, n_{cells} long. When analyzing mixtures of two ligands, we seek two $\mathbf{w}$ vectors, $\mathbf{w}_1$and $\mathbf{w}_2$, so that the estimated log-concentration of ligand 1 is $\mathbf{w}_1 \cdot \mathbf{r}$ and $\mathbf{w}_2 \cdot \mathbf{r}$ for ligand 2. Only cells that had an EC50 value $< 100\mu$M for at least one compound, indicating a cell that was responsive over the presented range of concentrations, were used ($n = 56$ cells).

Model parameters (the weights $\mathbf{w}_i$) were set using two procedures. First, we explored a "self-tuning" approach, using the pure compound responses for compound i to tune the weight vector $\mathbf{w}_i$. We generated a matrix of firing rates, $\mathbf{R}$, one for each trial (4–6 trials) per concentration per cell. We used a concentration vector, $\mathbf{c}$, covering the range from 300 nM to 100 μM in increments of half log units. $\mathbf{w}$ was tuned using linear least squares regression for each compound individually, yielding two $\mathbf{w}$ vectors in which each cell has 2 weights, one for each compound. The model efficacy was first tested using the aforementioned weights and average firing rates for all cells in response to each sulfated steroid when presented independently. The model was also tested using the firing rate for each cell in response to the mixture of components. To find the reproducibility of reconstruction, we recalculated concentration by using an average firing rate obtained by sampling 4/5 repeats. Samples were drawn randomly 100 times and the response was averaged. The error bars correspond to the standard error. All error values shown are calculated as $E = \sum(\log c_{actual} - \log \hat{c}_{model})^2$ summed across all stimuli and concentrations.

"Self-tuning," while straightforward, cannot properly handle mixtures; this can be demonstrated using a simple toy model of neuronal responses. Suppose that the population firing rate to pure compound 1 is $\mathbf{r}_1 = \mathbf{a_1}\log(c_1)$, where $\mathbf{a}_1$ is an arbitrary vector and c_1 is the actual concentration of compound 1; compound 2 behaves likewise with a different arbitrary vector $\mathbf{a}_2$. Suppose further that a mixture of these two compounds results simply in the sum of these firing rates, $\mathbf{r} = \mathbf{r}_1 + \mathbf{r}_2$. Using the mixture data, we would estimate the log concentration of each compound as

$$\log(\hat{c_1}) = \mathbf{w}_1 \cdot [\mathbf{a}_1 \log(c_1) + \mathbf{a}_2 \log(c_2)], \qquad \log(\hat{c_2}) = \mathbf{w}_2 \cdot [\mathbf{a}_1 \log(c_1) + \mathbf{a}_2 \log(c_2)]$$

Perfect "self-tuning" for this toy model implies $\mathbf{w}_i \cdot \mathbf{a}_i = 1$. However, to yield the correct result for mixtures, we require the additional constraints $\mathbf{w}_1 \cdot \mathbf{a}_2 = 0$ and $\mathbf{w}_2 \cdot \mathbf{a}_1 = 0$; these constraints are not imposed by the least-squares fit when each weight vector is tuned independently. These constraints can be (approximately) satisfied if the neurons have no overlapping stimulus responses, but it does not happen naturally when at least some neurons respond to both ligands.

Consequently, we developed an alternate procedure, which we call "cross-tuning," designed to account for neurons that have overlapping responses. This procedure also accounts for neurons that

violate the simplistic assumptions of the above toy model. In its most general form, the strategy is to use single-compound responses to fit a model describing the neuron's response properties, and then use the parameters to "simulate" responses to all possible tested mixtures. The simulated mixture responses are used in a least-squares sense to train the weight vectors to properly extract the log-concentration of each component. The model is then tested by comparing its reconstruction of log-concentration using actual mixture data.

More specifically, we calculated predicted mixture responses based on the Hill mixture model presented above, using the efficacy $c_{\text{eff}} = c_1/K_{1i} + c_2/K_{2i}$ for the ith neuron. For a particular simulated mixture and neuron, we computed c_{eff}. To include the effects of noise, we estimated firing rate responses using a "lookup table" procedure: we compared this efficacy to all of the efficacies tested with pure compound A and pure compound B, and the closest match was chosen to assign the Δr values for all simulated trials of this particular simulated mixture for this neuron. This was repeated for all possible mixtures (using concentrations ranging from 300 nM to 100 μM in half-log units) and all cells. This yielded a "response vector" of length 180 (36 mixtures and 5 trials) for each cell, or in total a 180×n-cells R matrix. Finally, least-squares minimization to reconstruct the actual concentrations of each component of the simulated mixtures was used to solve for $\mathbf{w}_1$ and $\mathbf{w}_2$.

Ratio computation Ratios were computed using the reconstructed log-concentrations. For each mixture, the reconstructed log-concentrations for each compound were subtracted to give the log-ratio: $\log \hat{c_1} - \log \hat{c_2} = \log \frac{\hat{c_1}}{\hat{c_2}}$. Error bars were computed as described above.

4.3 Results

The accessory olfactory system, like all other sensory systems, must be capable of representing information in a way that is robust to environmental uncertainties. Here, we explore the possibility that the activity of sensory neurons can be used to compute concentration ratios, as the ratio is insensitive to absolute changes in concentration yet still sensitive to relative changes (Figure 4.1A). As an initial step, we explore the degree to which the logarithm of concentration, a natural stepping-stone to computing ratios, might be represented. In principle this may be achieved by individual VSNs, or alternatively as a consequence of population activity (Figure 4.1B).

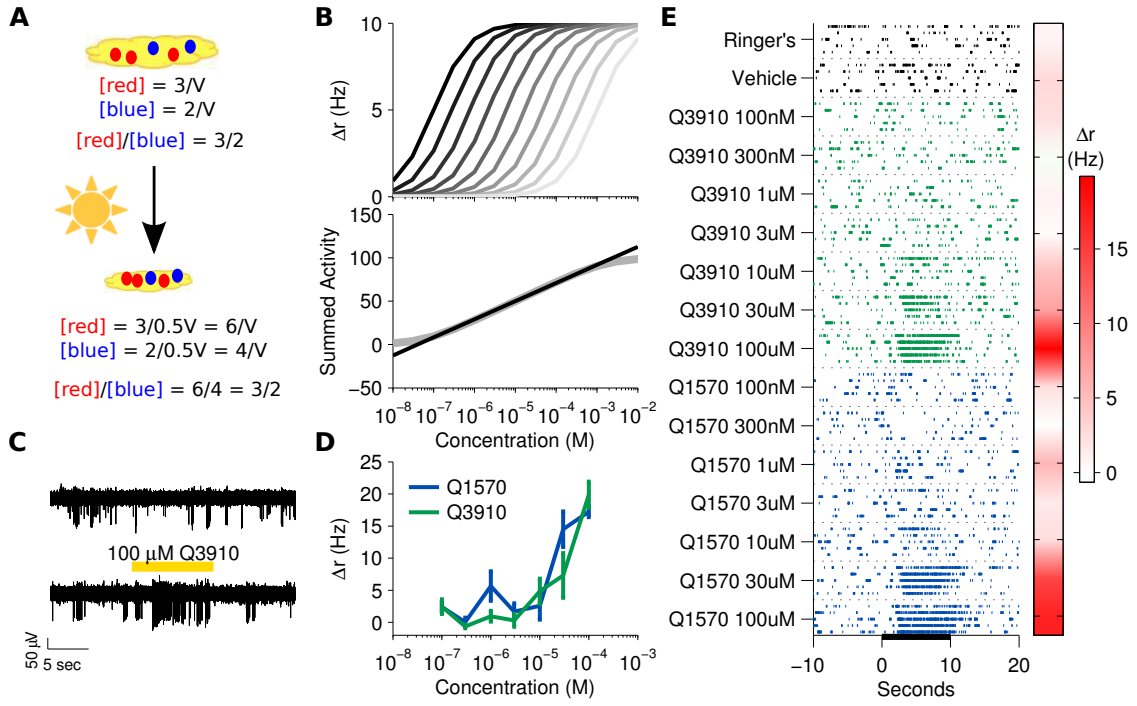

Figure 4.1: VSNs respond to a wide range of concentrations **A** An example of environmental uncertainty facing the AOS. The concentration of ligands measured in a pool of urine depends strongly on environmental uncertainties such as evaporation. However, ratios allow for robust representation of concentration invariant to environmental uncertainties. **B** A population of idealized cells with slightly different sensitivities to the same compound are shown (top). Summing their activity produces a result that is linear with respect to log-concentration (bottom) over the range spanned by the cells. **C** An example voltage trace from a single electrode in response to Ringer's solution control (top) and Q3910 (bottom). The tissue was stimulated for 10 seconds. **D** Summary of average firing rates in response to presented stimuli in the same cell as shown in **C**. Error bars correspond to the standard error of the mean. **E** A raster plot of the same cell shown in **C**,**D** in response to two negative controls and seven concentrations of two different sulfated steroids. Each stimulus was presented five times (rows within each block). Average firing rate is shown on the right.

We began by investigating how individual sensory neurons represent concentration across the large dynamic range of the system. We performed multielectrode array recordings of VSNs in response to three sulfated steroids: two glucocorticoids (Q1570 and Q3910, two "similar" odors) and one androgen (A0225, a more "dissimilar" odor). Each preparation was tested with two of these stimuli, each over a wide range of concentrations, and with binary mixtures of the two compounds. As has been previously reported ([178, 161, 44, 43, 220]), we observed that sulfated steroids induced activity in VSNs. Of 494 total cells (n = 18 mice), 95 were responsive to at least one sulfated steroid (rank-sum test, $p < 0.05$, see Methods).

4.3.1 Individual neurons provide poor representation of log-concentration across a large dynamic range

Receptor-ligand interactions are frequently described by a Hill model [2, 10]. Qualitatively, this model captures three regimes, one at low concentrations in which little or no response is observed, a rising phase where response increases with increasing ligand concentration, and a high-concentration regime in which the response saturates. Applied to the spiking rate of neurons, the Hill model can be written

$$r = r_0 + r_\infty \frac{(c/K)^n}{1 + (c/K)^n}, \tag{4.1}$$

where r is the firing rate, c indicates ligand concentration, K corresponds to the concentration at which the half-max response is achieved (EC_{50}), r_0 is the spontaneous firing rate, r_∞ is the maximum stimulus-induced increase in firing rate, and n reflects the receptor cooperativity. Using this model, the response can be viewed as being roughly linear with respect to log-concentration near EC_{50}. The extent of approximately-linear behavior depends on the Hill coefficient, n; larger values of n correspond to a more narrow dynamic range (Figure 4.2A top), while smaller values indicate a larger concentration span over which the response is approximately log-linear (Figure 4.2A bottom). To investigate whether individual sensory neurons can represent log-concentration across the large dynamic range, we explored the stimulus responses of a population of VSNs in terms of a Hill model.

We tested each VSN using two different sulfated steroids, at concentrations spanning five orders

of magnitude, ranging from 10 nM to 100 μM (Figure 4.1B–D). Of the 95 steroid-responsive cells, a sizable subset showed responses only to the highest concentrations, and thus the fitting parameters were not well-determined by the data. Therefore, here we focused on the 47 cells for which $EC_{50} < 100\mu M$ (for at least one of the two compounds) and $n < 5$. This group of cells was virtually synonymous with the subset responding to at least two of the presented concentrations. Each neuron's responses to both compounds was fit simultaneously to the Hill model, with all parameters shared between the two compounds except the EC_{50}, for which K_1 and K_2 describe the EC_{50} to each of the two compounds. Quality of fit was measured by the p-value of the χ^2 fit, as shown in Figure 4.2B. For 42/47 cells (89%), the Hill model served as a plausible description of their response, in the sense that this model could not be discounted ($p > 0.05$). The Hill coefficient, n, ranged from 0.39 to 4.9, with the majority (23/42) falling between 0.5 and 2 (Figure 4.2C). The EC_{50} varied from 7.7×10^{-8} to 1×10^{-1} M across the population; EC_{50}s greater than 1×10^{-4} M, the highest stimulated concentration, indicated that the cell was not responsive to that particular compound (Figure 4.2D).

As the value of n directly influences the dynamic range of the neuron, we considered individual neurons with high, medium, and low n-values (Figure 4.2E–G, respectively). We fit each cell with a rectified log model (see Methods) to test whether any portion of the cell's response was approximately log-linear (red dotted line). As shown in Figure 4.2E, the cell with a high n ($n = 4.9$) did not exhibit any sizable span over which the response was approximately log-linear, and an attempt at reconstructing log-concentration using a linear relationship (see Methods) exhibited very large errors (Figure 4.2H; mean 0.9 log units of error, maximum 1.81). A mid-range cell ($n = 2.0$) showed approximately log-linear behavior over a larger concentration range (Figure 4.2F). The activity of this neuron could be used to reconstruct log-concentration with slightly better accuracy (Figure 4.2I; mean 0.7 log units of error, maximum 1.1). A low-n cell ($n = 0.76$) appeared to be reasonably log-linear across the tested range (Figure 4.2G). We were able to decode log-concentration from this cell with an average error of 0.4 log-units, with a maximum difference of 0.8 log-units (6-fold). For this particular cell, a log-linear model, $r = m \log \frac{c}{c_0}$, was a statistically plausible ($p > 0.05$) fit. Out of 95 responsive cells, from an initial population of 494 cells, we observed only three cells that appeared to respond log-linearly over such a wide concentration range (3%

of responsive cells, 0.6% of all cells). None of the neurons that were stimulated by the androgen compound, A0225, displayed this property. While it is possible that a rare, specialized population encoding log-concentration exists, it is unclear whether the accessory olfactory system could rely on such neurons for general ratio computation. Consequently, we also explored the possibility of population coding for log-concentration.

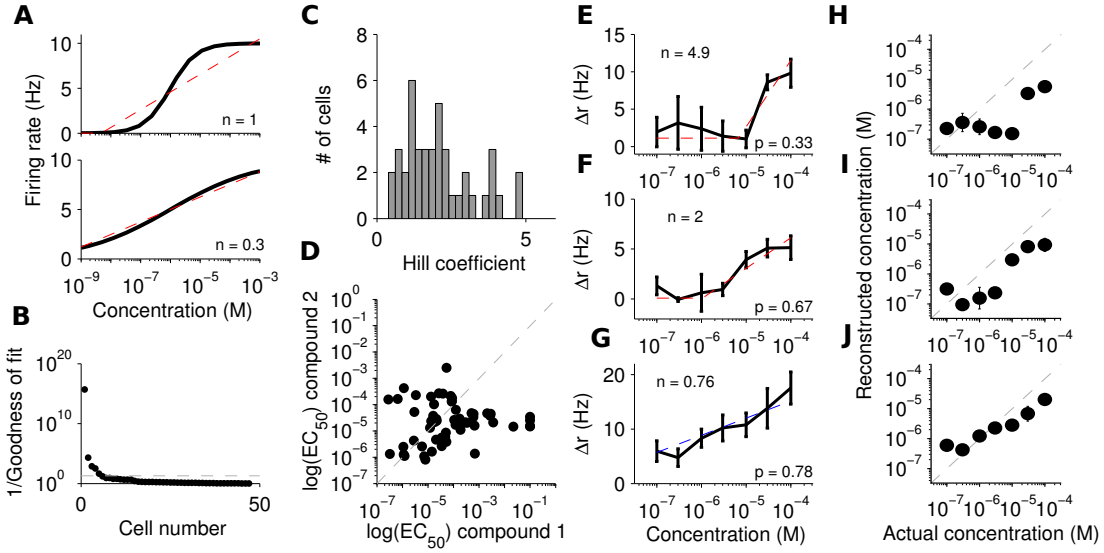

Figure 4.2: Single neuron encoding of log-concentration. **A** (top) Simulated cell with a "typical" Hill-response profile (black line). To demonstrate that the concentrations around the EC_{50} approximate log-concentration, we fit the response with a rectified-log model (red dotted line). (bottom) Another simulated cell with a smaller Hill coefficient. This cell approximates log-concentration over the entire range shown (red dotted line). **B** Goodness of fit to the Hill model for each VSN as measured by the $1/\mathrm{p}$ value to the χ^2 fit. Cells below the dotted line (p=0.05) are well described by the model. **C** Hill coefficients for each VSN. **D** EC_{50} to each compound. **E**–**G** Example cells with with a rectified-log model (red dotted line) or an unrectified log model (blue dotted line). **H**–**J** reconstruction of log-concentration using the response of the cell to the left. Note that while **J** provides a reasonable approximation of log-concentration, **I** does so only at a few higher concentration and **H** does only at non-resposnsive concentrations.

4.3.2 Populations of VSNs can reliably represent log-concentration across a large dynamic range

We tested the idea that populations of neurons could be used to reconstruct log-concentration by using a linear model in which the estimated log-concentration, $\log \hat{c}$, is calculated as $\log \hat{c} = \mathbf{w} \cdot \mathbf{r}$, where $\mathbf{r}$ is the vector of firing rates across the population and $\mathbf{w}$ is a vector of weights. We measured

the firing rate of each cell in the population (Figure 4.3A) to the different concentrations (see Methods) of a sulfated steroid; we then optimized the match between the estimated $\log \hat{c}$ and the actual $\log c$ by least-squares, thereby solving for the weights. Using the response of each cell to compounds presented individually, we were able to reconstruct log-concentration as shown in 4.3B,C. The reconstructed concentration differed from the actual concentration by at most 0.28 log units, less than two-fold, over three orders of magnitude. As compared to the concentration representation by individual cells (Figure 4.2H–J), this scheme proved to be substantially more accurate and robust over a larger range of concentrations, from 300 nM to 100 μM. This suggests that populations of sensory neurons may be better suited to the task of accurately representing concentrations than are individual neurons.

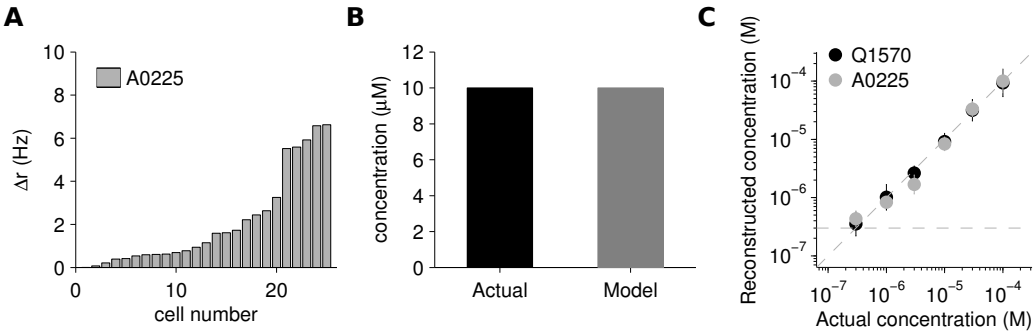

Figure 4.3: Population coding of log-concentration. **A** The activity of 25 cells that were stimulated with 10 μM A0225, sorted by response magnitude. **B** the actual concentration presented (black) and the model reconstruction (gray). **C** Using the firing rates obtained in response to six different concentrations of a sulfated steroid presented individually, log-concentration was accurately reconstructed.

4.3.3 Neuronal responses to stimulus mixtures

Natural stimuli for the AOS, such as urine and other secretions, are complex mixtures [158, 62, 43]. Estimating the relative concentrations of individual components in such mixtures is expected to be far more complex, and is a problem that, in terms of actual neuronal recordings, appears to have received little or no attention.

To explore how mixtures are represented, we presented VSNs with mixtures of two similar (Q1570 and Q3910) or two dissimilar (Q1570 and A0225) sulfated steroids at differing concentrations

and proportions. The two similar compounds have previously been shown to activate overlapping populations of neurons [161, 44], representing a challenging decoding problem with ambiguity in the meaning of each neuron's response. The two dissimilar compounds activate largely non-overlapping populations (data not shown), which might be expected to be a simpler decoding problem.

In addition to the mixtures, each neuron was presented with each pure compound, allowing us to fit the parameters of a Hill model (Figure 4.4A; section 4.3.1). We modeled the response to mixtures in terms of a competitive binding model,

$$r = r_0 + r_\infty \frac{c_{\text{eff}}^n}{1 + c_{\text{eff}}^n}, \qquad \text{where} \quad c_{\text{eff}} = \frac{c_1}{K_1} + \frac{c_2}{K_2}. \tag{4.2}$$

Note that the response to the mixture can be predicted based on the parameters of the fit to pure-compound responses. To test this model, only responsive cells that showed saturation to one or more compounds were used ($n = 24$ cells) (see Methods). An example cell's predicted response compared to the actual response is shown in Figure 4.4B, suggesting that this particular cell was well fit by the competitive binding model. The actual responses and predicted fits are shown for the population of cells in Figure 4.4C. A majority of recorded cells (16/24) were tolerably-well described by this model ($p > 0.001$, χ^2 test), and poorly-fitting cells did not have any obvious systematic departure from the competitive binding model (Figure 4.4C). It is also worth noting that when we re-fit the Hill parameters to the aggregate pure-compound and mixture data (using Eq. 2), the majority (19/24 cells) were well-described (p > 0:05; χ^2 -test). This suggests that this model provides a reasonable description of the responses. In what follows, we employ the more strenuous test of generalizability, where the parameters are fit using only pure-compound data, and then applied to the analysis of mixture data.

4.3.4 Populations of VSNs encode log-concentration of mixture elements

These results show that population activity of sensory neurons can be used to estimate log-concentration of sulfated steroids across a range of concentrations. Since natural stimuli exist as mixtures of active ligands, ultimately we are interested in knowing whether concentration of the individual components can be reconstructed from responses to a mixture. Therefore, we tested whether the same model

as previously described, $\log \hat{c}_i = \mathbf{w}_i \cdot \mathbf{r}$, suffices to reconstruct the log-concentration of all mixture elements (where the subscript refers to the ith compound) from a single set of neuronal responses $\mathbf{r}$.

Crucially, we tuned the weights without "access" to the measured firing rates to mixtures, as we wished to use these responses as an independent test. We therefore limited our tuning data set to responses recorded to each pure compound, across all concentrations. We first considered a "self-tuning" model, in which $\mathbf{w}_1$was tuned using responses to compound 1 but blind to the responses to compound 2, and likewise for $\mathbf{w}_2$. This model reproduces the pure compound log-concentrations well (Figure 4.3C), but performs relatively poorly on the mixtures, particularly in decoding the Q1570 compound (Figure 4.5). The model reconstruction differed from the actual concentration used by as much as 2.57 orders of magnitude, and consistently underestimated Q1570 by at least half a log unit. A likely cause of this poor performance is the fact that some cells respond to both ligands, but tuning the weights for each compound independently does not take this into account (see Methods).

We therefore implemented a "cross-tuning" model, in which the weights were tuned accounting for the possibility of mixtures. To implement this tuning without using the measured responses to mixtures, we used the Hill parameters to calculate the efficacy, c_{eff} (4.2), and then used this to "simulate" the responses to mixtures (see Methods). This produces a "predicted" response profile for each mixture condition, and hence is a "cross-tuning" model in the sense that an allowance is made in the least-squares procedure for the simultaneous presence of both compounds. However, all the data for tuning comes from just the pure compound responses.

We then tested this cross-tuning model against firing rates obtained in response to mixtures. As before, this was done for both the "easier" case (Q1570 and A0225) and the "harder" case (Q1570 and Q3910). As shown in Figure 4.6, the cross-tuning model was considerably more effective than naïve self-tuning. Over three orders of magnitude of concentration, the error ranged from 0.003 to 1.74 log-units (Q1570). This suggests that populations of VSNs could be used to represent both log-concentration and identity over a large range of concentrations.

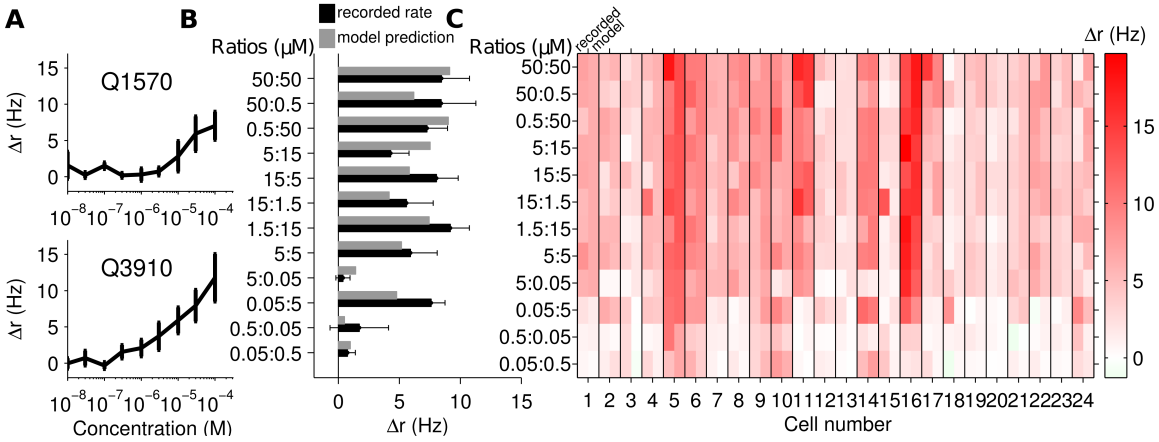

Figure 4.4: Competitive binding. **A** The response of a cell to a range of concentrations of Q1570 (top) and Q3910 (bottom). **B** The response of the same cell to binary mixtures of Q1570 and Q3910 (black). Using the Hill model parameters fit to this cell previously, we predicted the expected firing rate to these mixtures given that the cell follows competitive binding (gray). The model fit and recorded rates closely agree, evidence for the competitive binding model. **C** The recorded response (left side of each column) and predicted response (right side of each column) to sulfated steroid mixtures across the population.

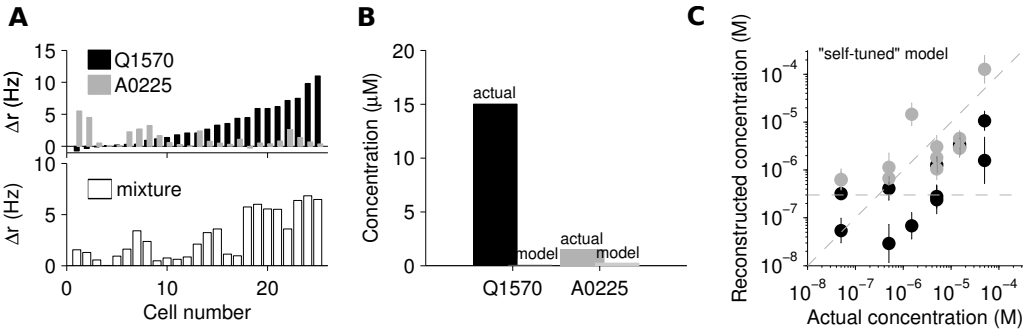

Figure 4.5: Population coding of log-concentration. **A** The response of a population of cells stimulated with 30 μM Q1570 (black) and 3 μM A0225 (gray), presented individually (top). (bottom) The response of the same population of cells to the mixture of the two compounds at half their concentrations (15 μM Q1570 and 1.5 μM A0225). **B** using weights set from responses to pure compounds, we tested the model with the responses to mixtures. The actual versus model reconstructed concentrations are shown. The model poorly reconstructs the concentration of both compounds. **C** Mixture element concentration reconstruction using the same technique described in **B** across a larger range of concentrations. The reconstructed concentration does not appear to accurately capture the stimulated concentration across the range of stimuli.

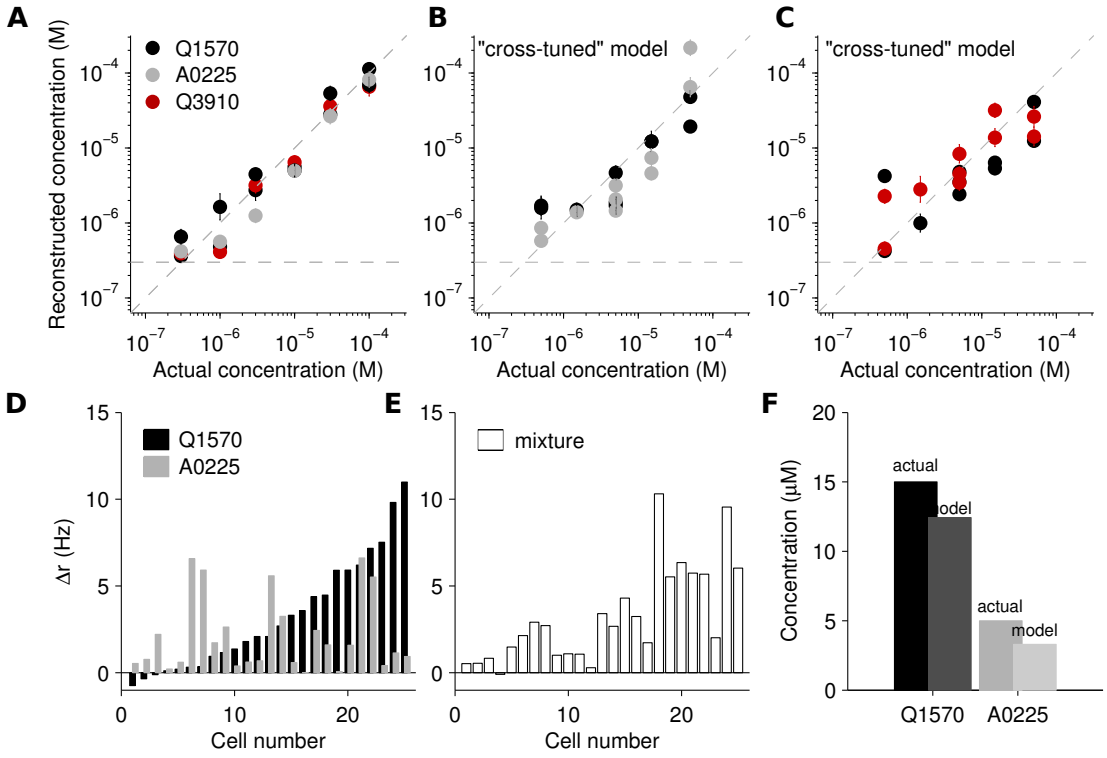

Figure 4.6: Population coding taking nonlinearities into account. **A** reconstructed versus actual concentration in response to the pure compounds of Q1570, A0225 and Q3910 presented individually. Error bars indicate standard error. **B,C** Reconstructed versus actual concentration of mixture components using two populations of neurons. Using the recorded responses to mixtures, the model was able to disambiguate mixture elements and concentrations. **D** The response of a population of cells to two sulfated steroids presented separately (30 μM Q1570 and 10 μM A0225). **E** the response of the same population in the same order, to the mixture of the two compounds at half their original concentrations (15 μM Q1570 and 5 μM A0225). **F** The model reconstruction of each element of the mixture compared to the actual concentrations of the mixture elements.

4.3.5 Model parameters

We explored the model parameters to identify what features the model emphasized when setting the optimal weights. In both populations of cells, a few cells were heavily utilized (Figure 4.7A,B). This suggests that perhaps equivalent results might be obtained using only a subset of the neuronal population (Figure 4.7C,D). To explore this dependence, we first identified the cell that was most accurate in reconstructing log-concentration. We then found the cell that when combined with the first, reduced the error the most, and kept adding the "best" cells until all were used. In the first population of cells stimulated with Q1570 and A0225 ("easier" case), 81% of error reduction was accomplished with only three cells, indicating that a quite small subset suffices for reasonably-accurate reconstruction. In the second population stimulated with Q1570 and Q3910 ("harder" case), the three "best" cells reduced the error by 62%. In both cases, the minimum error was obtained with a subset of neurons, 13/25 cells in the first case and 15/38 cells in the second, reflecting generalization error as the number of parameters in the model increased. In some cases, these "extra" cells incorporated beyond the minimum point were unreliable across trials, in other cases they were redundant cells in that there was a more reliable cell with a very similar response profile that was more valuable in recreating log-concentration. This emphasis on more reliable cells can be observed in Figure 4.7E,F, which reveals that model weight varied inversely with estimated variance in the EC_{50}. The general trend across both populations was that cells with lower variance, or more reproducibility, tended to be utilized in the reconstruction more heavily.

4.3.6 Populations of VSNs can be used to represent ratios

Using the log-concentration responses, we tested whether log-ratios could be computed from VSN activity, based on the idea that $\log c_1 - \log c_2 = \log c_1/c_2$. We used the log-concentrations decoded in response to sulfated steroid mixtures and compared the reconstruction to the actual log-ratio presented. As shown in Figure 4.8, the reconstructed ratios reflected the actual ratios. Ratios ranged from 1:1 to 1:100 with stimuli ranging from 300 nM to 100 μM. The greatest error observed was in the 1 μM : 100 μM Q1570:Q3910 mixture, which differed from the actual value by 1.75 orders of magnitude. The Q1570:Q3910 population is a harder case in that cells responded to both com-

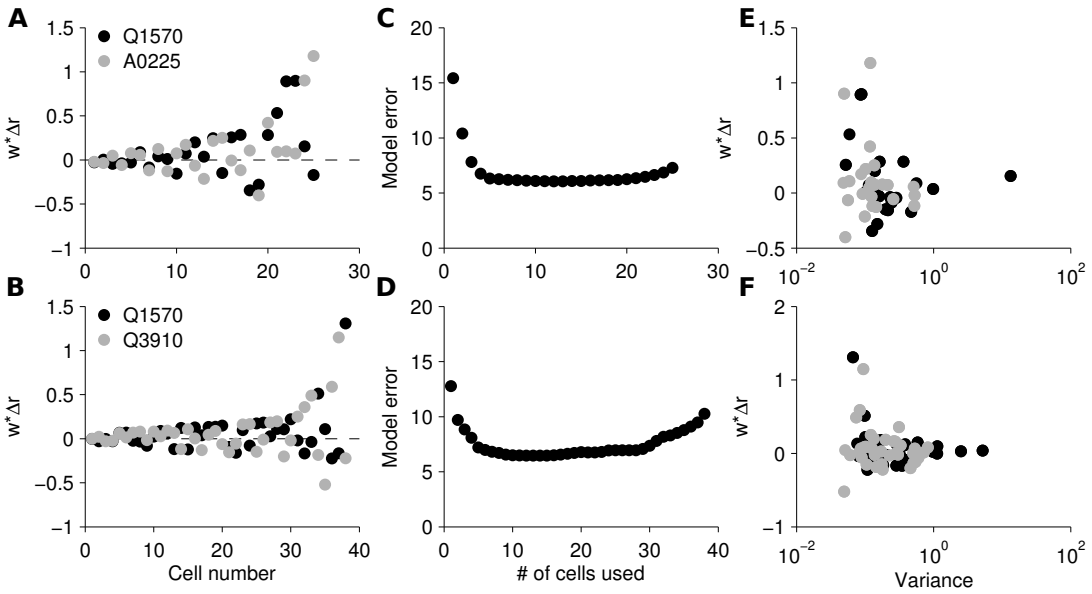

Figure 4.7: Contributions of individual neurons to reconstruction. **A,B** Weight times the maximum firing rate of that cell, corresponding to throughput, or how much information the cell contributed. Each cell has two weights, one per compound. Cells are ordered based on maximum $w \times \Delta r$. **C,D** Model error as a function of numbers of cells used (Q1570, A0225 top, Q1570, Q3910 bottom), starting with the most informative cells. Model error corresponds to the sum of squares error. **E,F** Weight times maximum firing rate (as in A,B) as a function of variance in the fit of the EC_{50} value in the Hill model fitting. The more reliable cells (with smaller variance) tend to be the most heavily used by the model.

pounds, often with equal affinity. Therefore, it is unsurprising that the reconstruction was slightly less accurate given the finite population of recorded cells.

These results provide the first evidence, to our knowledge, that ratio and logarithmic coding in olfaction can be generated from actual neuronal responses, thus providing a robust encoding scheme for the accessory olfactory system.

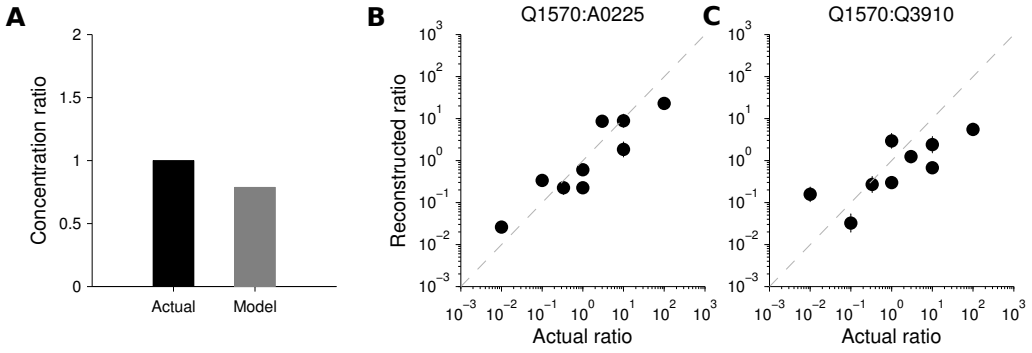

Figure 4.8: Log-ratio reconstruction. **A** Actual and model reconstructed ratio for an example ratio. The example mixture was of $5\mu M$ Q1570 and $5\mu M$ A0225. **B,C** Actual versus model reconstruction of the log-ratio using two different populations of VSNs. Error bars (s.e.m.) are typically smaller than the points .

4.4 Discussion

We have demonstrated that in principle the accessory olfactory system is capable of representing concentration information in a robust manner through the use of log-ratios. Activity of populations of VSNs can be weighted and summed to represent log-concentration and the log-ratio. In particular, with an appropriate model, it sufficed to tune the parameters using responses just to individual components; the resulting model was able to accurately reconstruct log-concentration of both components of mixtures. Using neuronal data recorded from sensory neurons, we demonstrated the viability of this coding scheme that allows the AOS to represent concentration in a robust manner that is both sensitive to changes in relative concentrations of stimuli yet insensitive to changes in absolute concentration.

4.4.1 Ratio coding and the accessory olfactory system

Ratio-computation is particularly well suited for the mouse AOS. This system is specialized to detect non-volatile ligands present as mixtures in bodily substances such as facial secretions and urine [158, 221]. The vomeronasal organ in the nasal cavity contains a blood vessel acting as a pump that draws the liquid stimuli into contact with receptor neurons when the mouse makes direct contact with the stimulus [111]. In contrast, the main olfactory system detects volatile compounds. Differences in volatility between ligands will result in different rates of evaporation and therefore non-stable concentration ratios. The non-volatile nature of AOS stimuli implies that these ligands do not evaporate when left in the environment. While the absolute concentration of each ligand will vary with solvent (water) evaporation, the relative concentration of compounds will not change. Consequently, this presents an ideal system to use, and explore, ratio coding.

4.4.2 Biological plausibility of log-ratio coding

A strength of this model is that it is based on biologically plausible constructs. It incorporates weighted summation and subtraction, operations that can be readily accomplished via synaptic scaling, pooling, and a combination of excitatory and inhibitory circuitry. One prerequisite for log-encoding over a large concentration range is diversity in the sensitivities of different sensory neurons (Figure 4.1B), a requirement that was met by our observed data (Figure 4.2C). It is unknown whether these differences in sensitivities are due to neurons expressing the same receptor with different expression levels [222] or due to expression of different, possibly closely related receptors, each with a different threshold. It is unlikely that this phenomenon results from combinatorial expression of multiple receptors as VSNs are thought to express one, or a few [117] types of receptors out of around 300 known varieties [110].

From the vomeronasal organ, it is known that receptor neurons project into glomeruli in the AOB in which an individual glomerulus receives input from only one type of receptor neuron [128, 116]. Unlike in the main olfactory bulb, mitral cells, the projection neuron out of the AOB, receive input from multiple glomeruli. Based on anatomical data, whether these mitral cells receive redundant input [131], input from different receptor types [132], input from similarly responsive sensory neu-

rons, or some combination thereof, is unknown. However, a comparison of sulfated steroid responses in VSNs versus in mitral cells in the AOB suggests that most processing streams largely maintain segregation, with a few cases of mixing observed [44]. This may support the notion that mixed inputs, when they exists, may serve to expand the dynamic range of the mitral cells but maintain the stimulus-specificity of VSNs.

The AOB also contains laterally-inhibitory circuitry [46, 88], which might in principle compute the difference between log-concentrations. Consequently, in the AOS it seems possible that ratio-representation might be observed as early as the mitral cell level.

4.4.3 Concentration response of VSNs and logarithmic coding

Using multielectrode array recordings of sensory neurons in the VNO, we measured the response of a group of cells to a range of concentrations of sulfated steroids as well as binary mixtures. The response of individual neurons could be modeled using the Hill model, which has previously been used to describe sensory neuron activity in both the accessory [150, 171, 220] and main olfactory systems [2, 10]. The rising phase of a Hill-fit response approximates logarithmic coding, and potentially is a possible way in which the system could represent log-concentration. In fact, a model of concentration invariance proposed by Hopfield [31, 30] and directly applied to ratio-coding by Uchida and Mainen [32] is based on the idea that logarithmic coding can be approximated by receptor-ligand interactions from threshold to saturation. The activities of VSNs were able to fit with a rectified-log model (Figure 4.2E-G). However, the concentration range over which the cells were linear varied widely across the population from a very narrow to a wider range (Figure 4.2C,D), and many cells did saturate over our target concentration range. We did observe a few neurons that responded in a nearly log-linear fashion over our tested concentration range (Figure 4.2G); however, these cells were very rare ($n = 3/494$ cells), and this pattern of activity was only observed in response to a subset of stimuli.

4.4.4 Population coding to represent log-concentration

Single-neuron encoding schemes face a major interpretive challenge: when a cell responds to more than one stimulus [44, 161] (Figure 4.1D), the readout of a neuron's response is ambiguous. For

this reason, the diversity of activity of VSNs is ideal for a population coding scheme that allows for a reliable representation of log-concentration across a large dynamic range. Our model implements a weighted summation of populations of sensory neurons in order to reconstruct log-concentration; log-ratios can then be computed by subtraction.

We identified a key computational challenge facing this system. Simply tuning the model weights in response to each compound individually yields poor results for mixtures (Figure 4.5) because of the existence of neurons responding to both components of the mixture. Significantly better results are obtained when these overlaps are taken into consideration (Figure 4.6).

This study extensively tested mixtures of two compounds. However natural stimuli for the AOS, like urine, are complex mixtures of many compounds. Therefore, for this to be a realistic coding scheme, it must be capable of scaling to larger numbers of ligands. At the level of two compounds, the "cross-tuning" model's success emphasized the importance of accounting for the complete receptive field of individual neurons. For an arbitrarily large number of stimuli, what kind of interactions may occur at the receptor level and how might the system, or model, handle the diversity? VSN tuning is determined by receptor expression, and the receptors are activated by only a specific set of stimuli. Previous studies have demonstrated that VSNs respond to one or a few sulfated steroids when presented individually [44, 161], implying that the response of single neurons will be determined by only a small number of compounds out of a complex mixture. This limits the scope of the "cross-tuning" required for more naturalistic, complex stimuli.

The log-concentration model essentially comes down to weighted summation, or synaptic weights, and inhibitory circuitry, or subtraction. How might the system set these weights? One possibility is that the AOS is wired in development to compute ratios — sensory neurons are pooled in glomeruli and lateral circuitry is established with specific strengths, set over the course of evolution. Another possibility is that experience shapes the computation, in which the AOS changes synaptic weights based on stimuli present in the environment or specific social cues that are relevant at particular times or environments.

This study is the first to demonstrate that both logarithmic and ratio coding can be obtained quantitatively from experimentally-observed neuronal data. This represents a biologically plausible model in which populations of neurons can be used to achieve robust detection of concentration

across a very wide dynamic range.

5 Behavioral investigation into accessory olfactory mediated stimulus detection

5.1 Introduction

A thorough understanding of a sensory system requires an exploration of stimulus-driven behavior. Ideally, this can be done both in a naturalistic setting as well as under tight experimental control and manipulation. Making a connection between stimulus and behavior and being able to explore components such as perceptibility, timing, and performance in an experimenter-controlled manner can provide a sophisticated understanding as to how the sensory system of an animal operates. For example, in the main olfactory field, much work has been done to characterize stimulus coding, perception and discriminability of complex mixtures and timing (for review see [223, 224, 225, 226]). Studies frequently use some variation of an olfactometer — a device that provides precise stimulus control, both in amount and timing, paired with an operant conditioning paradigm. This allows animals to be trained to associate a reward or punishment with a stimulus and then behave appropriately to maximize reward and minimize punishment, effectively self-reporting their detection abilities. By manipulating the stimuli, delivery, and conditions, the experimenter can learn a great deal about the sensory system.

The accessory olfactory system (AOS) is currently lacking in such an experimental paradigm, in part because it is in many ways a lesser understood sensory system. The AOS is a specialized olfactory system possessed by most terrestrial animals other than humans and old world apes. It is involved in detecting cues found in urine and other secretions that mediate social behaviors such as aggression, reproduction and individual recognition. Compared to the main olfactory or taste fields little is known about the AOS. While it is recognized that urine and facial secretions activate the AOS, the number of known specific stimuli is limited to sulfated steroids as the largest class [43],

exocrine secreting peptides [158], and more controversially, other proteins [153, 62, 126, 127] (see Chapter 1.2.5 for discussion). Main olfactory and taste system cues are assumed to be consciously perceived, however, it is not known if this is the case for AOS stimuli.. Behaviors mediated by the AOS include hormonal regulation such as estrous induction [42], pregnancy block [77], and aggression [42]. These are complex and often slow behaviors on the timescale of minutes, hours, or days. It is unclear as to how, or even if, stimuli eliciting such behavior may be perceived. In addition, AOS circuitry does not go through cortex directly [147], unlike other sensory systems. This suggests that AOS stimuli might not be consciously perceived [227, 42]. However, AOS stimuli might be detected at a level sufficient for awareness. It has been suggested that AOS stimuli are intrinsically rewarding [42]. In an experiment involving garter snakes, the animals were trained to discriminate two visual patterns to receive a reward of prey extract, known to activate the snake VNO [42], suggesting some level of awareness as the animals were able to link the AOS-mediated reward to a stimulus. Here, we test the ability to link an AOS-mediated stimulus with a reward for the purpose of developing an olfactometer-type behavioral paradigm.

A device allowing experimenters to control stimulus delivery and record detection would be of great use to the AOS field as no such behavioral setup exists. In addition to providing insight into whether or not AOS stimuli can be perceived, it can also be a useful stimulus screen to enrich the study of detection and encoding of ligands and mixtures in the AOS. Ultimately, it could be paired with in vivo recording, allowing us to investigate coding questions in an awake behaving animal with precisely controlled stimulus delivery. Therefore, we set out to develop a behavioral setup in which a mouse can be trained to indicate the presence of a particular AOS stimulus through operant conditioning in a go/no-go task. The taste field has its gustometer, main olfaction has its olfactometer. Here, we present our attempt to develop the AOS equivalent, termed "the vomerometer".

5.2 Materials and methods

5.2.1 Animals

Adult mice, both male and female 3 to 9 months of age were used. Wild type mice were of the C57B/6J strain. The TrpC2$^{-/-}$ animals had the TrpC2 channel genetically ablated [54]. TrpC2 animals were also on a C57B/6J background. As a control, litter-mates heterozygous for the TrpC2 mutation were used. Genetic identity was confirmed using genotyping for the mutant and wild-type TrpC2 gene. In studies using a mix of genotypes, the experimenter was blind to the genotype of the animals until all experiments were completed. All experimental protocols followed the United States Animal Welfare Acts and National Institutes of Health guidelines and were approved by the Washington University Animal Studies Committee.

5.2.2 Solutions

Sulfated steroid (Q1570) and Ringer's solutions were as described in Section 2. Mouse urine was collected from male mice of the CBA strain as described in Section 2.

5.2.3 Vomerometer

The vomerometer consists of a slightly modified computer-controlled eight-channel gustometer (Knosys, Lutz, FL) [228] (Figure5.1A). The device was attached to a computer and Knosys software, written in BBC basic, was used to control the apparatus. Mice were tested in a clear Plexiglas operant chamber (17x12x12 cm) with a metal floor and a 1 cm diameter opening 2 cm from the floor on one end and a fan on the other end to reduce olfactory cues. A metal lick-tube was positioned in the opening for dispensing stimuli. The lick tube contained eight independent stainless steel channels recessed 2 mm within the tube, each one attached to an unpressurized stimulus channel using c-flex tubing (Cole-Parmer, Court Vernon Hills, IL). The stimulus barrels consisted of 3 ml syringes with the plunger removed attached to a blunted 18-gauge needle. The needle attached to the c-flex tubing that runs through a computer controlled solenoid valve to stop and start fluid flow. The stimulus barrels were positioned at least 20 cm above the chamber. When the mouse licked the drink tube, a very mild current (65 μA) was passed from the tube to the floor through the mouse

to allow for monitoring of the lick behavior. A piece of paper folded in half was placed on top of the plexiglass chamber to darken the chamber and a white noise machine (White Noise Lite "App" played on an HTC Thunderbolt cellular phone) was placed below the paper, speakers facing the chamber, to generate a white noise sound at maximum volume. The chamber was wiped down with Clidox-S between animals and prior to beginning any session.

Stimulus barrels were calibrated prior to use such that each tube delivered approximately the same amount of stimulus over a 30 second time window when all valves were opened. By measuring the volume of liquid expelled over a set amount of time, we were able to determine how long to open each valve so as to deliver the ideal amount of stimulus. To deliver 4 μl of liquid, valves were opened for 200 msec.

5.2.4 Acclimation

10 days prior to beginning experimentation, mice were separated from their home cage and housed individually. They were kept on a restricted water schedule and given 1 ml water per day. Food was delivered *ad lib*. Mice were monitored for health daily and kept within 85% of their original body weight.

After 10 days of water deprivation, mice began acclimation to the testing chamber to learn the general licking procedure. A drop of water was placed on the end of the lick tube and the mouse was allowed to explore. The control program was designed to mimic the experimental setup in which the mouse licks the tube, the stimulus is dispensed, there is a decision window, and then an outcome followed by an inter-trial interval (ITI). The acclimation program used a 1 second decision window and a 4 second ITI delivering 4 μl of water for the stimulus and reward. The mice were given 15 minutes from the time of the first lick or 30 minutes maximum from being placed in the chamber to lick freely. Each mouse was trained at most once per day for as many days as required such that the mouse completed at least 100 trials in the allotted time (1–3 days). Upon completing the time interval, the mice were returned to their home cages and given 1 ml of water minus the amount of water received during training, at least 15 minutes after being returned to their cage.

5.2.5 Training procedure

Following successful completion of the acclimation protocol, we began training the mice to discriminate two stimuli. Two stimulus barrels were filled with the S^- or test solution and two with the S^+ solution, typically Ringer's solution or water. One barrel was filled with water used to reward correct completion of S^+ trials. While the specific timing of stimulus delivery varied, the general outline was consistent (see Figure 5.1B for a schematic outline). The mouse licked the tube and 4 μl of stimulus was randomly delivered. The mouse had a set time to decide followed by a set response period in which the mouse had to lick or not to report if the stimulus was an S^+ stimulus (lick) or an S^- stimulus (do not lick). If the mouse licked in response to an S^- stimulus, a mild shock was delivered to the mouse's tongue and a loud beep played. The intensity of the shock was set to the minimum voltage required to elicit a response, such as a very short break in licking, and was increased and decreased throughout the experiment as needed. The mouse was also given a punishment "time-out" of 3 times the ITI duration, in which licking the tube had no effect. When a mouse correctly responded to an S^+ stimulus by licking, a 4 μl water reward was delivered. Nothing happened following a correct S^- or incorrect S^+ trial. Each mouse performed anywhere from 80–120 trials. Initially, they were started on 80 trials and increased to 100 or 120 trials as they became faster. Following the experiment, mice were returned to their home cage and after at least 15 minutes, were given 1 ml water minus the amount given as reward during training.

5.2.6 Measuring performance

The outcome of each trial was automatically recorded by the Knosys software. Trials were divided into blocks of 20 and the percent correct within each block was recorded. The type of correct outcome, true positive or true negative, was also recorded. To assess significant performance, the percent correct of each block was quantified using a t-test.

5.2.7 Sulfated steroid purification

Thin-layer chromatography (TLC) was performed as previously described [43]. A 100 mM solution of Q1570 in water was diluted in methanol then run on chromatographic plates. A water control

was also diluted in methanol and run on plates following the same procedure. Compounds were extracted in methanol and further diluted in water. Purity and identity was verified using mass spectroscopy.

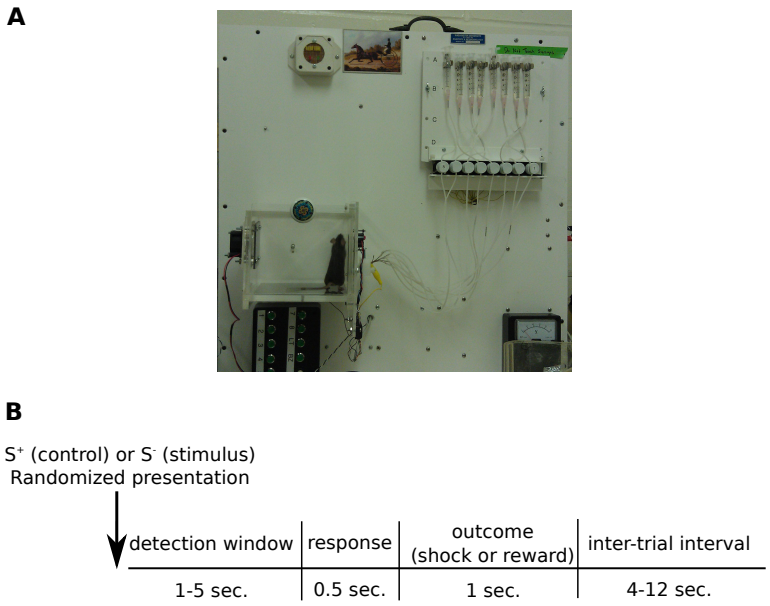

Figure 5.1: Vomerometer. **A,** Photograph of apparatus with a mouse in the chamber. A metal lick tube extends out of the chamber and connects with the eight stimulus valves. **B,** A schematic of the procedure.

5.3 Results

5.3.1 The vomerometer

As described in section 5.2, the vomerometer is largely an unmodified commercially available gustometer from Knosys, Inc. We took advantage of the fact that AOS stimuli are non-volatile and often occur in liquid form. The animal is required to make direct contact with a liquid stimulus which is drawn into contact with receptors in the vomeronasal organ (VNO) at the base of the nasal cavity by a pumping mechanism consisting of a blood vessel. Little is known about the pump dynamics, but it appears to be active in novel conditions [111]. While it is unknown whether or not stimuli can access the VNO during licking, and if so, if it is pump-dependent, some preliminary evidence using dye-spiked urine suggests that liquid can enter the VNO in response to nose contact with the liquid (T. Holy, unpublished observations).

A photograph of the device with a mouse in the operant chamber is shown in Figure 5.1A. The mouse has access to a lick tube which is connected to eight stimulus tubes. Precise opening and closing of solenoid valves gives temporal control over stimulus delivery. The lick tube maintains separate stimulus lines, avoiding cross contamination. The mouse licks the tube, stimulus is delivered, presumably the stimulus enters the VNO, and then the mouse has a time window to decide to lick or not.

5.3.2 Mice can be trained to discriminate tastants

To verify the experimental setup, we trained mice to discriminate a 1% NaCl solution (S^-) from water (S^+), a task previously demonstrated in rodents [228, 229] and in mice using the exact apparatus (Burt Slotnick, personal communication). The training procedure was as indicated above and in Figure 5.1B. Mice were given a 1 sec decision window with a 0.5 second reporting period. The ITI was 4 seconds. This process was initially conducted with no water reward for correct S^+ trials. After four days and 18–23 trial blocks, mice were only performing at an average percent correct rate of 56-76% ($n = 3$ mice) (Figure 5.2A). To boost performance, we added the water reward upon correct S^+ performance. A naïve group of three mice were trained with a water reward and learned more rapidly. On the second day of training two of the mice performed above 75% correct and the third mouse was capable of discrimination on the third day (Figure 5.2B).

5.3.3 Finding the optimal time window

The accessory olfactory system is known to be a very slow system compared to other sensory systems. In an awake, behaving mouse, stimulus responses in the AOB fail to appear for at least 3.6 seconds [151] or at least 4.3 seconds [113]. In addition, the AOS may mediate behaviors operating on a very slow timescale (hours to days) such as pregnancy block [83]. Therefore, the optimal time window for detection is not obvious. Initial NaCl tests used 1 second (Figure 5.2A), however, the minimum of 3 seconds needed to elicit a response in the AOB suggests that stimulus information may not fully propagate to the brain within 1 second. We decided to first use a time window greater than the largest minimum time to observe firing increases in the AOB: 5 seconds.

Five seconds is a much larger time window between the stimulus delivery and outcome than we

have observed in the gustometer or olfactometer literature. Therefore, it was unclear if this time window was too long for mice to link any stimulus and reward, and therefore, too long to learn. We tested naïve mice ($n = 3$) using 1% NaCl versus water to see if they could learn to associate the stimulus with the outcome over the 5 second time window. The mice rapidly learned the task (Figure 5.2B). In the interest of speeding up the task, we eventually decreased the decision window to 3 seconds.

5.3.4 Initial difficulties discriminating sulfated steroids

After successfully training mice to discriminate 1% NaCl solution from water, we reasoned that the mice may have an understanding of the task and might then be able to discriminate sulfated steroid in Ringer's solution from Ringer's solution. Therefore, using the same three mice and the same task, we changed the S^- stimulus to 100 μM Q1570 (corticosterone 21-sulfate) and the S^+ stimulus to Ringer's solution. After 5-7 days (25-35 blocks of trials), the mice were able to perform at a level better than chance (t-test, $p < 0.05$). However, their performance rarely exceeded 75% correct on any given trial block versus greater than 80% correct with NaCl (Figure 5.2C).

5.3.5 Gradual training increases performance

In the first round of sulfated steroid discrimination, we trained the mice to discriminate a tastant and then switched sensory modalities. A more gradual transition might be more instructive. Therefore, we devised a new training protocol in which mice were initially trained to discriminate mouse urine diluted in Ringer's with added sulfated steroid from Ringer's. Then we slowly decreased the urine concentration until the mouse was tested on sulfated steroid versus Ringer's solution. Urine is known to contain AOS-detected cues as well as main olfactory (even to human MOS), and likely taste cues. Therefore, the mouse might initially associate the stimulus with an AOS cue and learn to use this system. Since mice do not encounter isolated sulfated steroids in nature, the sudden introduction of sulfated steroid, as previously presented, may be sufficiently unnaturalistic.

We began training mice to discriminate 100 or 1000-fold diluted CBA male mouse urine with 50–100μM Q1570 from Ringer's solution. To test for AOS-dependance of performance, in Section 5.3.6 we will use mice with a genetically ablated TrpC2 gene, an essential part of the signal transduction

pathway in VSNs [54]. All mice used for initial training were wild type or heterozygous for a functional TrpC2 gene. The urine dilution was progressively reduced in 10-fold increments, waiting for each mouse to achieve criterion-level performance (>75% accuracy averaged over the day) at each dilution before progressing to the next. After a mouse was capable of discriminating 100,000-fold diluted urine with Q1570 from Ringer's, the mouse was tasked with discriminating between Q1570 in Ringer's and Ringer's solution. Mice learned to discriminate sulfated steroid from Ringer's after anywhere from 1 to 5 days (100-500 trials). The performance of all mice under the same conditions averaged over the last day of each stimulus is shown in Figure 5.3A. Mice were capable of discriminating sulfated steroid from Ringer's with approximately 65% accuracy on average. While this performance was below that observed in the tastant task, it is still above chance.

5.3.6 Sulfated steroid discrimination may not be AOS mediated

Mice appeared to be capable of discriminating sulfated steroids from Ringer's. However, this may not be due purely to AOS cues. While there is no evidence to suggest so, sulfated steroids may be detected by taste receptors or main olfactory receptors. There also may be non-chemosensory cues, such as different flow rates in the stimulus tubes or clicks made when valves open.

To address the AOS-dependance of sulfated steroid discrimination, we used a mouse with a non-functional TrpC2 channel. Previous studies have demonstrated a lack of response to urine [54] and sulfated steroids [43, 168] in TrpC2$^{-/-}$ sensory neurons. If the mice were detecting the difference between stimuli using their accessory olfactory systems, then the TrpC2$^{-/-}$ mice should be incapable of learning to discriminate sulfated steroids. However, they should still be able to discriminate urine from Ringer's, since urine contains MOS and presumably taste cues as well.

We tested 8 mice with non-functional AOS. Their behavioral results are shown in Figure 5.3B, compared with their TrpC2$^{+/-}$ litter-mates and other wild-type mice from the same genetic background in Figure 5.3A. These mice were capable not only of discriminating diluted urine, but also of discriminating sulfated steroids, contrary to what was expected. One possible explanation is that these mice were able to taste or smell sulfated steroids independently of their AOS. Another possibility is that there is still some residual AOS function left [230]. A third possibility is that the mice were using an external cue. We took care to remove sound cues by playing loud white noise,

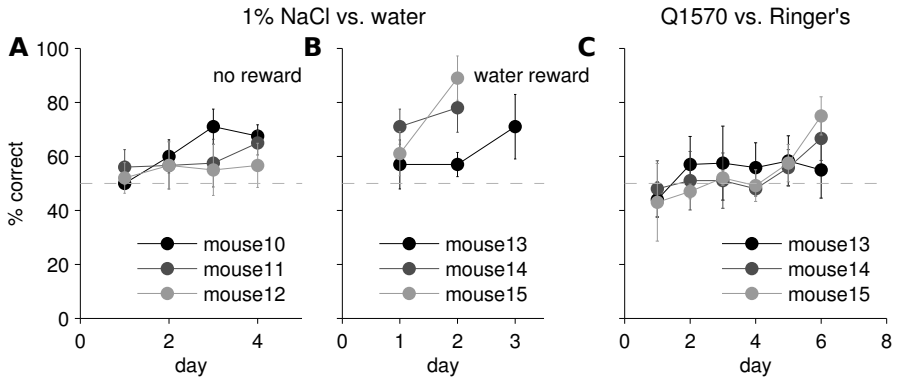

Figure 5.2: Mice can discriminate tastants. **A,** Three different mice can partially discriminate 1% NaCl solution from water. Each dot is the average of 80-100 trials performed in a single day. Error bars correspond to standard deviation. These mice were not rewarded for a correct S^+ trial, but were punished for an incorrect S^- trial. **B,** Three different mice were capable of learning to discriminate NaCl from water within 1-3 days. These mice were given a water reward upon completion of a correct S^+ trial. **C,** The same mice as in panel **B** were challenged to discriminate 100 μM Q1570 in Ringer's solution from Ringer's solution. By day seven, some of the mice may have demonstrated learning.

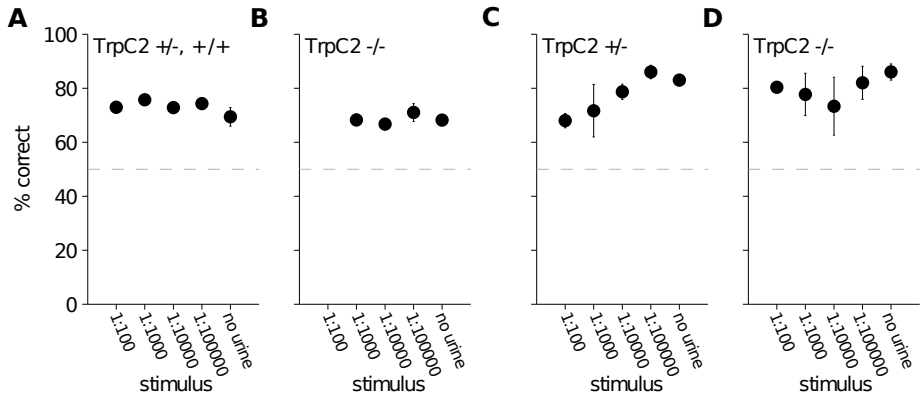

Figure 5.3: Mice with and without a functional TrpC2 channel can discriminate between sulfated steroid and Ringer's solution. **A,** The results of the final day of each stimulus (100 trials) averaged across 11 wild-type and $TrpC2^{+/-}$ mice. Mice were adept at discriminating each stimulus. **B**, Performance of 8 $TrpC2^{-/-}$ mice run in parallel to those in panel A. These mice were also capable of discriminating all stimuli. **C,D,** A separate group of 3 $TrpC2^{+/-}$ mice (**C**) and 3 $TrpC2^{-/-}$ (**D**) trained to discriminate sulfated steroid from Ringer's. Tube placement was scrambled and tubing was changed to eliminate unintended cues.

however, this may not have masked all sounds and would have no impact on any flow rate differences across stimulus tubes. To disambiguate these possibilities, we tested the mice on Ringer's versus Ringer's. This eliminates any taste or smell component of the stimulus but preserves flow rate and noise cues. In 6 of the mice shown in Figure 5.3A,B, we arbitrarily assigned two tubes of Ringer's to S^+ and two to S^- the day after discontinuing the sulfated steroid test (Figure 5.4A). We also trained a separate batch of four mice. First they were trained to discriminate diluted urine from Ringer's. Then, instead of using sulfated steroid, we used S^+ Ringer's and S^- Ringer's. As shown in Figure 5.4B day 1, there appeared to be a slight bias, indicating that the mice were picking up on some cue from the tube rather than from the stimulus source.

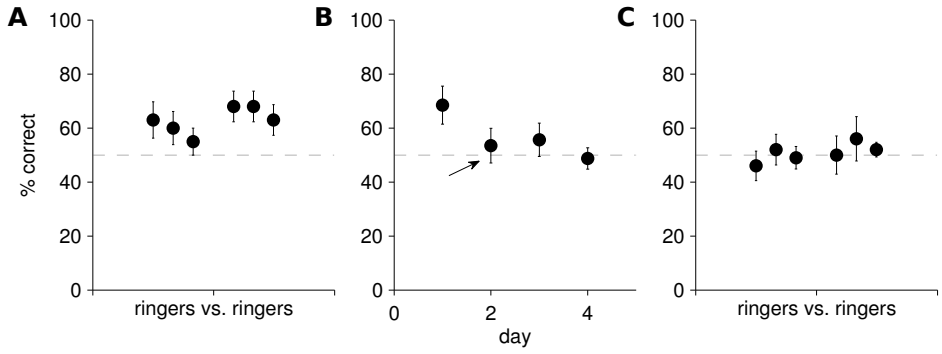

Figure 5.4: Non-stimulus dependent discrimination. **A,** Six mice were presented with identical S^+ and S^- tubes of Ringer's solution after completing sulfated steroid discrimination (these mice are included in Figure 5.3**A**,**B**). Each dot represents the average performance over 5 blocks of 20 trials. **B,** Four mice were trained to discriminate urine from Ringer's, then switched to Ringer's versus Ringer's. Each dot represents the average performance across all four mice on a single day. On the second and subsequent days, as indicated by the arrow, tube and valve locations were scrambled, removing any bias. **C,** Six mice were trained to discriminate sulfated steroid from Ringer's (Figure 5.3**C**,**D**), then presented with Ringer's versus Ringer's for one day (5 blocks of 20 trials). These conditions differ from those in **A** as the tubing was replaced and valves shuffled after each day.

Next, we took greater precaution with the stimulus tubes and scrambled the tube location and valve placement after each day. As shown in Figure 5.4B day 2-4, when the four mice trained on Ringer's versus Ringer's were tested with scrambled tubes, their bias was extinguished. This suggests that the mice may have been learning the task through non-chemosensory cues.

Finally, we tested a new batch of 6 mice, half $TrpC2^{-/-}$, and half heterozygous litter-mates. In addition to white noise, stimulus tube valve assignment and location were shuffled. Once the mice moved on to discriminate sulfated steroid versus Ringer's, completely new stimulus tubes and

connective tubing were used each day. Therefore, from day to day, the tubes and their location were different thus eliminating any possible long-term learning of tube-specific properties such as flow rate, valve click, or tube taste differences. As shown in Figure 5.3C,D, both TrpC2$^{+/-}$ and TrpC2$^{-/-}$ mice were proficient at discriminating sulfated steroid from Ringer's solution. However, when we switched the mice to S^{+} and S^{-} Ringer's discrimination, they performed at chance (Figure 5.4C). Because all tube-related cues were eliminated, this suggests that there was something detectable in the sulfated steroid solution.

It is possible that the sulfated steroid had some contaminants detectable by taste or main olfaction. Therefore, we purified Q1570 using TLC plates and verified its purity using mass spectrometry. As a control for any possible purification related contaminants, we ran a water control at all purification steps. The mice were then tested using purified Q1570 in Ringer's versus Ringer's with an equal amount of water control added. After one day of 100 trials, all mice were unable to discriminate purified sulfated steroid from Ringer's solution (Figure 5.5). This suggests that whatever cue the mice were attending to was removed during TLC purification. While this does not definitively indicate that the sulfated steroid detection assay was unsuccessful, it suggests that mice may not be able to self-report detection of AOS cues. However, the nature of the stimulus could be sufficiently different following purification. Therefore, we will test the mice over several more days to see if they are capable of learning to discriminate purified sulfated steroids.

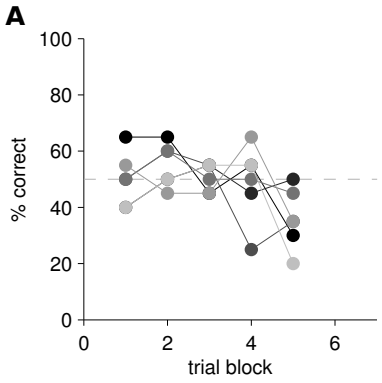

Figure 5.5: Purified sulfated steroid cannot be discriminated. **A,** The same six mice as in Figures 5.3**C**,**D** and 5.4**C** were tasked with discriminating TLC-purified Q1570 from Ringer's. Each line corresponds to a different mouse.

5.4 Discussion

5.4.1 Mice are adept at discriminating sensory cues

In attempting to develop a novel behavioral assay of the accessory olfactory system we gained insight into general mouse behavior. We were successful at training 37 mice to perform a go/no-go task to discriminate between two different sensory cues. This in itself is unremarkable, as numerous studies have demonstrated operant conditioning in response to taste [228, 231, 229] or main olfactory [232, 233, 234] stimuli. We also are unsure of what stimulus the mice were detecting. When discriminating NaCl, taste was likely used (Figure 5.2) and both taste and the MOS are capable of detecting urine (Figure 5.3). In the absence of any obvious odors or tastants, we can only speculate. The fact that mice were best able to perform the Q1570 versus Ringer's task following gradual training by beginning with an obvious urine stimulus and slowly tapering suggests that the cue they were responding to is subtle. The decrease in performance following sulfated steroid purification suggests that some contaminate in the sulfated steroid itself was this subtle cue.

5.4.2 Timing of sulfated steroid detection

Since the mice did not appear to have been using their AOS, we are unable to comment on the detection time window. The AOS is a slow sensory system, and firing in the AOB has been reported to lag seconds behind stimulus contact [151, 113]. However, it is possible that in a highly overtrained situation, control of the pump may change allowing for more rapid detection. It is also possible that downstream circuitry may be capable of detecting an increase in firing rate before we are able to observe it in individual cells. Evidence from drosophila olfaction suggests that circuits may be optimized to respond to the rising phase of a stimulus response [235]. A functional behavioral assay of this kind could shed light into the issue of temporal dynamics in the AOS.

As stimuli are pumped into the VNO, they also need to be pumped out of the VNO [113]. The time allotted between stimuli may be insufficient to allow for proper rinsing of the pump. The presence of residual stimuli may be sufficient for detection, making the Ringer's trials a slightly-diluted sulfated steroid trial. A lack of VNO flushing may be sufficient to further complicate this task.

5.4.3 Mice may not be capable of self-reporting AOS stimulus detection

While our failure to observe AOS-dependent discrimination is consistent with the idea the this task may not be possible, it is by no means conclusive. With continued testing of the purified sulfated steroid, the mice may be able to discriminate. It is also possible that the training paradigm or allotted time interval is not sufficient to cue the mouse to associate AOS stimuli with the outcome. The stimulus delivery method may not be allowing the stimuli to access the VNO, thus preventing detection. Or, it may be that linking stimulus with outcome is not possible within the mouse AOS — it truly is an unconscious sensory system mediating behaviors that fundamentally do not involve any conscious perception. With future investigation, we hope to provide more conclusive evidence.

6 Conclusions and future directions

6.1 Conclusions

Over the scope of this thesis, I investigated several aspects of the AOS, from single neuron representations of stimuli to population representations of stimulus concentration and behavioral readout. In exploring how single neurons represent information using multielectrode array recordings of explanted tissue, we identified that spontaneous and stimulus-evoked activity shared very similar bursting structure. Stimulus responses differed from spontaneous activity primarily by an increased number of bursts. Spontaneous activity confounded stimulus response identification with false positives, which were reduced by averaging activity across multiple trials. We also identified a role of the signal transduction cascade in setting both spontaneous and stimulus-driven activity in VSNs.

Next we studied how individual VSNs and populations of VSNs encode stimulus concentration also using multielectrode array recordings of explanted vomeronasal epithelium. Ultimately, the AOS must be capable of representing concentration in a manner that is invariant to environmental disruptions such as evaporation and dilution. Ratio coding provides a means of stability, as the ratio of AOS ligands will remain constant following environmental changes in urine concentration. Yet ratio coding will still reflect meaningful concentration varaince as changes in the relative concentration. Ratios can be encoded using logarithms; if a neural circuit represents log-concentration, inhibitory circuitry can compute the difference of log-concentrations, yielding the log-ratio. We identified that individual VSNs only encoded log-concentration over a narrow and variable range. However, the activity of populations of VSNs could be used to compute log-ratios of concentration spanning several orders of magnitude. While the ideas of logarithmic and ratio coding have previously been proposed (i.e. [32]), this provides the first neural evidence supporting ratio coding in an olfactory system.

Further investigation into coding in the AOS would benefit from a simple behavioral read-out. AOS-mediated behaviors typically involve complex functions such as hormonal regulation and aggression (Chapter 5), and it is unknown whether AOS stimuli are even consciously perceived. Therefore, we set out to develop a go/no-go task in which mice were trained to discriminate between AOS stimuli and Ringer's solution. Mice succeeded in discriminating sensory cues, but not sulfated steroids. Future work on this task may lead to the development of the first such assay of its kind in the AOS field.

Overall, these studies provide further insights into the field of accessory olfactory coding and representation of AOS stimuli at the levels of the individual neuron, populations of neurons, and behavior. While these studies were specific to the AOS, the results can be generalized to a broader perspective of sensory and intensity coding.

6.2 Future directions

Further exploration of ionic currents and signal transduction in VSNs In Chapter 3 we identified that VSNs displayed similar bursting behavior during spontaneous and stimulus driven activity and that the signal transduction cascade played a role in this activity. Several follow-up questions come to mind. A further exploration of the ionic currents that contribute to bursting would be interesting. The structured spontaneous activation of the signal transduction cascade calls to mind quantal activation of the G-protein observed in main olfactory sensory neurons [236]. An exploration of ligand-receptor and receptor-G-protein interactions and kinetics may illuminate how VSNs respond to stimuli. While there are obvious similarities to the MOS in function, different G-proteins and signal transduction elements are involved in the AOS, suggesting the mechanics may also differ.

Ratio coding in the AOS A logical next step in exploring ratio coding is to investigate the hypothesis proposed in Chapter 4, that mice use ratios to represent AOS stimuli in a stable manner. Two ways in which this can be done are through behavioral and electrophysiological assays. The behavioral paradigm described in Chapter 5 would be ideal if mice are able to self-report sulfated steroid detection. Assuming that the behavioral assay is successful, then we first need to demon-

strate that mice can discriminate between different sulfated steroids. Then mice can be trained to discriminate a particular ratio of sulfated steroids from Ringer's. The concentrations will then be changed while maintaining the same ratio, and the mouse will be tasked with discriminating between the two ratios. Changing the absolute concentration of one compound, and therefore the ratio, is another test. If the mouse cannot discriminate the two identical ratios but can discriminate the different ratio with the same components, then this implies that ratios are represented by the mouse AOS. Investigating the concentration range over which mice can discriminate ratios would be an interesting experiment. We demonstrated that ratios can be decoded from VSN population activity over more than three orders of magnitude, however rats have been shown to recognize ratios of MOS odorants over at least a ten-fold concentration range [32].

Electrophysiologically, we can directly test if neurons in the AOS encode ratios. The first level at which this is possible is with the mitral cells in the AOB which receive input from VSNs via glomeruli. Using an ex-vivo preparation that preserves the connections from the VNO to the AOB while allowing experimental access to the AOB, extracellular recordings from the mitral cell layer can be made [237]. Cannulation of the VNO allows for precise stimulus delivery. We would stimulate with a similar battery of stimuli as used in Chapter 4 to test whether a cell is tuned to the absolute concentration, ratios, or some other stimulus aspect. We predict that some population of mitral cells do encode ratios of concentration.

***In vivo* recording in the brain** A combination of electrophysiological recording and behavior in an awake-behaving recording preparation is an ideal experiment. The ability to record in the AOB during a precisely controlled behavior would allow us to explore a wide range of questions including temporal dynamics and decision making. Downstream brain areas, such as the medial amygdala, can also be targeted. Similar to what has been done in the main olfactory field (i.e. [238, 239]), awake behaving recordings can deeply advance understanding of the system.

Further investigations of the VNO All functional investigations of the VNO have been performed *ex vivo*, either using slice recordings [174, 87], tissue explants [150], or dissociated cells [173, 62]. In all of these conditions, the local environment surrounding VSNs differs from that *in*

vivo. Mucus and secretions are likely washed away, ion concentrations may be altered and tissue structure is affected. These perturbations can potentially change the firing and response properties of sensory neurons, affecting investigations of sensory coding. While there is no evidence from AOB recordings that the VNO is profoundly disrupted, a more naturalistic VNO environment is still of interest. I propose two experiments: mucus component identification and *in vivo* recording from VSNs.

In the main olfactory epithelium, mucus provides a micro environment, regulating ion concentration [240] and even containing enzymes that process odorants prior to reaching the receptors [241]. Mucus in the VNO likely contains similar compounds, and has been postulated to contain proteins that specifically bind "pheromones" [242], potentially allowing compounds to bind receptors that would otherwise not. There is evidence that the ionic environment in the VNO is disrupted in *ex vivo* experiments [243]. A thorough understanding of what is present in mucus would allow experimenters to better recapitulate the natural environment in *ex vivo* experiments. While this is a large scale undertaking, proteomics, mass spectroscopy and other biochemical assays can go a long way in determining the ion concentrations and protein composition of VNO mucus.

Another approach to obtaining a more naturalistic environment is to perform *in vivo* recordings of VSNs. This is a difficult task as the VNO is encased in a bony capsule and located deep in the nasal cavity. However, Meredith successfully performed chronic recordings of the VNO pump in hamsters [111]. Implanting a multielectrode array in the VNO may be feasible, allowing for long term recordings of VSNs. In addition to allowing for naturalistic recordings from VSNs, this technique would allow experimenters to study temporal dynamics in VSNs as they relate to pump timing.

6.3 Final conclusions

Here, I investigated sensory and concentration coding in the mouse AOS. The AOS is specialized to detect social odors such as urine and mediates behaviors involving reproduction, aggression and individual recognition. Using multielectrode array recordings and computational approaches, we identified that VSN activity consists of groups of action potentials that are very similar in structure during spontaneous and stimulus-evoked activity, likely due to the signal transduction cascade. We

also investigated concentration representation in the AOS and found that populations of sensory neurons can be used to robustly represent concentration. Finally, we set out to develop a behavioral assay to test whether it is possible to train mice to discriminate AOS cues as a means of further investigating detection and coding in the AOS. This assay was not yet successful, however, may be improved with continued effort. These investigations contribute to sensory coding at levels ranging from the single neuron to animal behavior, advancing the current understanding of the AOS and setting the stage for future investigations.

References

[1] Felleman, D. J., and Van Essen, D. C. (1991) Distributed hierarchical processing in the primate cerebral cortex. *Cereb Cortex 1*, 1–47.

[2] Wilson, R. I., and Mainen, Z. F. (2006) Early events in olfactory processing. *Annu Rev Neurosci 29*, 163–201.

[3] Fechner, G. T., Adler, H. E., Howes, D. H., and Boring, E. G. *Elements of psychophysics*; A Henry Holt edition in psychology; Holt, Rinehart and Winston: New York, 1966.

[4] Mountcastle, V. B., F, P. G., and Werner, G. (1963) The Relation Of Thalamic Cell Response To Peripheral Stimuli Varied Over an Intensive Continuum. *J Neurophysiol 26*, 807–34.

[5] Johnson, K. O., Hsiao, S. S., and Yoshioka, T. (2002) Neural coding and the basic law of psychophysics. *Neuroscientist 8*, 111–21.

[6] Barbour, D. L. (2011) Intensity-invariant coding in the auditory system. *Neurosci Biobehav Rev 35*, 2064–72.

[7] Benda, J., and Hennig, R. M. (2008) Spike-frequency adaptation generates intensity invariance in a primary auditory interneuron. *J Comput Neurosci 24*, 113–36.

[8] Billimoria, C. P., Kraus, B. J., Narayan, R., Maddox, R. K., and Sen, K. (2008) Invariance and sensitivity to intensity in neural discrimination of natural sounds. *J Neurosci 28*, 6304–8.

[9] Morita, K., Okada, M., and Aihara, K. (2007) Selectivity and stability via dendritic nonlinearity. *Neural Comput 19*, 1798–853.

[10] Firestein, S., Picco, C., and Menini, A. (1993) The relation between stimulus and response in olfactory receptor cells of the tiger salamander. *J Physiol 468*, 1–10.

[11] Trotier, D. (1994) Intensity coding in olfactory receptor cells. *Semin Cell Biol 5*, 47–54.

[12] Reisert, J., and Matthews, H. R. (2001) Response properties of isolated mouse olfactory receptor cells. *J Physiol 530*, 113–22.

[13] Rubin, B. D., and Katz, L. C. (1999) Optical imaging of odorant representations in the mammalian olfactory bulb. *Neuron 23*, 499–511.

[14] Meister, M., and Bonhoeffer, T. (2001) Tuning and topography in an odor map on the rat olfactory bulb. *J Neurosci 21*, 1351–60.

[15] Wachowiak, M., and Cohen, L. B. (2001) Representation of odorants by receptor neuron input to the mouse olfactory bulb. *Neuron 32*, 723–35.

[16] Cleland, T. A., Johnson, B. A., Leon, M., and Linster, C. (2007) Relational representation in the olfactory system. *Proc Natl Acad Sci U S A 104*, 1953–8.

[17] Engen, T., and Pfaffmann, C. (1959) Absolute judgments of odor intensity. *J Exp Psychol 58*, 23–6.

[18] Slotnick, B. M., and Ptak, J. E. (1977) Olfactory intensity-difference thresholds in rats and humans. *Physiol Behav 19*, 795–802.

[19] Duchamp-Viret, P., Duchamp, A., and Sicard, G. (1990) Olfactory discrimination over a wide concentration range. Comparison of receptor cell and bulb neuron abilities. *Brain Res 517*, 256–62.

[20] Pelz, C., Gerber, B., and Menzel, R. (1997) Odorant intensity as a determinant for olfactory conditioning in honeybees: roles in discrimination, overshadowing and memory consolidation. *J Exp Biol 200*, 837–47.

[21] Malnic, B., Hirono, J., Sato, T., and Buck, L. B. (1999) Combinatorial receptor codes for odors. *Cell 96*, 713–23.

[22] Semmelhack, J. L., and Wang, J. W. (2009) Select Drosophila glomeruli mediate innate olfactory attraction and aversion. *Nature 459*, 218–23.

[23] Wright, G. A., Thomson, M. G. A., and Smith, B. H. (2005) Odour concentration affects odour identity in honeybees. *Proc Biol Sci 272*, 2417–22.

[24] Reisert, J., and Matthews, H. R. (1999) Adaptation of the odour-induced response in frog olfactory receptor cells. *J Physiol 519 Pt 3*, 801–13.

[25] Spors, H., and Grinvald, A. (2002) Spatio-temporal dynamics of odor representations in the mammalian olfactory bulb. *Neuron 34*, 301–15.

[26] Rospars, J.-P., Lánský, P., Duchamp, A., and Duchamp-Viret, P. (2003) Relation between stimulus and response in frog olfactory receptor neurons in vivo. *Eur J Neurosci 18*, 1135–54.

[27] Grémiaux, A., Nowotny, T., Martinez, D., Lucas, P., and Rospars, J.-P. (2012) Modelling the signal delivered by a population of first-order neurons in a moth olfactory system. *Brain Res. 1434*, 123–35.

[28] VanRullen, R., Guyonneau, R., and Thorpe, S. J. (2005) Spike times make sense. *Trends Neurosci 28*, 1–4.

[29] Stopfer, M., Jayaraman, V., and Laurent, G. (2003) Intensity versus identity coding in an olfactory system. *Neuron 39*, 991–1004.

[30] Brody, C. D., and Hopfield, J. J. (2003) Simple networks for spike-timing-based computation, with application to olfactory processing. *Neuron 37*, 843–52.

[31] Hopfield, J. J. (1999) Odor space and olfactory processing: collective algorithms and neural implementation. *Proc Natl Acad Sci U S A 96*, 12506–11.

[32] Uchida, N., and Mainen, Z. F. (2007) Odor concentration invariance by chemical ratio coding. *Front Syst Neurosci 1*, 3.

[33] Karlson, P., and Luscher, M. (1959) Pheromones': a new term for a class of biologically active substances. *Nature 183*, 55–6.

[34] Butenandt, A., Beckmann, R., Stamm, D., and Hecker, E. (1959) über den Sexuallockstoff des Seidenspinners Bombyx mori. *Reindarstellung und Konstitution. Z. Naturforschg. 14b*, 283–84.

[35] Wyatt, T. D. (2009) Fifty years of pheromones. *Nature 457*, 262–3.

[36] Johansson, B. G., and Jones, T. M. (2007) The role of chemical communication in mate choice. *Biol Rev Camb Philos Soc 82*, 265–89.

[37] Wysocki, C. J. (1979) Neurobehavioral evidence for the involvement of the vomeronasal system in mammalian reproduction. *Neurosci Biobehav Rev 3*, 301–41.

[38] Xu, F., Schaefer, M., Kida, I., Schafer, J., Liu, N., Rothman, D. L., Hyder, F., Restrepo, D., and Shepherd, G. M. (2005) Simultaneous activation of mouse main and accessory olfactory bulbs by odors or pheromones. *J. Comp. Neurol. 489*, 491–500.

[39] Logan, D. W., Brunet, L. J., Webb, W. R., Cutforth, T., Ngai, J., and Stowers, L. (2012) Learned recognition of maternal signature odors mediates the first suckling episode in mice. *Curr Biol 22*, 1998–2007.

[40] Hudson, R., and Distel, H. (1986) Pheromonal release of suckling in rabbits does not depend on the vomeronasal organ. *Physiol Behav 37*, 123–8.

[41] Baxi, K. N., Dorries, K. M., and Eisthen, H. L. (2006) Is the vomeronasal system really specialized for detecting pheromones? *Trends Neurosci 29*, 1–7.

[42] Halpern, M. (1987) The organization and function of the vomeronasal system. *Annu. Rev. Neurosci. 10*, 325–62.

[43] Nodari, F., Hsu, F. F., Fu, X., Holekamp, T. F., Kao, L. F., Turk, J., and Holy, T. E. (2008) Sulfated steroids as natural ligands of mouse pheromone-sensing neurons. *J. Neurosci. 28*, 6407–6418.

[44] Meeks, J. P., Arnson, H. A., and Holy, T. E. (2010) Representation and transformation of sensory information in the mouse accessory olfactory system. *Nat Neurosci 13*, 723–30.

[45] Døving, K. B., and Trotier, D. (1998) Structure and function of the vomeronasal organ. *J. Exp. Biol. 201*, 2913–25.

[46] Larriva-Sahd, J. (2008) The accessory olfactory bulb in the adult rat: a cytological study of its cell types, neuropil, neuronal modules, and interactions with the main olfactory system. *J Comp Neurol 510*, 309–50.

[47] Bhatnagar, K. P., and Smith, T. D. (2003) The human vomeronasal organ. V. An interpretation of its discovery by Ruysch, Jacobson, or Kölliker, with an English translation of Kölliker (1877). *Anat Rec B New Anat 270*, 4–15.

[48] Jacobson, L., Trotier, D., and Døving, K. B. (1998) Anatomical description of a new organ in the nose of domesticated animals by Ludvig Jacobson (1813). *Chem Senses 23*, 743–54.

[49] Retzius, G. (1894) Die Riechzellen der Ophidier in der Riechschleimhaut und im Jacobson'schen Organ. *Biol. Untersuch. Neue Folge 6*, 48–51.

[50] Adrian, E. D. (1955) Synchronised activity in the vomero-nasal nerves with a note on the function of the organ of Jacobsen. *Pflugers Arch. 260*, 188–92.

[51] Clancy, A. N., Coquelin, A., Macrides, F., Gorski, R. A., and Noble, E. P. (1984) Sexual behavior and aggression in male mice: involvement of the vomeronasal system. *J. Neurosci. 4*, 2222–9.

[52] Wysocki, C. J., Nyby, J., Whitney, G., Beauchamp, G. K., and Katz, Y. (1982) The vomeronasal organ: primary role in mouse chemosensory gender recognition. *Physiol. Behav. 29*, 315–27.

[53] Wysocki, C. J., Katz, Y., and Bernhard, R. (1983) Male vomeronasal organ mediates female-induced testosterone surges in mice. *Biol. Reprod. 28*, 917–22.

[54] Stowers, L., Holy, T. E., Meister, M., Dulac, C., and Koentges, G. (2002) Loss of sex discrimination and male-male aggression in mice deficient for TRP2. *Science 295*, 1493–500.

[55] Leypold, B. G., Yu, C. R., Leinders-Zufall, T., Kim, M. M., Zufall, F., and Axel, R. (2002) Altered sexual and social behaviors in trp2 mutant mice. *Proc. Natl. Acad. Sci. U.S.A. 99*, 6376–81.

[56] Roberts, S. A., Simpson, D. M., Armstrong, S. D., Davidson, A. J., Robertson, D. H., McLean, L., Beynon, R. J., and Hurst, J. L. (2010) Darcin: a male pheromone that stimulates female memory and sexual attraction to an individual male's odour. *BMC Biol. 8*, 75.

[57] Roberts, S. A., Davidson, A. J., McLean, L., Beynon, R. J., and Hurst, J. L. (2012) Pheromonal induction of spatial learning in mice. *Science 338*, 1462–5.

[58] Kimchi, T., Xu, J., and Dulac, C. (2007) A functional circuit underlying male sexual behaviour in the female mouse brain. *Nature 448*, 1009–14.

[59] Martel, K. L., and Baum, M. J. (2009) Adult testosterone treatment but not surgical disruption of vomeronasal function augments male-typical sexual behavior in female mice. *J. Neurosci. 29*, 7658–66.

[60] Mugford, R. A., and Nowell, N. W. (1970) Pheromones and their effect on aggression in mice. *Nature 226*, 967–8.

[61] Bean, N. J. (1982) Modulation of agonistic behavior by the dual olfactory system in male mice. *Physiol. Behav. 29*, 433–7.

[62] Chamero, P., Marton, T. F., Logan, D. W., Flanagan, K., Cruz, J. R., Saghatelian, A., Cravatt, B. F., and Stowers, L. (2007) Identification of protein pheromones that promote aggressive behaviour. *Nature 450*, 899–902.

[63] Wysocki, C. J., and Lepri, J. J. (1991) Consequences of removing the vomeronasal organ. *J. Steroid Biochem. Mol. Biol. 39*, 661–9.

[64] Wang, Z., Sindreu, C. B., Li, V., Nudelman, A., Chan, G. C.-K., and Storm, D. R. (2006) Pheromone detection in male mice depends on signaling through the type 3 adenylyl cyclase in the main olfactory epithelium. *J. Neurosci. 26*, 7375–9.

[65] Bean, N. J., and Wysocki, C. J. (1989) Vomeronasal organ removal and female mouse aggression: the role of experience. *Physiol. Behav. 45*, 875–82.

[66] Lee, S. V. D., and Boot, L. M. (1955) Spontaneous pseudopregnancy in mice. *Acta Physiol Pharmacol Neerl 4*, 442–4.

[67] Reynolds, J., and Keverne, E. B. (1979) The accessory olfactory system and its role in the pheromonally mediated suppression of oestrus in grouped mice. *J. Reprod. Fertil. 57*, 31–5.

[68] Ma, W., Miao, Z., and Novotny, M. V. (1998) Role of the adrenal gland and adrenal-mediated chemosignals in suppression of estrus in the house mouse: the lee-boot effect revisited. *Biol. Reprod. 59*, 1317–20.

[69] Whitten, W. K. (1956) Modification of the oestrous cycle of the mouse by external stimuli associated with the male. *J. Endocrinol. 13*, 399–404.

[70] Whitten, W. K., Bronson, F. H., and Greenstein, J. A. (1968) Estrus-inducing pheromone of male mice: transport by movement of air. *Science 161*, 584–5.

[71] Johns, M. A., Feder, H. H., Komisaruk, B. R., and Mayer, A. D. (1978) Urine-induced reflex ovulation in anovulatory rats may be a vomeronasal effect. *Nature 272*, 446–8.

[72] Mora, O. A., Sánchez-Criado, J. E., and Guisado, S. (1985) Role of the vomeronasal organ on the estral cycle reduction by pheromones in the rat. *Rev. Esp. Fisiol. 41*, 305–10.

[73] Booth, K. K., and Webb, E. C. (2010) Effect of Blockage of the Ducts of the Vomeronasal Organ on LH Plasma Levels during the "Whitten Effect" in Does. *Vet Med Int 2010*, journal.

[74] Vandenbergh, J. G. (1969) Male odor accelerates female sexual maturation in mice. *Endocrinology 84*, 658–60.

[75] Kaneko, N., Debski, E. A., Wilson, M. C., and Whitten, W. K. (1980) Puberty acceleration in mice. II. Evidence that the vomeronasal organ isa receptor for the primer pheromone in male mouse urine. *Biol. Reprod. 22*, 873–8.

[76] Lomas, D. E., and Keverne, E. B. (1982) Role of the vomeronasal organ and prolactin in the acceleration of puberty in female mice. *J. Reprod. Fertil. 66*, 101–7.

[77] Bruce, H. M. (1959) An exteroceptive block to pregnancy in the mouse. *Nature 184*, 105.

[78] Bruce, H. M. (1960) A block to pregnancy in the mouse caused by proximity of strange males. *J. Reprod. Fertil. 1*, 96–103.

[79] Bruce, H. M., and Parrott, D. M. (1960) Role of olfactory sense in pregnancy block by strange males. *Science 131*, 1526.

[80] Parkes, A. S., and Bruce, H. M. (1962) Pregnancy-block in female mice placed in boxes soiled by males. *J. Reprod. Fertil. 4*, 303–8.

[81] Bellringer, J. F., Pratt, H. P., and Keverne, E. B. (1980) Involvement of the vomeronasal organ and prolactin in pheromonal induction of delayed implantation in mice. *J. Reprod. Fertil. 59*, 223–8.

[82] Rajendren, G., and Dominic, C. J. (1985) Effect of transection of the vomeronasal nerve on the male-induced implantation failure (the Bruce effect) in mice. *Indian J. Exp. Biol. 23*, 635–7.

[83] Brennan, P. A., and Keverne, E. B. (1997) Neural mechanisms of mammalian olfactory learning. *Prog. Neurobiol. 51*, 457–81.

[84] Brennan, P. A. (2009) Outstanding issues surrounding vomeronasal mechanisms of pregnancy block and individual recognition in mice. *Behav. Brain Res. 200*, 287–94.

[85] Brennan, P. A. (2004) The nose knows who's who: chemosensory individuality and mate recognition in mice. *Hormones and behavior 46*, 231–240.

[86] Hurst, J. L., Payne, C. E., Nevison, C. M., Marie, A. D., Humphries, R. E., Robertson, D. H., Cavaggioni, A., and Beynon, R. J. (2001) Individual recognition in mice mediated by major urinary proteins. *Nature 414*, 631–4.

[87] He, J., Ma, L., Kim, S., Nakai, J., and Yu, C. R. (2008) Encoding gender and individual information in the mouse vomeronasal organ. *Science 320*, 535–8.

[88] Hendrickson, R. C., Krauthamer, S., Essenberg, J. M., and Holy, T. E. (2008) Inhibition shapes sex selectivity in the mouse accessory olfactory bulb. *J Neurosci 28*, 12523–34.

[89] Boehm, N., and Gasser, B. (1993) Sensory receptor-like cells in the human foetal vomeronasal organ. *Neuroreport 4*, 867–70.

[90] Smith, T. D., Siegel, M. I., Mooney, M. P., Burdi, A. R., and Todhunter, J. S. (1996) Vomeronasal organ growth and development in normal and cleft lip and palate human fetuses. *Cleft Palate Craniofac. J. 33*, 385–94.

[91] Trotier, D., Eloit, C., Wassef, M., Talmain, G., Bensimon, J. L., Døving, K. B., and Ferrand, J. (2000) The vomeronasal cavity in adult humans. *Chem. Senses 25*, 369–80.

[92] Bhatnagar, K. P., and Smith, T. D. (2001) The human vomeronasal organ. III. Postnatal development from infancy to the ninth decade. *J. Anat. 199*, 289–302.

[93] Stensaas, L. J., Lavker, R. M., Monti-Bloch, L., Grosser, B. I., and Berliner, D. L. (1991) Ultrastructure of the human vomeronasal organ. *J. Steroid Biochem. Mol. Biol. 39*, 553–60.

[94] Meredith, M. (2001) Human vomeronasal organ function: a critical review of best and worst cases. *Chem. Senses 26*, 433–45.

[95] Zhang, J., and Webb, D. M. (2003) Evolutionary deterioration of the vomeronasal pheromone transduction pathway in catarrhine primates. *Proc. Natl. Acad. Sci. U.S.A. 100*, 8337–41.

[96] Liman, E. R. (2012) Changing senses: chemosensory signaling and primate evolution. *Adv. Exp. Med. Biol. 739*, 206–17.

[97] Giorgi, D., Friedman, C., Trask, B. J., and Rouquier, S. (2000) Characterization of nonfunctional V1R-like pheromone receptor sequences in human. *Genome Res. 10*, 1979–85.

[98] Kouros-Mehr, H., Pintchovski, S., Melnyk, J., Chen, Y. J., Friedman, C., Trask, B., and Shizuya, H. (2001) Identification of non-functional human VNO receptor genes provides evidence for vestigiality of the human VNO. *Chem. Senses 26*, 1167–74.

[99] Rodriguez, I., Greer, C. A., Mok, M. Y., and Mombaerts, P. (2000) A putative pheromone receptor gene expressed in human olfactory mucosa. *Nat Genet 26*, 18–9.

[100] Liman, E. R., and Innan, H. (2003) Relaxed selective pressure on an essential component of pheromone transduction in primate evolution. *Proc. Natl. Acad. Sci. U.S.A. 100*, 3328–32.

[101] Foltán, R., and Sedý, J. (2009) Behavioral changes of patients after orthognathic surgery develop on the basis of the loss of vomeronasal organ: a hypothesis. *Head Face Med 5*, 5.

[102] Wyatt, T. D. *Pheromones and animal behaviour: communication by smell and taste*; Cambridge University Press, 2003.

[103] McClintock, M. K. (1971) Menstrual synchorony and suppression. *Nature 229*, 244–5.

[104] Strassmann, B. I. (1999) Menstrual synchrony pheromones: cause for doubt. *Hum. Reprod. 14*, 579–80.

[105] Dorries, K. M., Adkins-Regan, E., and Halpern, B. P. (1997) Sensitivity and behavioral responses to the pheromone androstenone are not mediated by the vomeronasal organ in domestic pigs. *Brain Behav. Evol. 49*, 53–62.

[106] Wyart, C., Webster, W. W., Chen, J. H., Wilson, S. R., McClary, A., Khan, R. M., and Sobel, N. (2007) Smelling a single component of male sweat alters levels of cortisol in women. *J. Neurosci. 27*, 1261–5.

[107] Wysocki, C. J., and Beauchamp, G. K. (1984) Ability to smell androstenone is genetically determined. *Proc. Natl. Acad. Sci. U.S.A. 81*, 4899–902.

[108] Keller, A., Zhuang, H., Chi, Q., Vosshall, L. B., and Matsunami, H. (2007) Genetic variation in a human odorant receptor alters odour perception. *Nature 449*, 468–72.

[109] Wysocki, C. J., and Preti, G. (2004) Facts, fallacies, fears, and frustrations with human pheromones. *Anat Rec A Discov Mol Cell Evol Biol 281*, 1201–11.

[110] Touhara, K., and Vosshall, L. B. (2009) Sensing odorants and pheromones with chemosensory receptors. *Annu Rev Physiol 71*, 307–32.

[111] Meredith, M. (1994) Chronic recording of vomeronasal pump activation in awake behaving hamsters. *Physiol Behav 56*, 345–54.

[112] Meredith, M., and O'Connell, R. J. (1979) Efferent control of stimulus access to the hamster vomeronasal organ. *J. Physiol. (Lond.) 286*, 301–16.

[113] Ben-Shaul, Y., Katz, L. C., Mooney, R., and Dulac, C. (2010) In vivo vomeronasal stimulation reveals sensory encoding of conspecific and allospecific cues by the mouse accessory olfactory bulb. *Proc Natl Acad Sci U S A*.

[114] Ogura, T., Krosnowski, K., Zhang, L., Bekkerman, M., and Lin, W. (2010) Chemoreception regulates chemical access to mouse vomeronasal organ: role of solitary chemosensory cells. *PLoS One 5*, e11924.

[115] Liman, E. R., Corey, D. P., and Dulac, C. (1999) TRP2: a candidate transduction channel for mammalian pheromone sensory signaling. *Proc. Natl. Acad. Sci. U.S.A. 96*, 5791–6.

[116] Rodriguez, I., Feinstein, P., and Mombaerts, P. (1999) Variable patterns of axonal projections of sensory neurons in the mouse vomeronasal system. *Cell 97*, 199–208.

[117] Martini, S., Silvotti, L., Shirazi, A., Ryba, N. J., and Tirindelli, R. (2001) Co-expression of putative pheromone receptors in the sensory neurons of the vomeronasal organ. *J Neurosci 21*, 843–8.

[118] Halpern, M., Shapiro, L. S., and Jia, C. (1995) Differential localization of G proteins in the opossum vomeronasal system. *Brain Res. 677*, 157–61.

[119] Dulac, C., and Axel, R. (1995) A novel family of genes encoding putative pheromone receptors in mammals. *Cell 83*, 195–206.

[120] Jia, C., and Halpern, M. (1996) Subclasses of vomeronasal receptor neurons: differential expression of G proteins (Gi alpha 2 and G(o alpha)) and segregated projections to the accessory olfactory bulb. *Brain Res 719*, 117–28.

[121] Matsunami, H., and Buck, L. B. (1997) A multigene family encoding a diverse array of putative pheromone receptors in mammals. *Cell 90*, 775–84.

[122] Saito, H., Mimmack, M. L., Keverne, E. B., Kishimoto, J., and Emson, P. C. (1998) Isolation of mouse vomeronasal receptor genes and their co-localization with specific G-protein messenger RNAs. *Brain Res. Mol. Brain Res. 60*, 215–27.

[123] Loconto, J., Papes, F., Chang, E., Stowers, L., Jones, E. P., Takada, T., Kumánovics, A., Lindahl, K. F., and Dulac, C. (2003) Functional expression of murine V2R pheromone receptors involves selective association with the M10 and M1 families of MHC class Ib molecules. *Cell 112*, 607–18.

[124] Ishii, T., Hirota, J., and Mombaerts, P. (2003) Combinatorial coexpression of neural and immune multigene families in mouse vomeronasal sensory neurons. *Curr. Biol. 13*, 394–400.

[125] Ishii, T., and Mombaerts, P. (2008) Expression of nonclassical class I major histocompatibility genes defines a tripartite organization of the mouse vomeronasal system. *J. Neurosci. 28*, 2332–41.

[126] Rivière, S., Challet, L., Fluegge, D., Spehr, M., and Rodriguez, I. (2009) Formyl peptide receptor-like proteins are a novel family of vomeronasal chemosensors. *Nature 459*, 574–7.

[127] Liberles, S. D., Horowitz, L. F., Kuang, D., Contos, J. J., Wilson, K. L., Siltberg-Liberles, J., Liberles, D. A., and Buck, L. B. (2009) Formyl peptide receptors are candidate chemosensory receptors in the vomeronasal organ. *Proc. Natl. Acad. Sci. U.S.A. 106*, 9842–7.

[128] Belluscio, L., Koentges, G., Axel, R., and Dulac, C. (1999) A map of pheromone receptor activation in the mammalian brain. *Cell 97*, 209–20.

[129] Jia, C., and Halpern, M. (1997) Segregated populations of mitral/tufted cells in the accessory olfactory bulb. *Neuroreport 8*, 1887–90.

[130] Takami, S., and Graziadei, P. P. (1991) Light microscopic Golgi study of mitral/tufted cells in the accessory olfactory bulb of the adult rat. *J Comp Neurol 311*, 65–83.

[131] Del Punta, K., Puche, A., Adams, N. C., Rodriguez, I., and Mombaerts, P. (2002) A divergent pattern of sensory axonal projections is rendered convergent by second-order neurons in the accessory olfactory bulb. *Neuron 35*, 1057–66.

[132] Wagner, S., Gresser, A. L., Torello, A. T., and Dulac, C. (2006) A multireceptor genetic approach uncovers an ordered integration of VNO sensory inputs in the accessory olfactory bulb. *Neuron 50*, 697–709.

[133] Yokosuka, M. (2012) Histological properties of the glomerular layer in the mouse accessory olfactory bulb. *Exp Anim 61*, 13–24.

[134] Raisman, G. (1972) An experimental study of the projection of the amygdala to the accessory olfactory bulb and its relationship to the concept of a dual olfactory system. *Exp Brain Res 14*, 395–408.

[135] Davis, B. J., Macrides, F., Youngs, W. M., Schneider, S. P., and Rosene, D. L. (1977) Efferents and centrifugal afferents of the main and accessory olfactory bulbs in the hamster. *Brain Res. Bull. 3*, 59–72.

[136] Fan, S., and Luo, M. (2009) The organization of feedback projections in a pathway important for processing pheromonal signals. *Neuroscience 161*, 489–500.

[137] Mohedano-Moriano, A., de la Rosa-Prieto, C., Saiz-Sanchez, D., Ubeda-Bañon, I., Pro-Sistiaga, P., de Moya-Pinilla, M., and Martinez-Marcos, A. (2012) Centrifugal telencephalic afferent connections to the main and accessory olfactory bulbs. *Front Neuroanat 6*, 19.

[138] Winans, S. S., and Scalia, F. (1970) Amygdaloid nucleus: new afferent input from the vomeronasal organ. *Science 170*, 330–2.

[139] Scalia, F., and Winans, S. S. (1975) The differential projections of the olfactory bulb and accessory olfactory bulb in mammals. *J Comp Neurol 161*, 31–55.

[140] Martínez-Marcos, A., and Halpern, M. (1999) Differential projections from the anterior and posterior divisions of the accessory olfactory bulb to the medial amygdala in the opossum, Monodelphis domestica. *Eur J Neurosci 11*, 3789–99.

[141] Mohedano-Moriano, A., Pro-Sistiaga, P., Ubeda-Bañón, I., Crespo, C., Insausti, R., and Martinez-Marcos, A. (2007) Segregated pathways to the vomeronasal amygdala: differential projections from the anterior and posterior divisions of the accessory olfactory bulb. *Eur J Neurosci 25*, 2065–80.

[142] Salazar, I., and Brennan, P. A. (2001) Retrograde labelling of mitral/tufted cells in the mouse accessory olfactory bulb following local injections of the lipophilic tracer DiI into the vomeronasal amygdala. *Brain Res 896*, 198–203.

[143] Mohedano-Moriano, A., Pro-Sistiaga, P., Ubeda-Bañon, I., de la Rosa-Prieto, C., Saiz-Sanchez, D., and Martinez-Marcos, A. (2008) V1R and V2R segregated vomeronasal pathways to the hypothalamus. *Neuroreport 19*, 1623–6.

[144] Kang, N., Baum, M. J., and Cherry, J. A. (2009) A direct main olfactory bulb projection to the 'vomeronasal' amygdala in female mice selectively responds to volatile pheromones from males. *Eur. J. Neurosci. 29*, 624–34.

[145] Halpern, M., and MartÃ-nez Marcos, A. (2003) Structure and function of the vomeronasal system: an update. *Prog Neurobiol 70*, 245–318.

[146] Beynon, R. J., and Hurst, J. L. (2003) Multiple roles of major urinary proteins in the house mouse, Mus domesticus. *Biochem. Soc. Trans. 31*, 142–6.

[147] Tirindelli, R., Dibattista, M., Pifferi, S., and Menini, A. (2009) From pheromones to behavior. *Physiol. Rev. 89*, 921–56.

[148] Halem, H. A., Cherry, J. A., and Baum, M. J. (1999) Vomeronasal neuroepithelium and forebrain Fos responses to male pheromones in male and female mice. *J. Neurobiol. 39*, 249–63.

[149] Inamura, K., Matsumoto, Y., Kashiwayanagi, M., and Kurihara, K. (1999) Laminar distribution of pheromone-receptive neurons in rat vomeronasal epithelium. *J. Physiol. (Lond.) 517 (Pt 3)*, 731–9.

[150] Holy, T. E., Dulac, C., and Meister, M. (2000) Responses of vomeronasal neurons to natural stimuli. *Science 289*, 1569–1572.

[151] Luo, M., Fee, M. S., and Katz, L. C. (2003) Encoding pheromonal signals in the accessory olfactory bulb of behaving mice. *Science 299*, 1196–201.

[152] Vandenbergh, J. G., Whitsett, J. M., and Lombardi, J. R. (1975) Partial isolation of a pheromone accelerating puberty in female mice. *J. Reprod. Fertil. 43*, 515–23.

[153] Leinders-Zufall, T., Brennan, P., Widmayer, P., Prashanth Chandramani, S., Maul-Pavicic, A., Jager, M., Li, X.-H., Breer, H., Zufall, F., and Boehm, T. (2004) MHC class I peptides as chemosensory signals in the vomeronasal organ. *Science 306*, 1033–7.

[154] Leinders-Zufall, T., Ishii, T., Mombaerts, P., Zufall, F., and Boehm, T. (2009) Structural requirements for the activation of vomeronasal sensory neurons by MHC peptides. *Nat. Neurosci. 12*, 1551–8.

[155] Böcskei, Z., Groom, C. R., Flower, D. R., Wright, C. E., Phillips, S. E., Cavaggioni, A., Findlay, J. B., and North, A. C. (1992) Pheromone binding to two rodent urinary proteins revealed by X-ray crystallography. *Nature 360*, 186–8.

[156] Sharrow, S. D., Vaughn, J. L., Zídek, L., Novotny, M. V., and Stone, M. J. (2002) Pheromone binding by polymorphic mouse major urinary proteins. *Protein Sci. 11*, 2247–56.

[157] Mucignat-Caretta, C., Caretta, A., and Cavaggioni, A. (1995) Acceleration of puberty onset in female mice by male urinary proteins. *J. Physiol. (Lond.) 486 (Pt 2)*, 517–22.

[158] Kimoto, H., Haga, S., Sato, K., and Touhara, K. (2005) Sex-specific peptides from exocrine glands stimulate mouse vomeronasal sensory neurons. *Nature 437*, 898–901.

[159] Haga, S., Hattori, T., Sato, T., Sato, K., Matsuda, S., Kobayakawa, R., Sakano, H., Yoshihara, Y., Kikusui, T., and Touhara, K. (2010) The male mouse pheromone ESP1 enhances female sexual receptive behaviour through a specific vomeronasal receptor. *Nature 466*, 118–22.

[160] Papes, F., Logan, D. W., and Stowers, L. (2010) The vomeronasal organ mediates interspecies defensive behaviors through detection of protein pheromone homologs. *Cell 141*, 692–703.

[161] Turaga, D., and Holy, T. E. (2012) Organization of vomeronasal sensory coding revealed by fast volumetric calcium imaging. *J Neurosci 32*, 1612–21.

[162] Novotny, M., Jemiolo, B., Harvey, S., Wiesler, D., and Marchlewska-Koj, A. (1986) Adrenal-mediated endogenous metabolites inhibit puberty in female mice. *Science 231*, 722–5.

[163] Punta, K. D., Leinders-Zufall, T., Rodriguez, I., Jukam, D., Wysocki, C. J., Ogawa, S., Zufall, F., and Mombaerts, P. (2002) Deficient pheromone responses in mice lacking a cluster of vomeronasal receptor genes. *Nature 419*, 70–4.

[164] Leinders-Zufall, T., Lane, A. P., Puche, A. C., Ma, W., Novotny, M. V., Shipley, M. T., and Zufall, F. (2000) Ultrasensitive pheromone detection by mammalian vomeronasal neurons. *Nature 405*, 792–6.

[165] Boschat, C., Pélofi, C., Randin, O., Roppolo, D., Lüscher, C., Broillet, M.-C., and Rodriguez, I. (2002) Pheromone detection mediated by a V1r vomeronasal receptor. *Nat. Neurosci. 5*, 1261–2.

[166] Sam, M., Vora, S., Malnic, B., Ma, W., Novotny, M. V., and Buck, L. B. (2001) Neuropharmacology. Odorants may arouse instinctive behaviours. *Nature 412*, 142.

[167] Contreras, C. M., Gutiérrez-García, A. G., Molina-Jiménez, T., and Mendoza-López, R. (2012) 2-Heptanone increases the firing rate of the basal amygdala: role of anterior olfactory epithelial organs. *Neuropsychobiology 66*, 167–73.

[168] Arnson, H. A., and Holy, T. E. (2011) Chemosensory burst coding by mouse vomeronasal sensory neurons. *J. Neurophysiol. 106*, 409–20.

[169] Sorensen, P. W., Scott, A. P., Stacey, N. E., and Bowdin, L. (1995) Sulfated 17,20 beta-dihydroxy-4-pregnen-3-one functions as a potent and specific olfactory stimulant with pheromonal actions in the goldfish. *Gen. Comp. Endocrinol. 100*, 128–42.

[170] Sorensen, P. W., Fine, J. M., Dvornikovs, V., Jeffrey, C. S., Shao, F., Wang, J., Vrieze, L. A., Anderson, K. R., and Hoye, T. R. (2005) Mixture of new sulfated steroids functions as a migratory pheromone in the sea lamprey. *Nat. Chem. Biol. 1*, 324–8.

[171] He, J., Ma, L., Kim, S., Schwartz, J., Santilli, M., Wood, C., Durnin, M. H., and Yu, C. R. (2010) Distinct Signals Conveyed by Pheromone Concentrations to the Mouse Vomeronasal Organ. *J. Neurosci. 30*, 7473–7483.

[172] Isogai, Y., Si, S., Pont-Lezica, L., Tan, T., Kapoor, V., Murthy, V. N., and Dulac, C. (2011) Molecular organization of vomeronasal chemoreception. *Nature 478*, 241–5.

[173] Liman, E. R., and Corey, D. P. (1996) Electrophysiological characterization of chemosensory neurons from the mouse vomeronasal organ. *J Neurosci 16*, 4625–37.

[174] Ukhanov, K., Leinders-Zufall, T., and Zufall, F. (2007) Patch-clamp analysis of gene-targeted vomeronasal neurons expressing a defined V1r or V2r receptor: ionic mechanisms underlying persistent firing. *J Neurophysiol 98*, 2357–69.

[175] Hagendorf, S., Fluegge, D., Engelhardt, C., and Spehr, M. (2009) Homeostatic control of sensory output in basal vomeronasal neurons: activity-dependent expression of ether-Ã -go-go-related gene potassium channels. *J Neurosci 29*, 206–21.

[176] Spehr, J., Hagendorf, S., Weiss, J., Spehr, M., Leinders-Zufall, T., and Zufall, F. (2009) Ca2+ -calmodulin feedback mediates sensory adaptation and inhibits pheromone-sensitive ion channels in the vomeronasal organ. *J Neurosci 29*, 2125–35.

[177] Kepecs, A., Uchida, N., and Mainen, Z. F. (2006) The sniff as a unit of olfactory processing. *Chem Senses 31*, 167–79.

[178] Arnson, H. A., Fu, X., and Holy, T. E. (2010) Multielectrode array recordings of the vomeronasal epithelium. *J Vis Exp*.

[179] Segev, R., Goodhouse, J., Puchalla, J., and Berry, M. J. (2004) Recording spikes from a large fraction of the ganglion cells in a retinal patch. *Nat. Neurosci. 7*, 1154–1161.

[180] Marre, O., Amodei, D., Deshmukh, N., Sadeghi, K., Soo, F., Holy, T. E., and Berry, M. J., 2nd (2012) Mapping a complete neural population in the retina. *J Neurosci 32*, 14859–73.

[181] van Rossum, M. C. (2001) A novel spike distance. *Neural Comput 13*, 751–63.

[182] Rieke, F., Warland, D., van Steninck, R. R., and Bialek, W. *Spikes-Exporing the neural codes*; MIT press, 1997.

[183] Silverman, B. *Density Estimation for Statistics and Data Analysis*; Chapman and Hall, New York, 1986.

[184] Cover, T., and Thomas, J. *Elements of information theory*; Wiley-Interscience, 1991.

[185] Knutsen, P. M., and Ahissar, E. (2009) Orthogonal coding of object location. *Trends Neurosci 32*, 101–9.

[186] Maler, L. (2007) Neural strategies for optimal processing of sensory signals. *Prog Brain Res 165*, 135–54.

[187] Gillespie, P. G., and Muller, U. (2009) Mechanotransduction by hair cells: models, molecules, and mechanisms. *Cell 139*, 33–44.

[188] Tsunozaki, M., and Bautista, D. M. (2009) Mammalian somatosensory mechanotransduction. *Curr Opin Neurobiol 19*, 362–9.

[189] Yau, K.-W., and Hardie, R. C. (2009) Phototransduction motifs and variations. *Cell 139*, 246–64.

[190] Singer, J. H., Glowatzki, E., Moser, T., Strowbridge, B. W., Bhandawat, V., and Sampath, A. P. (2009) Functional properties of synaptic transmission in primary sense organs. *J Neurosci 29*, 12802–6.

[191] Ishimaru, Y. (2009) Molecular mechanisms of taste transduction in vertebrates. *Odontology 97*, 1–7.

[192] Berry, M. J., Warland, D. K., and Meister, M. (1997) The structure and precision of retinal spike trains. *Proc Natl Acad Sci U S A 94*, 5411–6.

[193] Shadlen, M. N., and Newsome, W. T. (1998) The variable discharge of cortical neurons: implications for connectivity, computation, and information coding. *J Neurosci 18*, 3870–96.

[194] Reich, D., Mechler, F., Purpura, K., and Victor, J. (2000) Interspike intervals, receptive fields, and information encoding in primary visual cortex. *Journal of Neuroscience 20*, 1964.

[195] Green, D., and Swets, J. (1966) Signal detection theory and psychophysics.

[196] Britten, K., Shadlen, M., Newsome, W., and Movshon, J. (1992) The analysis of visual motion: a comparison of neuronal and psychophysical performance. *Journal of Neuroscience 12*, 4745.

[197] Dayan, P., Abbott, L., and Abbott, L. *Theoretical neuroscience: Computational and mathematical modeling of neural systems*; MIT Press, 2001.

[198] Spehr, M., Hatt, H., and Wetzel, C. H. (2002) Arachidonic acid plays a role in rat vomeronasal signal transduction. *J Neurosci 22*, 8429–37.

[199] Yang, C., and Delay, R. J. (2010) Calcium-activated chloride current amplifies the response to urine in mouse vomeronasal sensory neurons. *J Gen Physiol 135*, 3–13.

[200] Krahe, R., and Gabbiani, F. (2004) Burst firing in sensory systems. *Nat Rev Neurosci 5*, 13–23.

[201] Bean, B. P. (2007) The action potential in mammalian central neurons. *Nat Rev Neurosci 8*, 451–65.

[202] Eyherabide, H. G., Rokem, A., Herz, A. V. M., and Samengo, I. (2008) Burst firing is a neural code in an insect auditory system. *Front Comput Neurosci 2*, 3.

[203] Rospars, J. P., LÃ¡nskÃÂœ, P., Duchamp-Viret, P., and Duchamp, A. (2000) Spiking frequency versus odorant concentration in olfactory receptor neurons. *Biosystems 58*, 133–41.

[204] Kepecs, A., Wang, X.-J., and Lisman, J. (2002) Bursting neurons signal input slope. *J Neurosci 22*, 9053–62.

[205] DeBusk, B. C., DeBruyn, E. J., Snider, R. K., Kabara, J. F., and Bonds, A. B. (1997) Stimulus-dependent modulation of spike burst length in cat striate cortical cells. *J Neurophysiol 78*, 199–213.

[206] Martinez-Conde, S., Macknik, S. L., and Hubel, D. H. (2002) The function of bursts of spikes during visual fixation in the awake primate lateral geniculate nucleus and primary visual cortex. *Proc Natl Acad Sci U S A 99*, 13920–5.

[207] Oswald, A.-M. M., Doiron, B., and Maler, L. (2007) Interval coding. I. Burst interspike intervals as indicators of stimulus intensity. *J Neurophysiol 97*, 2731–43.

[208] Eggermont, J. J., Smith, G. M., and Bowman, D. (1993) Spontaneous burst firing in cat primary auditory cortex: age and depth dependence and its effect on neural interaction measures. *J Neurophysiol 69*, 1292–313.

[209] Rospars, J.-P., Lansky, P., Chaput, M., and Duchamp-Viret, P. (2008) Competitive and noncompetitive odorant interactions in the early neural coding of odorant mixtures. *J Neurosci 28*, 2659–66.

[210] Tan, J., Savigner, A., Ma, M., and Luo, M. (2010) Odor information processing by the olfactory bulb analyzed in gene-targeted mice. *Neuron 65*, 912–26.

[211] Johnston, D., and Wu, S. *Foundations of Cellular Neurophysiology*; The MIT Press, 1995.

[212] Meeks, J. P., Jiang, X., and Mennerick, S. (2005) Action potential fidelity during normal and epileptiform activity in paired soma-axon recordings from rat hippocampus. *J Physiol 566*, 425–41.

[213] Holekamp, T. F., Turaga, D., and Holy, T. E. (2008) Fast three-dimensional fluorescence imaging of activity in neural populations by objective-coupled planar illumination microscopy. *Neuron 57*, 661–72.

[214] Leinders-Zufall, T., Ishii, T., Mombaerts, P., Zufall, F., and Boehm, T. (2009) Structural requirements for the activation of vomeronasal sensory neurons by MHC peptides. *Nat Neurosci 12*, 1551–8.

[215] Riesenhuber, M., and Poggio, T. (2002) Neural mechanisms of object recognition. *Curr Opin Neurobiol 12*, 162–8.

[216] Bhagavan, S., and Smith, B. H. (1997) Olfactory conditioning in the honey bee, Apis mellifera: effects of odor intensity. *Physiol Behav 61*, 107–17.

[217] Cleland, T. A., Chen, S.-Y. T., Hozer, K. W., Ukatu, H. N., Wong, K. J., and Zheng, F. (2011) Sequential mechanisms underlying concentration invariance in biological olfaction. *Front Neuroeng 4*, 21.

[218] Baker, T. C., Cardé, R. T., and Roelofs, W. L. (1976) Behavioral responses of male Argyrotaenia velutinana (Lepidoptera: Tortricidae) to components of its sex pheromone. *Journal of Chemical Ecology 2*, 333–352, 10.1007/BF00988281.

[219] Hurst, J. L., and Beynon, R. J. (2004) Scent wars: the chemobiology of competitive signalling in mice. *Bioessays 26*, 1288–98.

[220] Celsi, F., D'Errico, A., and Menini, A. (2012) Responses to Sulfated Steroids of Female Mouse Vomeronasal Sensory Neurons. *Chem Senses*.

[221] Chamero, P., Leinders-Zufall, T., and Zufall, F. (2012) From genes to social communication: molecular sensing by the vomeronasal organ. *Trends Neurosci 35*, 597–606.

[222] Cleland, T. A., and Linster, C. (1999) Concentration tuning mediated by spare receptor capacity in olfactory sensory neurons: A theoretical study. *Neural Comput 11*, 1673–90.

[223] Uchida, N., Kepecs, A., and Mainen, Z. F. (2006) Seeing at a glance, smelling in a whiff: rapid forms of perceptual decision making. *Nat Rev Neurosci 7*, 485–91.

[224] Wachowiak, M. (2011) All in a sniff: olfaction as a model for active sensing. *Neuron 71*, 962–73.

[225] Wilson, D. A., and Sullivan, R. M. (2011) Cortical processing of odor objects. *Neuron 72*, 506–19.

[226] Su, C.-Y., Menuz, K., and Carlson, J. R. (2009) Olfactory perception: receptors, cells, and circuits. *Cell 139*, 45–59.

[227] Keverne, E. B. (1979) The dual olfactory projections and their significance for behaviour. *Chemical Ecology: Odour Communication in Animals* 75–83.

[228] Brosvic, G. M., and Slotnick, B. M. (1986) Absolute and intensity-difference taste thresholds in the rat: evaluation of an automated multi-channel gustometer. *Physiol. Behav. 38*, 711–7.

[229] Eylam, S., and Spector, A. C. (2003) Oral amiloride treatment decreases taste sensitivity to sodium salts in C57BL/6J and DBA/2J mice. *Chem. Senses 28*, 447–58.

[230] Zhang, P., Yang, C., and Delay, R. J. (2010) Odors activate dual pathways, a TRPC2 and a AA-dependent pathway, in mouse vomeronasal neurons. *Am J Physiol Cell Physiol 298*, C1253–64.

[231] Delay, E. R., Hernandez, N. P., Bromley, K., and Margolskee, R. F. (2006) Sucrose and monosodium glutamate taste thresholds and discrimination ability of T1R3 knockout mice. *Chem. Senses 31*, 351–7.

[232] Uchida, N., and Mainen, Z. F. (2003) Speed and accuracy of olfactory discrimination in the rat. *Nat. Neurosci. 6*, 1224–9.

[233] Slotnick, B., and Restrepo, D. (2005) Olfactometry with mice. *Curr Protoc Neurosci Chapter 8*, Unit 8.20.

[234] Frederick, D. E., Rojas-Líbano, D., Scott, M., and Kay, L. M. (2011) Rat behavior in go/no-go and two-alternative choice odor discrimination: differences and similarities. *Behav. Neurosci. 125*, 588–603.

[235] Bhandawat, V., Olsen, S. R., Gouwens, N. W., Schlief, M. L., and Wilson, R. I. (2007) Sensory processing in the Drosophila antennal lobe increases reliability and separability of ensemble odor representations. *Nat Neurosci 10*, 1474–82.

[236] Bhandawat, V., Reisert, J., and Yau, K.-W. (2005) Elementary response of olfactory receptor neurons to odorants. *Science 308*, 1931–4.

[237] Meeks, J. P., and Holy, T. E. (2009) An ex vivo preparation of the intact mouse vomeronasal organ and accessory olfactory bulb. *J Neurosci Methods 177*, 440–7.

[238] Kepecs, A., Uchida, N., Zariwala, H. A., and Mainen, Z. F. (2008) Neural correlates, computation and behavioural impact of decision confidence. *Nature 455*, 227–31.

[239] Spors, H., Albeanu, D. F., Murthy, V. N., Rinberg, D., Uchida, N., Wachowiak, M., and Friedrich, R. W. (2012) Illuminating vertebrate olfactory processing. *J Neurosci 32*, 14102–8.

[240] Kaneko, H., Putzier, I., Frings, S., Kaupp, U. B., and Gensch, T. (2004) Chloride accumulation in mammalian olfactory sensory neurons. *J Neurosci 24*, 7931–8.

[241] Nagashima, A., and Touhara, K. (2010) Enzymatic conversion of odorants in nasal mucus affects olfactory glomerular activation patterns and odor perception. *J Neurosci 30*, 16391–8.

[242] Miyawaki, A., Matsushita, F., Ryo, Y., and Mikoshiba, K. (1994) Possible pheromone-carrier function of two lipocalin proteins in the vomeronasal organ. *EMBO J 13*, 5835–42.

[243] Kim, S., Ma, L., Jensen, K. L., Kim, M. M., Bond, C. T., Adelman, J. P., and Yu, C. R. (2012) Paradoxical contribution of SK3 and GIRK channels to the activation of mouse vomeronasal organ. *Nat Neurosci 15*, 1236–44.